Dynamics of Phobos

Reconciling the ephemerides and rotation models

AE4020: Literature Study

Jorge Martinez Castillo

Delft University of Technology

TU Delft

Dynamics of Phobos

Reconciling the ephemerides and rotation models

by

Jorge Martinez Castillo

Student number: 5626919
Project duration: September 2022 – November, 2024
Supervisor: Dominic Dirkx

Cover: "3d illustration of the moon Phobos and the planet Mars" - Esteban De Armas at shutterstock.com
Style: TU Delft Report Style, with modifications by Daan Zwaneveld

TU Delft

Contents

Nomenclature

Note: In the whole text, the symbol denoting a vectorial quantity or magnitude will have an overhead arrow: $\vec{u}$, $\vec{v}$. The Euclidean norm of these vectorial quantities will be denoted indistinctly by either the same letter without the overhead arrow or the vectorial quantity inside two vertical lines: $u = \left|\vec{u}\right|$, $v = \left|\vec{v}\right|$. Unitary vectors will be denoted with the same letter as the non-unitary ones but will have an overhead hat notation: $\hat{u}$, $\hat{v}$. Note that $\vec{u} = u\hat{u}$, $\vec{v} = v\hat{v}$. Matrices will be denoted by bold capital letters - $\boldsymbol{A}$, $\boldsymbol{B}$, ... - and quaternions will be denoted by bold lower-case letters - $\boldsymbol{q}$, $\boldsymbol{p}$, ...

Gradient notation

Given a scalar function $f(\vec{x}) : \mathbb{R}^n \longrightarrow \mathbb{R}$, its derivative or gradient with respect to $\vec{x}$ is by definition a row vector, where the i-th component is given as follows:

$$\frac{\partial f}{\partial \vec{x}} \in \mathbb{R}^{1\times n} \quad \text{with} \quad \frac{\partial f}{\partial \vec{x}}(i) = \frac{\partial f}{\partial x_i}$$

Alternatively, the ∇ symbol can be used to denote a column vector corresponding to the transpose of the derivative:

$$\nabla f = \left(\frac{\partial f}{\partial \vec{x}}\right)^T$$

Given a vector function $\vec{g}(\vec{x}) : \mathbb{R}^n \longrightarrow \mathbb{R}^m$, its gradient or derivative is an m-by-n matrix whose entries are defined as follows:

$$\nabla \vec{g} = \frac{\partial \vec{g}}{\partial \vec{x}} \in \mathbb{R}^{m\times n} \quad \text{with} \quad \frac{\partial \vec{g}}{\partial \vec{x}}(i,j) = \frac{\partial g_i}{\partial x_j}$$

Note that this applies in a straight forward manner to the second derivative of $f(\vec{x})$. This derivative will be an n-by-n square matrix whose entries are defined as follows:

$$\frac{\partial^2 f}{\partial \vec{x}^2} \in \mathbb{R}^{n\times n} \quad \text{with} \quad \frac{\partial^2 f}{\partial \vec{x}^2}(i,j) = \frac{\partial^2 f}{\partial x_j \partial x_i} = \frac{\partial}{\partial x_j}\left(\frac{\partial f}{\partial x_i}\right) = \frac{\partial}{\partial x_j}\left(\frac{\partial f}{\partial \vec{x}}(i)\right) = \frac{\partial}{\partial x_j}\left(\nabla f(i)\right)$$

Note that, since the component-wise definition of ∇f and $\partial f / \partial \vec{x}$ is the same, we will be able to write the following as true:

$$\frac{\partial}{\partial \vec{x}}\left(\frac{\partial f}{\partial \vec{x}}\right) = \frac{\partial}{\partial \vec{x}}\left(\nabla f\right) = \frac{\partial^2 f}{\partial \vec{x}^2} = \nabla^2 f$$

Note the notation $\nabla^2 f$ for the gradient of the gradient, as opposed to its traditional meaning of the divergence of the gradient - i.e. the Laplacian.

Cross product notation

Consider two vectors $\vec{v}, \vec{u} \in \mathbb{R}^3$. Their cross product is defined as follows:

$$\vec{v} \times \vec{u} = \begin{bmatrix} v_2u_3 - v_3u_2 \\ v_3u_1 - v_1u_3 \\ v_1u_2 - v_2u_1 \end{bmatrix} = \begin{bmatrix} 0 & -v_3 & v_2 \\ v_3 & 0 & -v_1 \\ -v_2 & v_1 & 0 \end{bmatrix} \vec{u} = \begin{bmatrix} 0 & u_3 & -u_2 \\ -u_3 & 0 & u_1 \\ u_2 & -u_1 & 0 \end{bmatrix} \vec{v}$$

We can define the following matrices:

$$[\vec{v}_\wedge] = \begin{bmatrix} 0 & -v_3 & v_2 \\ v_3 & 0 & -v_1 \\ -v_2 & v_1 & 0 \end{bmatrix} \qquad [_\wedge\vec{u}] = \begin{bmatrix} 0 & u_3 & -u_2 \\ -u_3 & 0 & u_1 \\ u_2 & -u_1 & 0 \end{bmatrix}$$

Note that, for a generic vector $\vec{x}$, $[_\wedge\vec{x}] = -[\vec{x}_\wedge] = -[_\wedge\vec{x}]^T$. These definitions allow to write $\vec{v} \times \vec{u} = [\vec{v}_\wedge]\vec{u} = [_\wedge\vec{u}]\vec{v}$. This is convenient for the computation of derivatives because:

$$\frac{d}{d\vec{u}}(\vec{v} \times \vec{u}) = [\vec{v}_\wedge] \qquad \frac{d}{d\vec{v}}(\vec{v} \times \vec{u}) = [_\wedge\vec{u}]$$

This allows to write the following. Given two vectors $\vec{v}(\vec{x})$ and $\vec{u}(\vec{x})$, both of which depend on $\vec{x}$, the gradient of their cross-product is given as follows:

$$\nabla(\vec{v} \times \vec{u}) = \frac{\partial}{\partial\vec{v}}(\vec{v} \times \vec{u})\nabla\vec{v} + \frac{\partial}{\partial\vec{u}}(\vec{v} \times \vec{u})\nabla\vec{u} = [_\wedge\vec{u}]\nabla\vec{v} + [\vec{v}_\wedge]\nabla\vec{u}$$

Higher order tensors

It may happen that we come across mathematical objects with several dimensions. They are called *tensors* and their dimension is referred to as their *order*. A scalar can be regarded as a tensor of order 0, a vector as a tensor of order 1, and a matrix as a tensor of order 2. Higher order tensors exist, but we will at most encounter tensors of order 3, always in the context of computing the gradient of a vector that is in turn given as a multiplication of a matrix and another vector.

Consider a vector $\vec{u} = \boldsymbol{A}\vec{v}$, where $\vec{u} \in \mathbb{R}^n$, $\vec{v} \in \mathbb{R}^m$ and $\boldsymbol{A} \in \mathbb{R}^{n\times m}$. All three of these terms depend on a vector $\vec{x} \in \mathbb{R}^l$. By definition, the derivative of $\vec{u}$ is an n-by-l matrix. But if we apply the chain rule, how do we define the derivative of $\boldsymbol{A}$ with respect to $\vec{x}$? Direct application of the chain rule looks as follows:

$$\frac{d\vec{u}}{d\vec{x}} = \frac{d\boldsymbol{A}}{d\vec{x}}\vec{v} + \boldsymbol{A}\frac{d\vec{v}}{d\vec{x}}$$

The aim is to find an expression for the first term on the right-hand side. We begin by writing the derivative as follows:

$$\frac{d\vec{u}}{d\vec{x}} = \begin{bmatrix} \frac{d\vec{u}}{dx_1} & \frac{d\vec{u}}{dx_2} & \frac{d\vec{u}}{dx_3} & \dots & \frac{d\vec{u}}{dx_l} \end{bmatrix} \in \mathbb{R}^{n\times l}$$

Taking the k-th of those derivatives, we can write:

$$\frac{d\vec{u}}{dx_k} = \frac{d\boldsymbol{A}}{dx_k}\vec{v} + \boldsymbol{A}\frac{d\vec{v}}{dx_k}$$

This allows to separate the derivative as follows:

$$\frac{d\vec{u}}{d\vec{x}} = \begin{bmatrix} \frac{d\boldsymbol{A}}{dx_1}\vec{v} & \frac{d\boldsymbol{A}}{dx_2}\vec{v} & \frac{d\boldsymbol{A}}{dx_3}\vec{v} & \dots & \frac{d\boldsymbol{A}}{dx_l}\vec{v} \end{bmatrix} + \begin{bmatrix} \boldsymbol{A}\frac{d\vec{v}}{dx_1} & \boldsymbol{A}\frac{d\vec{v}}{dx_2} & \boldsymbol{A}\frac{d\vec{v}}{dx_3} & \dots & \boldsymbol{A}\frac{d\vec{v}}{dx_l} \end{bmatrix}$$

The final term in the first and last equations can be identified to be the same, by definition. The other terms must therefore be equivalent as well. Thus, we can define the following product between the third-order tensor $d\boldsymbol{A}/d\vec{x} \in \mathbb{R}^{n\times m\times l}$ and vector $\vec{v} \in \mathbb{R}^m$ as follows:

$$\frac{d\boldsymbol{A}}{d\vec{x}}\vec{v} = \begin{bmatrix} \frac{d\boldsymbol{A}}{dx_1}\vec{v} & \frac{d\boldsymbol{A}}{dx_2}\vec{v} & \frac{d\boldsymbol{A}}{dx_3}\vec{v} & \dots & \frac{d\boldsymbol{A}}{dx_l}\vec{v} \end{bmatrix} \implies \boldsymbol{M}\vec{v} = \boldsymbol{N} \qquad \text{with } \boldsymbol{M} = \frac{d\boldsymbol{A}}{d\vec{x}} \in \mathbb{R}^{n\times m\times l}$$

Notice that given a third-order tensor $\boldsymbol{M} \in \mathbb{R}^{n\times m\times l}$ and a vector $\vec{v} \in \mathbb{R}^m$, their product is a second-order tensor $\boldsymbol{N} = \boldsymbol{M}\vec{v} \in \mathbb{R}^{n\times l}$. For this, the entries along the last dimension of $\boldsymbol{M}$ must be compatible with the length of $\vec{v}$, namely the product $\boldsymbol{M}_k\vec{v}$ must be defined.

1 Introduction

1.1. Discovery and early observations of the Martian satellites

Everyone knows Mars - and the Martians. What not everyone knows is that Mars has two moons: Phobos and Deimos. Their discovery is surrounded by an aura of mystery and mysticism, and came by the hand of Asaph Hall on August 17th 1877 (Hall, 1878), during the Earth-Mars opposition [1] of that year. A bit over 250 years prior, Kepler had predicted that Mars would have two satellites, based on the fact that the Earth had one and Jupiter was at the time known to have four. So it only made sense that Mars had two (Burns, 1972). Even more striking is that, for reasons unknown to everyone but the author, *Gulliver's Travels*, written by Jonathan Swift 150 years before Hall's discovery, featured two moons orbiting Mars in orbits that are suspiciously close to the the now known ones (Burns, 1972). Over the course of two months, the moons were observed all around the globe, named, and their orbits computed. Specifically, the first particularity of Phobos then became obvious: it orbited Mars three times a Martian day, which means that it rises in the west and sets in the east.

Both Phobos and Deimos received the same amount of interest and were subject to the same type of research. Between their discovery and the advent of Martian orbiters, they could only be observed from ground during Earth-Mars oppositions, occurring roughly once every 2 years. Publications of observations were abundant in the first 20 years since their discovery (Pickering et al., 1879; Hall, 1880; Pritchett, 1880; Keeler, 1888, 1890; Campbell, 1892; Newall, 1895; Barnard, 1897) and the first ephemerides were generated as early as 1879 (Marth, 1879). Their sizes were also estimated in 1879 (Barnard, 1897). After almost 40 years, longer observation arcs revealed long term changes in its orbit. The precessions of the node and pericenter were studied in 1944 (Woolard, 1944). A secular acceleration in the longitude of the satellites was confirmed by Sharpless (1945). For Phobos in particular, this meant that the moon was spiraling inward onto the surface. Possible explanations for this phenomenon were gathered by Kerr and Whipple (1951). The most probable explanation for this was tidal friction. However, an unfortunate misunderstanding lead Jeffreys (1957) to wrongly read Sharpless' results and conclude that tidal friction could not be the cause of Phobos' longitude acceleration. Out of options, Iosif Shklovsky proposed in 1959 the possibility of Martian exospheric drag being the cause of this acceleration. The calculations were again carried out by Schilling (1964a), who concluded that such a theory was compatible with existing observations, but Phobos needed to be hollow. This spurred theories of Phobos being an artificial satellite built by Martian intelligent life. Nevertheless, that same year, Schilling (1964b) himself together with Schelling (1964) resolved the misunderstanding about Sharpless' results and Schilling (1964b) concluded that tidal friction was also compatible with existing observations and that more data was needed.

The theory of a hollow Phobos being deorbited by atmospheric drag was never again mentioned in scientific literature as a serious possibility. Therefore, it is safe to assume that the scientific community discarded such a theory. Thus, the leading theory on the origin of Phobos was based on general considerations of orbital mechanics. With a (near-)circular and (near-)equatorial orbit, Phobos'

[1] When the Earth and an outer planet - Mars or beyond - lie at the same side of the Sun - especially if in a straight line - the Sun and the planet are seen in opposite sides of the Earth's sky. This configuration is called opposition. Oppositions offer great opportunities for astronomical observations because the Sun is nowhere near the planet.

formation in the Martian proto-planetary disk by aggregation seemed the most plausible Correspondent (1969).

1.2. Space-borne research of Phobos

Up until the 60s, the study of Phobos had been dynamical, i.e. its orbit had put constraints on mass, density, environment and origin. However, the 60s marked the beginning of a new era for the research of the Martian system: Martian orbiters. Although their main purpose was generally not a focused study of the Martian moons, some pictures taken by the different spacecraft included them. Pictures provided a better measurement of the position of the moons, because now observations involved spacecraft ranging - orders of magnitude more accurate than telescopic observations from Earth - which helped improve knowledge on the moons' dynamics. In addition, Phobos' low orbit caused it to be closer to Martian orbiters than Deimos, which made it easier to explore visually. Photography from spacecraft could provide the first look at Phobos' surface features, as well as better estimates of its albedo.

It was the US who initiated the study of Phobos from space. The first space-borne sighting of Phobos occurred in 1969, as it sneaked into four pictures taken by *Mariner 7* (Siddiqi, 2018) during its single Martian flyby. These showed the moon to have an irregular shape but did not offer a good sight of its surface features. One of these pictures was analyzed a year later by Smith (1970) and revealed Phobos had a very low albedo and was stunningly dark. Further photographs of the moon were taken by *Mariner 9* in 1971, an orbiter which came as close as 5465km from the moon (Pollack et al., 1972). These pictures discerned surface features such as craters and helped constrain Phobos' composition (Veverka, 1978). *Mariner 9* discovered big craters, such as *Stickney*, *Hall* and *Roche*. The areas that had not been surveyed by *Mariner 9* were to be photographed by *Viking 1*'s orbiter (Veverka, 1978). *Viking 1* was the most fruitful Martian orbiter when it comes to Phobos. Launched in 1975, the photographs taken by *Viking 1* were far better than those of *Mariner 9* pSiddiqi (2018). On the one hand, their resolution was enough to make out small craters (Veverka, 1978) and reveal the famous grooves that run across the moon (Thomas et al., 1979). On the basis of these grooves being stress fractures, the stress state of Phobos was computed by Dobrovolskis (1982) and its breakup predicted. On the other hand, *Viking 1*'s pictures were colored, which allowed a preliminary identification of the surface composition by Veverka (1978). As it turns out, Phobos shared an extraordinary resemblance with carbonaceous chondrites, i.e. asteroids. The theory of Phobos being a captured asteroid then began gaining strength (Veverka, 1978). By 1985, the scientific community was already proposing in-situ measurements, which would require a Phobos lander (Illés et al., 1985).

The first mission to have Phobos as one of its primary objectives was the Soviet *Phobos 2* mission, which included a Mars orbiter and a Phobos lander (Siddiqi, 2018). Prior to the release of the lander, the orbiter mapped 80% of Phobos' surface and got as close as 190km. A bit over a week before lander release, however, *Phobos 2* went silent and the mission was lost. Another Phobos targeted mission was the *Aladdin* mission, finalist of NASA's *Discovery* program in 1998. It was a sample return mission that would collect material from Phobos and bring it back to Earth for study three years later. The mission lost the final selection process to *MESSENGER* and was never realized.

The exploration of the Martian system during the 20th century culminated in 1996 with the launch of the *Mars Global Surveyor (MGS)*, which would orbit Mars for almost ten years. Although it photographed Phobos a few times (JPL, 2000), no significant improvement on existing science was provided by this mission.

1.3. Phobos in the 21st century

At the turn of the century, Phobos had been studied visually in many wavelengths. Its dynamics were known and good estimates existed on its geophysical properties. However, the question still remained about its formation: had it been aggregated in the Martian proto-planetary disk or was it a captured asteroid? Its orbit favoured the former, its composition favoured the latter.

The 2000s began with *MGS* already in Martian orbit, and would see the addition of *Mars Express (MEX)* in December 2003 and *Mars Reconnaissance Orbiter (MRO)* in March 2006 (Siddiqi, 2018). Imagery by *MEX* helped map the grooves throughout the whole moon (Murray et al., 2006) and proved that they are not related to Stickney crater or its formation, as previously thought. They also helped refine models on the dynamics of Phobos - see, for example, the works of Jacobson (2010) or Oberst et al. (2014) - whose orbit can be used to study Mars' past (Samuel et al., 2019). Nevertheless, the focus of

the 21st century's exploration of the Martian moon(s) is landing and returning a sample, although there have been more proposals than actual missions. Mission proposals include *PRIME* in 2008 (Lee et al., 2008), *M-PADS* in 2009 (Ball et al., 2009), *Hall* in 2010 (Lee et al., 2010), *MMSR* in 2011 (Michel et al., 2011), *PCROSS* and *OSIRIS-REx* in 2012 (Colaprete et al., 2012; Elifritz, 2012), *MERLIN*, *Phootprint*, *PADME* and *PANDORA* in 2014 (Murchie et al., 2014; Barraclough et al., 2014; Lee et al., 2014; Prettyman et al., 2014), and *DePhine* in 2018 (Oberst et al., 2018). None of these have flown: some never will and others are still under development. Only *Phobos-Grunt*, proposed in 2004 (Marov et al., 2004), got to be launched. However, it didn't make it past Earth orbit (Siddiqi, 2018). Russia plans to recover it and a second mission, *Phobos-Grunt-2* nicknamed *Bumerang*, is under preparation (Golub' and Popel, 2021). Possibly the best-known mission "on its way to the Martian moons" is JAXA's *Martian Moon eXploration (MMX)* mission (Nakamura et al., 2021). *MMX* is a sample return mission planned for launch in 2024 that aims at unraveling the mystery of the origin of the Martian moon(s). It is to come back to Earth in 2029 with at least 10g of Phobian regolith with it. A detailed explanation of how such a mission - and the subsequent analysis of the recovered regolith - can answer the question of the moons' origin was given by Usui et al. (2020).

While we wait for *MMX* to return, the question on the origin and evolution of Phobos still stands.

1.4. Getting ready to visit Phobos

The exploration of Phobos in search for answers about its origin is entering a new era: the era of landers, of which *MMX* seems to be the spearhead. This presents new challenges, both technological and scientific. Many of these are related to knowing Phobos' position and orientation accurately enough for a spacecraft to land successfully in Phobos' weak gravitational field. Others lie on the methods to use the new data, and whether existing tools are good enough to use this data to its fullest. In the intersection of these two disciplines sits the dynamics of Phobos. On the one hand, better dynamical models are able to better predict Phobos' *state* - to be defined in the following chapters - and provide better guidance for spacecraft, both landers and orbiters. On the other hand, a good knowledge of the elements of the dynamics of Phobos, together with the interplay between them, allows for the isolation of certain dynamical effects. The better these effects are singled out, the better they will be able to be recognized in the data products of the mission and the more accurately they can be *estimated*.

As will be expanded on in future chapters, the position and orientation of Phobos - or, more technically, the translation and rotation - are studied separately and individually. Interactions between the two are widely acknowledged, but these are generally regarded as negligible. As we will see, quantitative analyses of these interactions have not been conducted as of yet. Thus, the study of the dynamics of Phobos is currently limited by this barrier, beyond which little is known. The aim of the master thesis that will follow this literature study is to explore that uncharted territory by studying translation and rotation as one. The present text will document the necessary knowledge required to understand these two motions in theory (see Ch. 2), as well as survey current methods and approaches to their study (see Ch. 3). Lastly, we will briefly go over the way in which Phobos' dynamics are used to analyze data (see Ch. 4). All these will be recovered in Ch. 6, and the text will culminate in the generation of a science question which the subsequent thesis will have to answer.

2

Dynamics

2.1. General dynamics

2.1.1. Newton's second law of motion and inertial frames

The motion of celestial bodies - planets and moons - is very well described by classical mechanics, summarized in Newton's three laws of motion. These laws apply to two different realms: translation and rotation. Of most interest is Newton's second law applied to both linear and angular motion (i.e. translation and rotation). These are stated in Eq.(2.1a) and Eq.(2.1b), respectively (Villalba et al., 2018). They apply to any generic body. The reader should keep in mind that the position and velocity "of the body" reference to the position and velocity "of the body's center of mass". It is to that point that Eq.(2.1a) applies.

$$\frac{d\vec{p}}{dt} = \sum \vec{F} \tag{2.1a}$$

$$\frac{d\vec{L}}{dt} = \sum \vec{T} \tag{2.1b}$$

In these equations, the different terms are defined below:

- t: Time.
- $\vec{p} = m\vec{v}$: It is the body's linear momentum, product of its mass m and its velocity $\vec{v}$.
- $\vec{F}$: It is a force applied onto the body. The sum of all forces is called the *resultant*.
- $\vec{L} = \boldsymbol{I}\vec{\omega}$: It is the angular momentum of the body, product of the body's *inertia tensor* $\boldsymbol{I}$ and the body's angular velocity $\vec{\omega}$.
- $\vec{T} = \vec{r}_a \times \vec{F}$: It is a torque applied on the body, obtained from the cross product of a force $\vec{F}$ and the vector $\vec{r}_a$ that goes from the body's center of mass to the point of application of the force.

In this text we will only treat bodies with constant mass. In this case, one usually brings the mass from inside the time derivative on the left of Eq.(2.1a) to the right. Furthermore, the velocity of the body is by definition the time derivative of the body's position, so we substitute the first derivative of the velocity by the second derivative of the position, using Newton's notation for the time derivative. The form it will be used in this text is seen in Eq.(2.2). Unless otherwise stated, an acceleration will be denoted $\vec{a}$ or $\ddot{\vec{r}}$ indistinctly. Similarly, a velocity will be denoted $\vec{v}$ or $\dot{\vec{r}}$ indistinctly, although the former will be preferred. Note that $\dot{\vec{v}} = \vec{a}$.

$$\ddot{\vec{r}} = \sum \frac{\vec{F}}{m} \tag{2.2}$$

A key aspect of these equations is that they only hold in *inertial* reference frames. An inertial frame is defined as one that (a) does not rotate and (b) its origin is not subject to any type of acceleration. Note that a reference frame moving through space in a straight line at constant speed meets these two conditions and is therefore an inertial frame. If applied in a non-inertial frame, additional terms should

be added to these equations. These terms will be discussed later as needed. Newton's second law of linear motion is preferably applied in inertial frames. That is however **not** the case for the rotational counterpart.

Newton's second law of rotational motion involves the body's inertia tensor $\boldsymbol{I}$[1]. This tensor describes how the mass of the body is distributed around its center of mass, and is expressed in relation to some coordinate system. Writing Newton's second law of angular motion in an inertial reference frame rises a problem: if the body is rotating with respect to this frame the inertia tensor will be time dependent. With the angular velocity vector $\vec{\omega}$ being time dependent as well, the derivative of their dot product becomes quite complicated. That is why Newton's second law of angular motion is usually written in a reference frame that is attached to the rotating body and rotates with it. The origin of the frame is made to coincide with the center of mass of the body and the directions of the three axes may, in principle, be chosen freely. There is however a convenient way of aligning these axes, and hereby the concept of *principal axes of inertia* is introduced. Conceptually, every extended body - i.e. a body with volume rather than a point particle - has a set of three perpendicular axes which, if used as coordinate system to write the inertia tensor, this tensor turns out to be diagonal. Mathematically, this is a consequence of the diagonalization that can be applied to any matrix, which is in the end a linear transformation describing a rotation. A reference frame attached to a body, centered at the body's center of mass, rotating with said body and with its axes aligned with the body's principal axes of inertia is called the *body frame*.

Writing Newton's second law in a non-inertial reference frame creates the necessity of additional terms in the equation. More specifically, the time derivative - which needs to be expressed in an inertial frame - has to be written in terms of the time derivative expressed in a non-inertial frame. This is done through what is known as *Coriolis theorem* (Villalba et al., 2018), mathematically stated in Eq.(2.3), where $\vec{u}$ is a generic vector. The derivative on the left is taken in an inertial reference frame, while the derivative on the right is taken in a non-inertial frame that rotates with respect to the inertial at a rate of $\vec{\omega}_{\mathcal{NI}/\mathcal{I}}$.

$$\left.\frac{d\vec{u}}{dt}\right|_{\mathcal{I}} = \left.\frac{d\vec{u}}{dt}\right|_{\mathcal{NI}} + \vec{\omega}_{\mathcal{NI}/\mathcal{I}} \times \vec{u} \tag{2.3}$$

By means of this theorem, Eq.(2.1b) will be written as in Eq.(2.4), where the time derivative is now taken in the non-inertial body frame. Note that $\vec{L} = \boldsymbol{I}\vec{\omega}$ and, in this body frame, $\boldsymbol{I}$ is simplified to a diagonal tensor.

$$\frac{d\vec{L}}{dt} + \vec{\omega} \times \vec{L} = \sum \vec{T} \tag{2.4}$$

These few equations summarize the basis of the physics the text will use. Other theories on motion, like those of relativity or quantum mechanics, will not be used in the text.

2.1.2. Newton's law of gravitation, the two body problem and elliptical orbits

As stated in the first line of this section, we will study the motion of celestial bodies as governed by Newton's laws, a discipline known as *celestial mechanics* or *orbital dynamics*, terms that will be used indistinctly along the text. The simplest - and most idealized - case of the motion of orbiting bodies is that of what is known as the *two body problem (2BP)*. In the 2BP scenario, two bodies are modelled as perfect spheres with consequently spherically symmetric gravitational fields that orbit their (common) center of mass.

In a limit sometimes referred to as "one body problem", one of the bodies - the *central body* or *primary* - is considered to be orders of magnitude more massive than the other, with the latter having negligible mass. This assumption places the center of mass of the system at the center of mass of the primary, and the other body orbits around it. This is a good approximation for most star-planet or planet-moon systems and, more importantly, it is a good approximation for the Mars-Phobos system, where the mass of Phobos is only 2×10^{-6}% the mass of Mars. In common language, the *two body problem* is usually understood in this way as well. This will also be the case in this text.

In this scenario, the motion of the orbiting body is described in an inertial frame centered at the center of mass of the primary (see Sec. 2.1.4). In this reference frame, the equation of motion of the

[1]To avoid confusing the inertia tensor $\boldsymbol{I}$ with the identity matrix - usually called $\boldsymbol{I}$ as well - this text will always indicate the dimensions of an identity matrix as subscripts. This means that $\boldsymbol{I}_{n\times n}$ is the n-by-n identity matrix while $\boldsymbol{I}$ will always be the inertia tensor.

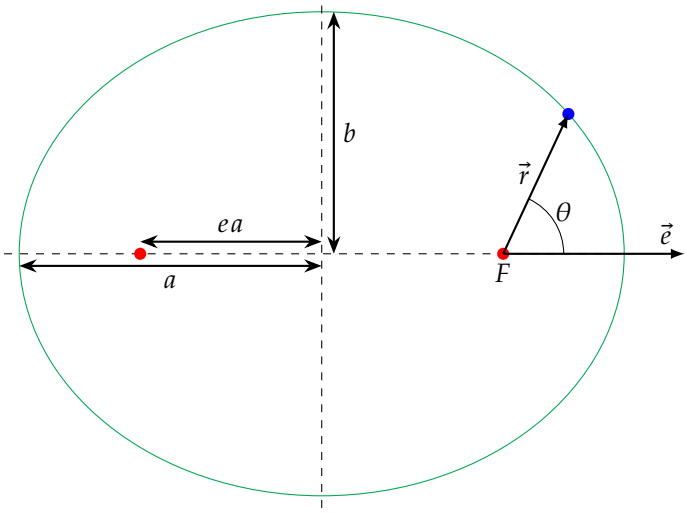

Figure 2.1: Planar geometry of an ellipse. Indicated here are the foci in red, the semi-major and semi-minor axes a and b, the eccentricity and position vectors $\vec{e}$ and $\vec{r}$, and the true anomaly θ.

orbiting body is written in Eq.(2.5). In this equation, μ is the *gravitational parameter* of the central body, the product of its mass M and the universal gravitational constant G, while $\vec{r}$ is the position vector of the orbiting body. This equation is known as *Newton's law of gravitation*.

$$\ddot{\vec{r}} = -\frac{\mu}{r^3}\vec{r} \tag{2.5}$$

Although not by direct integration, the solution to this equation can be shown to be conic section as done by Montenbruck and Gill (2005), a generalization of the case observed by Kepler of elliptical closed orbits - those of the planets around the Sun. The solution to an equation of motion is the *state vector* of the body, containing both its position and velocity. For the case of the elliptic orbit, however, another set of 6 independent parameters exists that describes the position of the body and, through some dynamical considerations, also its velocity. This set is the so-called *classical orbital elements (COEs)*. They are:

- a : Semimajor axis
- e : Eccentricity
- i : Inclination
- Ω : Right ascension of ascending node (RAAN)
- ω : Argument of pericenter
- θ : True anomaly. Sometimes denoted with ν.

The two state vectors are gathered in Eq.(2.6), while Fig.[2.1] and Fig[2.2] depict the planar and three-dimensional geometries of an ellipse and give geometrical interpretation to the COEs. The XY plane - the reference horizontal plane - is usually taken to be the equatorial plane if the primary is a planet or the *ecliptic*[2] if the primary is the Sun.

$$\vec{x} = \begin{bmatrix}\vec{r}\\ \vec{v}\end{bmatrix} = \begin{bmatrix}X\\ Y\\ Z\\ \dot{X}\\ \dot{Y}\\ \dot{Z}\end{bmatrix} \iff \vec{x} = \begin{bmatrix}a\\ e\\ i\\ \Omega\\ \omega\\ \theta\end{bmatrix} \tag{2.6}$$

In an elliptical orbit, the primary sits in one of the two foci of the ellipse, while the other focus remains empty. As such, there is a point in the orbit that is closest to the primary and one that is farthest.

[2]The ecliptic plane is the plane of Earth's orbit, and is the reference horizontal plane of the Solar System

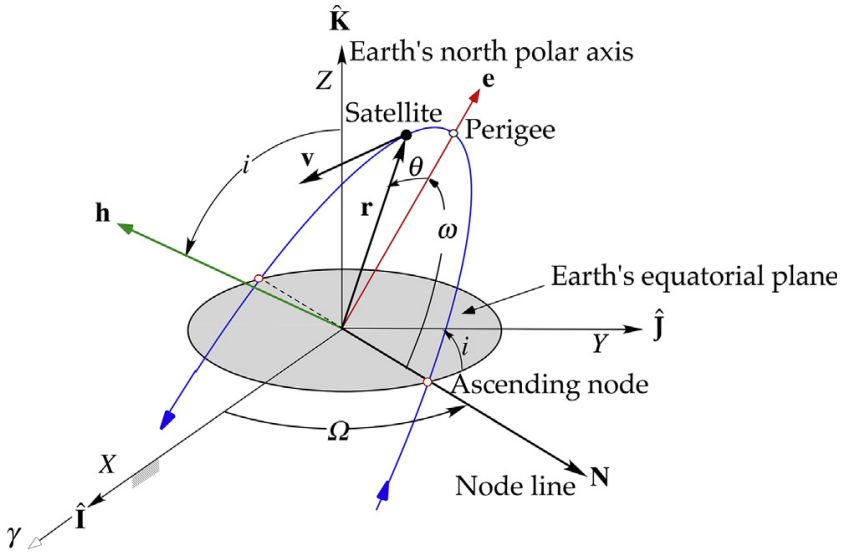

Figure 2.2: Three dimensional geometry of an ellipse. For reference, a geocentric frame is shown. Source: *Orbital mechanics for engineering students - Howard D. Curtis*

The former is called *periapsis* and the latter is called *apoapsis* - or *pericenter* and *apocenter*[3] respectively. The line joining them across the focci is called the *line of apsides* or *line of apses*. Although cyclic, the orbit is "thought to start" at pericenter, a point at which $\theta = 0$. Another important element of the orbit is the line at which the orbital plane intersects the reference horizontal plane. It is called the *line of nodes*. For equatorial orbits, $i = x0$ and such a line is not defined, together with Ω. In this case, the quantity $L = \Omega + \omega$ is used for the location of the pericenter. On the other hand, circular orbits have $e = 0$ and don't have a defined line of apsides or ω. Then, the *argument of latitude* $u = \omega + \theta$ is used instead. For circular, equatorial orbits, where neither ω nor Ω are defined, the *longitude* $l = \Omega + \omega + \theta$ is used.

Two relevant properties of an orbit are its period T and its energy $\mathcal{E}$, both collected in (2.7). Note how both depend solely on the semimajor axis and the primary. It can be seen that smaller orbits "are quicker" than bigger orbits, but also that the bigger the orbit the bigger its energy (note that $\mathcal{E}$ is always negative).

$$T = 2\pi\sqrt{\frac{a^3}{\mu}} \qquad \mathcal{E} = -\frac{\mu}{2a} \tag{2.7}$$

When there exists a dissipative disturbance that drains energy from the orbiter - such as drag or, as will be discussed later, tidal friction - the orbit *decays* and it speeds up - i.e. a and T decrease.

2.1.3. Orbital perturbations: third body forces

Last subsection was devoted to the very idealized two body problem. Although a good approximation in many cases, precise orbits are to be computed using the full dynamics of a system. This means getting rid of the assumptions one by one. Remember that the main assumptions of the two body body problem were:

- Only two bodies in the system.
- Spherical bodies (ergo spherical gravitational fields)
- Non-accelerated central body - due, among others, to the negligible mass of the orbiting body.

The first and third of those assumptions are removed in the same way: by including in the equations of motion the forces of all other bodies that are "close-by" in the form of what is known as *third body perturbations* or *third body forces*. However, one does **not** have to just add them to the orbiting body, but rather include the difference between the orbiting and central bodies. Effectively, this is just adding all

[3]For orbits around Earth, special names *perigee* and *apogee* can be used, while orbits around the Sun accept names *perihelion* and *aphelion*.

fictitious accelerations that appear on the truly non-inertial reference frame attached to the central body. One of these forces will be the force that the orbiting body itself exerts on the central body. Now the question is what the shape of these accelerations is.

Before doing that, and now that more bodies and forces appear in the equations, we will introduce some subscript notation borrowed from Dirkx (2022). Vector $\vec{r}_{AB}$ represents the position of body B with respect to body A (i.e. it is a vector going from A to B). If a body is situated at the origin of the reference frame - and therefore its position vector is $\vec{0}$ - we will allow ourselves to drop the subscript of this body in position vectors expressed with respect to it. For example, if body A is located at the origin, we will write $\vec{r}_B = \vec{r}_{AB}$ to express the position of body B with respect to body A. Similarly, vector $\vec{v}_{AB}$ represents the position of body B with respect to body A and, if body A is at rest in the reference of interest, $\vec{v}_B = \vec{v}_{AB}$. If deemed useful, a comma between the two subscripts might be added without a change in meaning. This logic is somewhat different for accelerations, where acceleration vector $\vec{a}_{AB}$ is not the acceleration of body B with respect to body A, but rather the acceleration that is exerted on body B by body A. In other words, $\vec{a}_{AB}$ is the acceleration that A exerts on B.

Let's now add more bodies to the problem. The shape of the acceleration of a third body C on body B that orbits body A is seen in Eq.(2.8). Note that body A - the central body - sits at the origin and, in this non-inertial reference frame, it is also at rest. The subscript $3B$ on the left hand side indicates that the acceleration is of third-body type. Term ① is the gravitational acceleration that body C exerts on body B, while term ② is the gravitational acceleration that body C exerts on the origin itself. Notice that, in order to evaluate these accelerations, we need $\vec{r}_C$, which requires either integrating it as part of the problem or having a known model for the position of the third body. The latter is usually preferred, and the so-called *ephemerides* are used. These are just a table with the location of the bodies at different points in time.

$$\vec{a}_{CB,3B} = \underbrace{-\frac{\mu_C}{r_{CB}^3}\vec{r}_{CB}}_{①} + \underbrace{\frac{\mu_C}{r_C^3}\vec{r}_C}_{②} = -\mu_C\left(\frac{\vec{r}_{CB}}{r_{CB}^3} - \frac{\vec{r}_C}{r_C^3}\right) \tag{2.8}$$

The question might arise on how applicable this is when introducing the force of the orbiting body itself - body B - on the origin, namely because it would be the case where B and C are the same body and $r_{BC} = 0$. It is a very valid concern and the approach should be somewhat different. For this, we will use Newton's third law, whereby every action has an equal and opposite reaction. More particularly, we will consider that the force that body A - the primary - exerts on body B - the orbiting - can be written as $\vec{F}_{AB} = m_B\vec{a}_{AB}$. This force will be met with a reaction, an opposing force that B will exert on A, given by $\vec{F}_{BA} = m_A\vec{a}_{BA}$, such that $\vec{F}_{BA} = -\vec{F}_{AB}$. Eq.(2.9) shows how this principle leads to an expression for $\vec{a}_{BA}$.

$$\vec{F}_{BA} = -\vec{F}_{AB} \quad \rightarrow \quad m_B\vec{a}_{AB} = -m_A\vec{a}_{BA} \quad \rightarrow \quad \vec{a}_{BA} = -\frac{m_B}{m_A}\vec{a}_{AB} = -\frac{\mu_B}{\mu_A}\vec{a}_{AB} \tag{2.9}$$

Including this term in the equations of motion of the 2BP turns the reference frame attached to A into a non-inertial frame. This acceleration of the reference frame should then be included as a non-inertial acceleration, i.e. *subtracting* it from the acceleration that A exerts on B. This is depicted in Eq.(2.10a). Note that this form is general and does not assume an expression of $\vec{a}_{AB}$. In the case of two spherical bodies, Eq.(2.5) can be used to write $\vec{a}_{AB}$, with $\mu = \mu_A$ and $\vec{r} = \vec{r}_B$. This particularization has been done in Eq.(2.10b).

$$\vec{a}_B = \vec{a}_{AB} - \vec{a}_{BA} = \vec{a}_{AB} + \frac{\mu_B}{\mu_A}\vec{a}_{AB} \quad \rightarrow \quad \vec{a}_B = \left(1 + \frac{\mu_B}{\mu_A}\right)\vec{a}_{AB} \tag{2.10a}$$

$$\vec{a}_B = -(\mu_A + \mu_B)\frac{\vec{r}_B}{r_B^3} \tag{2.10b}$$

Putting everything together, we can write the equations of motion of the orbiting body B around central body A in a non-inertial frame attached to A which is subjected to the accelerations of body B itself and any number N of *third bodies*. This is seen in Eq.(2.11).

$$\vec{a}_B = -(\mu_A + \mu_B)\frac{\vec{r}_B}{r_B^3} - \sum_{i=1}^{N} \mu_i \left(\frac{\vec{r}_{iB}}{r_{iB}^3} - \frac{\vec{r}_i}{r_i^3} \right) \tag{2.11}$$

Up to this point, and referring back to the three assumptions listed at the beginning of this subsection, we have been able to remove the first and last of them. The second one, due to the relevance it has in the topic at hand, will be treated separately and on its own in the next subsection. Other minor perturbations that are common for Earth orbiters, like atmospheric drag and solar radiation pressure, play little to no role in the Mars-Phobos dynamics that we will study here.

2.1.4. Useful reference frame definitions

We will finish this section by defining different reference frames and coordinate system that will become necessary later on.

We will begin talking about the quintessential inertial frame: the *Body Centered Inertial (BCI)*. As its name indicates, this is an inertial frame used to study the motion of objects around a celestial body and is centered at the body's center of mass. The Z axis of this frame is aligned with the rotation axis of the body and the X axis points to a reference direction in distant space, more specifically the direction known as *the first point of aries*, which coincides with the more common *Vernal equinox* for the Earth. The Y axis completes the right handed triad. An important aspect of the BCI frame is that, if the spin axes of two bodies A and B are (quasi-)parallel - which is often the case in planet-satellite systems - the BCI bases of both bodies are parallel, and a vector given in BCI components of body A is also given in BCI components of body B.

A natural second to the previous frame is the *Body Centered Body Fixed (BCBF)* reference frame, which we will also call *body-fixed frame* in this text indistinctly. This frame is concentric with the BCI frame and shares its same Z axis. However, the BCBF frame rotates around its Z together with the rotation of the body. Thus, the direction of the X axis is not referred to distant space anymore, but rather an equatorial point on the body is selected to be this reference direction. Note that the BCBF frame is not inertial.

The BCBF is particularly popular among bodies with a near-spherical shape, like planets and big moons such as our own or the Jovian moons. For bodies that are far from being spherical, the body frame is used as substitute (see Sec. 2.1.1). In this frame, the x, y and z axes correspond to the principal axes of inertia, which are chosen such that $I_x \leq I_y \leq I_z$. In both cases, the XY plane is usually referred to as the equatorial plane. In this text we will use the BCBF or body-body-fixed frames for both Mars and Phobos, the same way it is done by Rambaux et al. (2012).

The transformation between the BCI and BCBF frames is given by a general rotation matrix $\boldsymbol{R}^{\mathcal{B}/\mathcal{I}}$, that converts vectors written in BCI to vectors written in body-fixed frame. The inverse of this transformation is given by the rotation matrix $\boldsymbol{R}^{\mathcal{I}/\mathcal{B}} = (\boldsymbol{R}^{\mathcal{B}/\mathcal{I}})^{-1} = (\boldsymbol{R}^{\mathcal{B}/\mathcal{I}})^T$. For convenience, the vector basis attached to a body will be denoted by the body identifier itself, namely $\mathcal{P}$ for Phobos and $\mathcal{M}$ for Mars.

Another popular vector basis is the so-called *RTN* frame. It is most frequently centered at an orbiter around the primary - although placing the origin at the center of the primary is sometimes useful - and is composed of the right-handed triad $\{\hat{r}, \hat{t}, \hat{n}\}$. Vector $\hat{r}$ points in the direction of the position vector (i.e. from the center of mass of the primary to the orbiter), vector $\hat{n}$ points in the direction direction of the angular momentum of the body and $\hat{t}$ completes the triad.

Other reference frames that are secondary to the work at hand are the *J200* and *ICRF* reference frames - the latter stands for *International Celestial Reference Frame*. Definitions will not be given here, but the reader is referred to Ma et al. (1998) for a comprehensive explanation of the ICRF and to Sec. 2 by Archinal et al. (2018) for the relationship between the two frames.

2.2. Full 2 body problem and spherical harmonics

This section will focus solely on the dynamics of extended, non-spherical bodies. When two of these bodies are used in the 2BP, the new scenario is usually called *full 2BP* (F2BP). The force between them is not equivalent anymore to the force between to point particles and the dynamics are quite different. These dynamics will now be the sum of different accelerations, which luckily obey the principle of superposition. In other words, the complicated dynamics of the F2BP can be decomposed is different terms, some of which are simpler. We will dissect the F2BP in its different components and we will later give mathematical expressions for these terms.

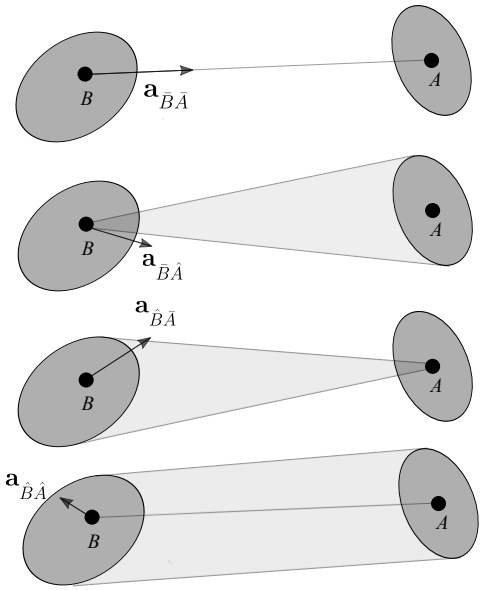

Figure 2.3: The different terms of the F2BP. Source: *Tudat mathematical model definition* - Dirkx (2022)

2.2.1. Anatomy of the F2BP

The 4 terms of the F2BP are depicted in Fig.[2.3], taken from Dirkx (2022). In words, these are:

- The acceleration of the center of mass of body A on the center of mass of body B. This is the classical 2BP term from Eq.(2.5).
- The acceleration of the rest of body A on the center of mass of body B. This is a new term.
- The acceleration of the center of mass of body A on the rest of body B.
- The acceleration of the rest of body A on the rest of body B.

We can immediately see a pattern: "point-on-point", "volume-on-point", "point-on-volume" and "volume-on-volume". The "volume" of the body is usually termed its "extended body", "dynamic figure" or just "figure", terminology that we will use indistinctly in this text. Terms related to the center of mass of a body will be indicated with a bar over the body subscript, while terms related to the figure of a body will be indicated with a hat over the body subscript, just as done by Dirkx (2022). For instance, the acceleration that the center of mass of A exerts on the center of mass of B will be indicated as $\vec{a}_{\bar{A}\bar{B}}$.

Note that we are only considering accelerations that body A exerts on body B. If we were to only include these terms in the equations of motion, we would be considering A to be an inertial frame. This fact can be easily corrected for using Eq.(2.10a). The only difference is that, now, $\vec{a}_{AB}$ will be composed by all the terms listed above, namely Eq.(2.12).

$$\vec{a}_{AB} = \vec{a}_{\bar{A}\bar{B}} + \vec{a}_{\hat{A}\bar{B}} + \vec{a}_{\bar{A}\hat{B}} + \vec{a}_{\hat{A}\hat{B}} \tag{2.12}$$

As we will see, there exist tools to write $\vec{a}_{A\bar{B}} = \vec{a}_{\bar{A}\bar{B}} + \vec{a}_{\hat{A}\bar{B}}$ in a direct manner, but not to write $\vec{a}_{\bar{A}\hat{B}}$ and much less to write $\vec{a}_{\hat{A}\hat{B}}$. The latter is highly non-trivial, and we will ignore it for now. We will focus on the former. The fact that there exists a way to write $\vec{a}_{\hat{A}\bar{B}}$ means that there is also a way to write $\vec{a}_{\hat{B}\bar{A}}$. We can then apply Newton's third law of action and reaction to obtain a relationship between the two accelerations by means of the masses of the two bodies, the same way as we did in (2.9). This process is outlined in (2.13).

$$\vec{F}_{\bar{A}\hat{B}} = -\vec{F}_{\hat{B}\bar{A}} \quad \rightarrow \quad m_B\vec{a}_{\bar{A}\hat{B}} = m_A\vec{a}_{\hat{B}\bar{A}} \quad \rightarrow \quad \vec{a}_{\bar{A}\hat{B}} = -\frac{m_A}{m_B}a_{\hat{B}\bar{A}} = -\frac{\mu_A}{\mu_B}a_{\hat{B}\bar{A}} \tag{2.13}$$

Plugging Eq.(2.13) into Eq.(2.12), dropping $\vec{a}_{\hat{A}\hat{B}}$ and further plugging that into Eq.(2.10a) yields Eq.(2.14) after simplification.

$$\vec{a}_B = \left(1 + \frac{\mu_B}{\mu_A}\right)(\vec{a}_{\bar{A}\bar{B}} + \vec{a}_{\hat{A}\bar{B}}) - \left(1 + \frac{\mu_A}{\mu_B}\right)\vec{a}_{\hat{B}\bar{A}} \tag{2.14}$$

We are only left with two types of accelerations: that exerted by the center of mass of a body onto the center of mass of another body, and that exerted by the figure of a body onto the center of mass of another body. We already have an expression for the first - Newton's law of gravitation. Now we need an expression of the second. The next subsection will be devoted to finding such an expression.

To finalize this subsection, we will justify the decision of dropping the $\vec{a}_{\hat{A}\hat{B}}$ term, that will hold for the remainder of this text and the subsequent thesis. There are two dynamics we are interested in: translation and rotation. The effect of the figure-figure term on the former was shown to be small by Dirkx et al. (2019). More specifically, it is said in the source that the strongest figure-figure effects are about 0.5% as relevant as the weakest figure-point effects. On the rotation side of the dynamics, it was shown by Rambaux et al. (2012) that figure-figure effects are below 0.01% of the main point-figure term. Changes on libration amplitudes (see Sec. 2.2.3) are of the order of 10^{-3} degrees.

2.2.2. Describing the gravitational field of an extended body

Gravity fields without spherical symmetry can be represented in many ways. Before dwelling in how we will do it, we will explicitly state some implications of working with non-spherical gravity fields. It is important to realize that, when asymmetries are introduced in the gravity field of a body, their descriptions will necessarily be coordinate-dependent. This means that (1) a coordinate system, with its vector basis and probably a reference frame attached to it, becomes absolutely necessary and (2) different coordinate systems will inevitably yield different descriptions of the same (physically identical) gravity field.

In this text, we will use the widest-spread description of gravity fields in astrodynamics, the so-called *spherical harmonics expansion* (Battin, 1999). This description makes use of a vector basis and frame attached to the moving body, such as the BCBF, and the associated geographical coordinates to describe the gravitational *potential* U of the attracting body as an infinite series. The subsequent gravitational field follows from the definition of this potential, whereby $\vec{g} = \nabla U$. The potential generated by a body A is given in this expansion form in Eq.(2.15). Notice that, in order for this infinite series to converge to an actual function, this potential can only be defined for $r > R$.

$$U_A(r,\theta,\phi) = \sum_{l=0}^{\infty}\sum_{m=0}^{l} U_{A,l,m}(r,\theta,\phi) \tag{2.15a}$$

$$U_{A,l,m}(r,\theta,\phi) = \frac{\mu_A}{r}\left(\frac{R}{r}\right)^l P_{l,m}(\sin\phi)\big(C_{l,m}\cos(m\theta) + S_{l,m}\sin(m\theta)\big) \tag{2.15b}$$

Indices l and m are usually termed *degree* and *order* respectively, and R is the reference radius of the body. The term $P_{l,m}$ represents the so called *associated Legendre functions* (Battin, 1999) of degree l and order m, which are commonly known as *Legendre polynomials* in astrodynamics. These are given in Eq.(2.16) for an argument x.

$$P_{l,m}(x) = \frac{(1-x^2)^{m/2}}{(-2)^l\, l!}\frac{d^{l+m}}{dx^{l+m}}(1-x^2)^l \tag{2.16}$$

The terms $C_{l,m}$ and $S_{l,m}$ are the *spherical harmonics coefficients* and are what gives the gravity field its shape. A gravity field an be fully described by a set of $C_{l,m}$ and $S_{l,m}$ through Eq.(2.15). Its values for a given gravity field are usually empirically obtained through their estimation from orbit determination processes. The harmonic coefficients are often given in one of their (many) normalized versions. In this text, we will use the *full normalization* if any. This normalization brings along a normalization of the Legendre polynomials as well, such that the normalized $\bar{C}_{l,m}$, $\bar{S}_{l,m}$ and $\bar{P}_{l,m}(x)$ satisfy $\bar{P}_{l,m}\bar{C}_{l,m} = P_{l,m}C_{l,m}$ and $\bar{P}_{l,m}\bar{S}_{l,m} = P_{l,m}S_{l,m}$. A normalization constant $N_{l,m}$ is defined and acts inversely on the Legendre polynomials, i.e. Eq.(2.17a) and Eq.(2.17b). In this (full) normalization, $\bar{N}_{l,m}$ is defined as in Eq.(2.17c). Here, $\delta_{0,m}$ is the Kronecker delta, meaning that $\delta_{0,m} = 1$ if $m = 0$ and $\delta_{0,m} = 0$ otherwise.

$$\bar{P}_{l,m} = \bar{N}_{l,m}P_{l,m} \qquad \text{(multiplication)} \tag{2.17a}$$

$$\bar{C}_{l,m} = \frac{C_{l,m}}{\bar{N}_{l,m}} \quad \text{and} \quad \bar{S}_{l,m} = \frac{S_{l,m}}{\bar{N}_{l,m}} \qquad \text{(division)} \tag{2.17b}$$

$$\bar{N}_{l,m} = \sqrt{\frac{(2-\delta_{0,m})(2l+1)(l-m)!}{(l+m)!}} \tag{2.17c}$$

As we said, the harmonic coefficients $C_{l,m}$ and $S_{l,m}$ describe the shape of the gravity field of a body, which is dependent, among other things, on the shape of the body itself. Deformable bodies will therefore have time-dependent coefficients associated to them. It should be the time to address whether we will consider Phobos to be a deformable body based on the impact that such a consideration will have on its dynamics. Luckily, it was shown by Yang et al. (2020) that the deformation of Phobos - represented by the k_2 parameter - has a negligible effect on its rotation. Deformation changed libration amplitudes (see Sec. 3.1) only in the order of 10^{-4} degrees (in the case of longitudinal librations) and 10^{-6} degrees (in the case of other librations). Therefore, we can treat Phobos as a rigid body and consider its harmonic coefficients to be constant.

If one wanted to use this potential in real life, they would run into problems. As it so happens, infinite series are not practical in engineering and they have to be truncated for real application. Thus, a maximum degree and order $l_{\max}$ and $m_{\max}$ are set and only terms up to that term are included. The expression we will use in practice is then that of Eq.(2.18), where $m^* = \min(l, m_{\max})$. This is further justified by the fact that, for $r > R$, the $(R/r)^l$ term decays very quickly with increasing l.

$$U_A(r,\theta,\phi) = \sum_{l=0}^{l_{\max}} \sum_{m=0}^{m^*} U_{A,l,m}(r,\theta,\phi) \tag{2.18}$$

If we look closer and we do the numbers, we can see that the potential of degree and order 0 corresponds to the potential of the point particle, namely Eq.(2.19), where $C_{0,0} = 1$ by definition.

$$U_{A,0,0} = \bar{C}_{0,0}\frac{\mu_A}{r} \tag{2.19}$$

Referring to Eq.(2.12), this term of degree 0 corresponds to $\vec{a}_{\bar{A}\bar{B}}$ if body B is immersed in this gravity field of body A, while all other terms of degree $l \geq 1$ are included in the term $\vec{a}_{\bar{A}\bar{B}}$.

Another point of interest is that all terms of order 0 (i.e. $m = 0$) have $\sin(m\theta) = 0$. In these terms, $S_{l,m}$ doesn't play any role, and therefore it is convention to set them to 0: $S_{l,0} = 0$.

As mentioned earlier, one should now compute the gravitational field as $\vec{g} = \nabla U$. There is a subtlety in this gradient. No matter how we write it - spherical or Cartesian coordinates - the potential in Eq.(2.15a) and Eq.(2.15b) is a function of the position vector from the center of mass of the source and to a point in space *given in body fixed frame*. If we call this vector $\vec{\rho}$, we can definitely write $U(\vec{\rho})$. The gradient, however, is by definition the derivative with respect to a vector in the inertial frame, namely $\vec{r}$. The relationship between $\vec{r}$ and $\vec{\rho}$ is given by $\vec{r} = \boldsymbol{R}^{\mathcal{I}/\mathcal{B}}\vec{\rho}$ or, conversely, $\vec{\rho} = \boldsymbol{R}^{\mathcal{B}/\mathcal{I}}\vec{r}$. The required gradient, call it $\nabla_{\mathcal{I}}U$, is related to the gradient in body fixed, call it $\nabla_{\mathcal{B}}U$ as in Eq.(2.20).

$$\nabla_{\mathcal{I}}U = \left(\frac{\partial U}{\partial \vec{r}}\right)^T = \left(\frac{\partial U}{\partial \vec{\rho}}\frac{\partial \vec{\rho}}{\partial \vec{r}}\right)^T = \left(\frac{\partial U}{\partial \vec{\rho}}\boldsymbol{R}^{\mathcal{B}/\mathcal{I}}\right)^T = \boldsymbol{R}^{\mathcal{I}/\mathcal{B}}\nabla_{\mathcal{B}}U \tag{2.20}$$

To wrap up the potential expansion we have developed so far, we will collect these procedures and write the dynamics of a body B around a central body A in an F2BP. This is written in Eq.(2.21), where $\boldsymbol{R}^{\mathcal{I}/\mathcal{A}}$ denotes the rotation matrix from $BCBF$ of body A to BCI - and similarly for B. Notice that, whenever $l_{\max} \geq 1$ for one of the bodies, a rotation model of that body becomes necessary in order to evaluate $\nabla_{\mathcal{B}}U$ and $\boldsymbol{R}^{\mathcal{I}/\mathcal{B}}$.

$$\vec{a}_B = (\mu_A + \mu_B)\left(-\frac{\vec{r}_{AB}}{|\vec{r}_{AB}|^3} + \frac{1}{\mu_A}\sum_{l=1}^{l_{\max,A}}\sum_{m=0}^{m^*_A}\boldsymbol{R}^{\mathcal{I}/\mathcal{A}}\nabla_{\mathcal{A}}U_{A,l,m} - \frac{1}{\mu_B}\sum_{l=1}^{l_{\max,B}}\sum_{m=0}^{m^*_B}\boldsymbol{R}^{\mathcal{I}/\mathcal{B}}\nabla_{\mathcal{B}}U_{B,l,m}\right) \tag{2.21}$$

To finalize this subsection, we will go over some common lingo that will likely come up in this (and future) works. This lingo arises from the properties of the spherical harmonic functions, which are visually represented in Fig.[2.4], taken from Chung et al. (2008). We can see that the harmonics of order 0 ($m = 0$) look like rings of constant longitude (the spheres are "lying on their side", with the North Pole where the concentric red circles are located). These harmonics are often called *zonal* harmonics. On the

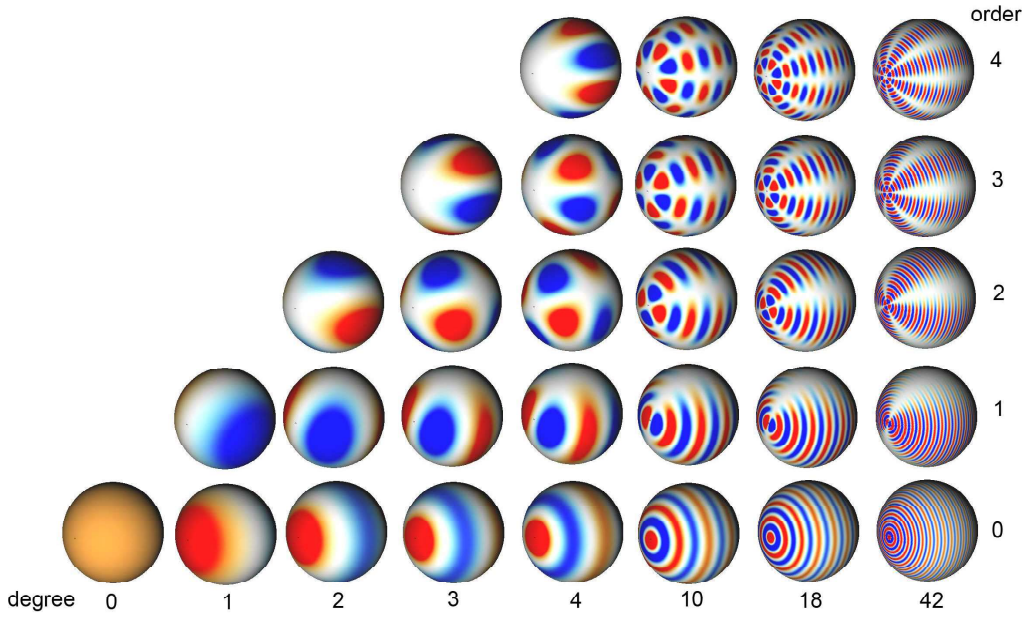

Figure 2.4: Visual representation of different degree (l) and order (m) potential harmonic functions. Only the angle-dependant part has been depicted. Source: Chung et al. (2008)

other hand, harmonics with $m = l$ look like sections in an orange and are sometimes called *sectorial* harmonics. All other harmonics are usually referred to as *tesseral* harmonics. It is often the case that the most important harmonics are those with $(l, m) = (2, 0)$ and $(l, m) = (2, 2)$ together. This combination of coefficients is often known as *quadrupole* (quadrupole gravity field, quadrupole potential, ...). For most big bodies that can be modelled as ellipsoids - like planets - the most important harmonics are the zonal ones. Such is the case that they have been given a particular name, namely J_l, such that $J_l = C_{l,0}$. The most common of them is the J_2 term, often times termed the *oblateness* (of the Earth, Mars, ...). It is noted in page 528 of Wakker (2015) that there exists in convention to use a negative sign in the definition of J_l, so that $J_l = -C_{l,0}$, arising from the fact that $C_{l,0}$ is always negative and there is a tendency to like positive numbers better. However, it is not universal and may create some confusion. Therefore, this text will avoid using J_l and will stick to $C_{l,0}$.

2.2.3. Rotational dynamics of the F2BP

As of now, the 2BP only concerned translation, while the dynamics of the F2BP were seen to involve the orientation of the bodies. This means that, in order for us to have a useful formulation of Newton's laws of motion in the F2BP, a model for this orientation becomes necessary. Usually, this is done by assuming that the translational dynamics and the rotational dynamics are uncoupled. This is not to say that forces are not dependent on attitude, but rather that the accelerations in Eq.(2.21) do not modify the rotational states of the two bodies. This way, an orientation model can be used without worries that it will become invalid at some point. This is fair play in most cases. The very point of this thesis is that, for the Mars-Phobos case, it is not, and all the terms in Eq.(2.21) will affect the orientation of, potentially, both bodies. In truth, given the size of Mars, only Phobos' orientation is affected. This subsection will focus on formulating the rotational dynamics caused by the accelerations of Eq.(2.21) on Phobos.

As mentioned in Sec. 2.1.1, the rotational equations of motion are expressed in a body-fixed frame and are given by Eq.(2.4). This equation involves $\vec{T} = \vec{r}_a \times \vec{F}$. There is one thing we can immediately see: if $\vec{r}_a = \vec{0}$, then $\vec{T} = 0$ as well, meaning that those forces that act on the center of mass of the body will not affect its orientation. If we take a look at Eq.(2.21), we can see that two out of the three terms happen to act on Phobos' center of mass, namely $\vec{a}_{\bar{A}\bar{B}}$ and $\vec{a}_{\hat{A}\bar{B}}$. These will not impact its rotation and therefore will play no role in this subsection, so we can focus on $\vec{a}_{\hat{B}\bar{A}}$ alone. Physically, this is an acceleration that the center of mass of Mars exerts on the extended body of Phobos. The torque created on Phobos by this acceleration, call it $\vec{T}_{\bar{A}\hat{B}}$, is mathematically given by Eq.(2.22) (see App. A). In this equation, M is the mass of Mars, $\vec{r}$ is the position vector from Phobos' center of mass to that of Mars, and U_{P} is the

potential of Phobos. Its gradient should be evaluated in a consistent manner: at the position of Mars in Phobos' body-fixed frame.

$$\vec{T}_{\hat{A}\hat{B}} = -M\vec{r} \times \nabla_I U_P = -M\vec{r} \times (\boldsymbol{R}^{\mathcal{I}/\mathcal{P}} \nabla_{\mathcal{P}} U_P) \tag{2.22}$$

Although brief, that is really the full analysis of all the torques that are exerted on Phobos. One could consider torques exerted by other bodies. However, notice that the central term - degree 0 - of ∇U_P evaluated at the location of those bodies is negligibly small. Remember that additional torques might have been included if the term $\vec{a}_{\hat{A}\hat{B}}$ from Eq.(2.12) had been preserved, but these torques were deemed to have negligible effects (see Sec. 2.2.1 and Rambaux et al. (2012)). This torque in Eq.(2.22) could now be entered in Eq.(2.4) and integrated for $\vec{\omega}$ and the orientation of Phobos. Note the dependency of this torque on the position of Phobos $-\vec{r}$ as well as its orientation $\boldsymbol{R}^{\mathcal{I}/\mathcal{P}}$.

2.2.4. Harmonic coefficients and moments of inertia

Since it will be necessary for future chapters, we will see the relationship between the degree-two harmonic coefficients and the elements of the inertia tensor. Both describe, in their own way, the mass distribution of a body, so it is intuitive that they are related in some way. We will not give proof of derivation to the equations and relationships presented here, because they would entail manipulations of volume integrals and would not offer any insight to the problem. Rather, we will just present the equations that have been gathered from Dirkx et al. (2019) (Eq.(105) in the source), Lainey et al. (2019) (Eq.(7) and Eq.(18) in the source) and Le Maistre et al. (2019) (Eq.(4) in the source).

The relationships between the six moments of inertia and the five unnormalized degree-two harmonic coefficients is given in Eq.(2.23). In this equation, I is the mean moment of inertia of a sphere of mass M and radius R, $I = \frac{2}{5}MR^2$.

$$\begin{bmatrix} I_{xx} \\ I_{yy} \\ I_{zz} \\ I_{xy} \\ I_{xz} \\ I_{yz} \end{bmatrix} = MR^2 \begin{bmatrix} 1/3 & 0 & 0 & -2 & 0 \\ 1/3 & 0 & 0 & 2 & 0 \\ -2/3 & 0 & 0 & 0 & 0 \\ 0 & 0 & 0 & 0 & -2 \\ 0 & -1 & 0 & 0 & 0 \\ 0 & 0 & -1 & 0 & 0 \end{bmatrix} \begin{bmatrix} C_{2,0} \\ C_{2,1} \\ S_{2,1} \\ C_{2,2} \\ S_{2,2} \end{bmatrix} + I \begin{bmatrix} 1 \\ 1 \\ 1 \\ 0 \\ 0 \\ 0 \end{bmatrix} \tag{2.23}$$

This relationship between the moment of inertia and the harmonic coefficients holds regardless of the vector basis or reference frame in which they are expressed. Thus, one is allowed to freely choose said vector basis. A convenient choice of frame is the body-fixed frame (see Sec. 2.1.4). By definition, this frame satisfies $I_{xy} = I_{xz} = I_{yz} = 0$. This automatically implies that $C_{2,1} = S_{2,1} = S_{2,2} = 0$. Removing these terms and equations from the system in Eq.(2.23) and replacing I_{xx}, I_{yy}, I_{zz} for the most common names A, B, and C respectively yields Eq.(2.24). Remember that, by convention, $A \leq B \leq C$ (see Sec. 2.1.4).

$$\begin{bmatrix} A \\ B \\ C \end{bmatrix} = MR^2 \begin{bmatrix} 1/3 & -2 \\ 1/3 & 2 \\ -2/3 & 0 \end{bmatrix} \begin{bmatrix} C_{2,0} \\ C_{2,2} \end{bmatrix} + I \begin{bmatrix} 1 \\ 1 \\ 1 \end{bmatrix} \tag{2.24}$$

These equations indicate that changes in the harmonic coefficients of Phobos will propagate into changes in its inertia matrix. Therefore not only $\nabla_{\mathcal{P}} U_P$ in Eq.(2.22) but also $\vec{L} = \boldsymbol{I}\vec{\omega}$ in Eq.(2.4) will change.

2.3. Variational equations

Last section covered the forces, accelerations and torques that exist in the context of the F2BP. These should then go into Eq.(2.2) and Eq.(2.4) to form the so-called *equations of motion (EOMs)* and the state vector of the body is integrated for. From a mathematical perspective, this state vector can be regarded as a dynamical system that is governed by a *dynamical model*, namely the equations of motion. This dynamical model will be determined by a number of parameters - in the case of Phobos' motion around Mars, one of this parameters is, for example, Mars' gravitational parameter. It will be beneficial for the rest of the section - and future chapters - if we write this *dynamical problem* in a general sense.

Consider a state vector with n_s dynamical variables $\vec{x} \in \mathbb{R}^{n_s}$, which is governed by a dynamical model $\vec{f} \in \mathbb{R}^{n_s}$. This dynamical model is determined by a number n_p of parameters, that can be gathered in a parameter vector $\vec{p} \in \mathbb{R}^{n_p}$. If we provide an initial state $\vec{x}_o \in \mathbb{R}^{n_s}$, then the evolution of $\vec{x}$ will be uniquely defined by this initial state, the shape of $\vec{f}$ and the model parameters $\vec{p}$. In mathematical terms, this is written as in Eq.(2.25), where t is the independent variable - usually time.

$$\dot{\vec{x}} = \vec{f}(\vec{x}, \vec{p}, t) \qquad \text{with} \quad \vec{x}(t=0) = \vec{x}_o \quad \text{and} \quad \vec{x} = \vec{x}(\vec{x}_o, \vec{p}, t) \tag{2.25}$$

As we can see, for a given model $\vec{f}$, there are some "knobs" that we can tweak to change the solution, namely the parameters $\vec{p}$ and the initial state $\vec{x}_o$. One may now ask the question of what happens when this knobs are turned. A straight-forward answer would be to change them and run the simulation again. While that is a perfectly valid answer, there is great insight in a more analytical approach. Sometimes, there is even the necessity for it. On the one hand, one might not want to blindly change the knobs, but rather look for those that are most useful to turn. In other words, the aim is to find what elements the solution is most sensitive to. Or, even, what *parts* of the solution are most sensitive to what elements, and in which way. Other times, such an analysis is required because the values that the knobs should be turned to are unknown. Imagine, for example, that we are unsure of what the value of Phobos' $C_{2,0}$ is, and we would like to find out how this uncertainty affects our solution. How different does $C_{2,0}$ have to be in order for our solution to go out of admissible margins - whatever those are? We can definitely start trying out values of $C_{2,0}$ and we can run up to 10 or 1000 simulations with different values, depending on how good our intuition is about the relationship between $C_{2,0}$ and $\vec{x}(t, C_{2,0})$. And now we need to do that for all, say, 20 parameters in our model. Given the time and resources, we can definitely run a million simulations and investigate the subsequent ocean of numbers. We have used a model parameter as an example, but uncertainties exist as well for the initial state. We may think that the system starts somewhere, but in fact it starts "2m more to one side". Now, is that enough to change our solution completely? Is it fine if our initial state is off by 30km also, or is that too much already? All these questions could be answered by running simulations nonstop, and maybe extracting the information in some years from now. Luckily, there is a smarter way of finding these answers, and such a technique is the focus of this section.

The question to be answered quantitatively is, simply put, how changes in $\vec{x}_o$ or $\vec{p}$ translate into changes in $\vec{x}$. In mathematics, this is the same as asking for the *partial derivatives* of $\vec{x}$ with respect to $\vec{x}_o$ and $\vec{p}$, written out in Eq.(2.26). Given that $\vec{x}$ changes with time, it is only natural to think that these partials are themselves functions of time. In the most general case, these partials are matrices, and have particular names: they are the *state transition matrix (STM)*, $\boldsymbol{\Phi}$ and the *sensitivity matrix*, $\boldsymbol{S}$. It is important to keep in mind that they are functions of time.

$$\frac{\partial \vec{x}}{\partial \vec{x}_o} = \boldsymbol{\Phi} \in \mathbb{R}^{n_s \times n_s} \qquad \frac{\partial \vec{x}}{\partial \vec{p}} = \boldsymbol{S} \in \mathbb{R}^{n_s \times n_p} \tag{2.26}$$

Closed expressions for $\boldsymbol{\Phi}(t)$ and $\boldsymbol{S}(t)$ do not exist - in principle - but rather they are given in differential equations, the so-called *variational equations*, developed in Eq.(2.27). Note the remarks in Eq.(2.27c). These variational equations are usually propagated together with the equations of motion themselves.

$$\frac{d\boldsymbol{\Phi}}{dt} = \frac{d}{dt}\frac{\partial \vec{x}}{\partial \vec{x}_o} = \frac{\partial}{\partial \vec{x}_o}\frac{d\vec{x}}{dt} = \frac{\partial \vec{f}}{\partial \vec{x}_o} = \frac{\partial \vec{f}}{\partial \vec{x}}\frac{\partial \vec{x}}{\partial \vec{x}_o} \quad \Longrightarrow \quad \dot{\boldsymbol{\Phi}} = \boldsymbol{D}\boldsymbol{\Phi} \tag{2.27a}$$

$$\frac{d\boldsymbol{S}}{dt} = \frac{d}{dt}\frac{\partial \vec{x}}{\partial \vec{p}} = \frac{\partial}{\partial \vec{p}}\frac{d\vec{x}}{dt} = \frac{\partial \vec{f}}{\partial \vec{p}} = \frac{\partial \vec{f}}{\partial \vec{x}}\frac{\partial \vec{x}}{\partial \vec{p}} + \frac{\partial \vec{f}}{\partial \vec{p}} \quad \Longrightarrow \quad \dot{\boldsymbol{S}} = \boldsymbol{D}\boldsymbol{S} + \boldsymbol{\Pi} \tag{2.27b}$$

$$\boldsymbol{\Phi} \in \mathbb{R}^{n_s \times n_s} \qquad \boldsymbol{S} \in \mathbb{R}^{n_s \times n_p} \qquad \boldsymbol{D} = \frac{\partial \vec{f}}{\partial \vec{x}} \in \mathbb{R}^{n_s \times n_s} \qquad \boldsymbol{\Pi} = \frac{\partial \vec{f}}{\partial \vec{p}} \in \mathbb{R}^{n_s \times n_p} \tag{2.27c}$$

As any other differential equation, the variational equations need initial conditions to be integrated. By definition, the initial condition for the STM needs to meet $\Delta\vec{x}_o = \boldsymbol{\Phi}_o \Delta\vec{x}_o$, so that $\boldsymbol{\Phi}_o = \boldsymbol{I}_{n_s \times n_s}$. On the other hand, the sensitivity matrix needs to meet $\Delta\vec{x}_o = \boldsymbol{S}_o \Delta\vec{p}$. If initial conditions are not changed, then the only way is that $\boldsymbol{S}_o = \boldsymbol{0}_{n_s \times n_p}$. Note that $\boldsymbol{\Phi}$ and $\boldsymbol{S}$ are also the coefficients of the first-order

Taylor expansions in Eq.(2.28). If $\Delta\vec{x}_o$ and $\Delta\vec{p}$ are not "too big" - whatever that means in the context at hand - the state transition and sensitivity matrices offer linear mappings between increments in initial conditions or state parameters and increments in the state vector at any later point in time. Remember that these increments are only valid for a reference trajectory.

$$\vec{x} = \vec{x}_{\text{ref}} + \left.\frac{\partial\vec{x}}{\partial\vec{x}_o}\right|_{\vec{x}_o=\vec{x}_{o,\text{ref}}} (\vec{x}_o - \vec{x}_{o,\text{ref}}) \quad \Longrightarrow \quad \Delta\vec{x} = \boldsymbol{\Phi}\Delta\vec{x}_o \tag{2.28a}$$

$$\vec{x} = \vec{x}_{\text{ref}} + \left.\frac{\partial\vec{x}}{\partial\vec{p}}\right|_{\vec{p}=\vec{p}_{\text{ref}}} (\vec{p} - \vec{p}_{\text{ref}}) \quad \Longrightarrow \quad \Delta\vec{x} = \boldsymbol{S}\Delta\vec{p} \tag{2.28b}$$

These matrices offer the possibility to answer all questions above at the cost of integrating an extra $n_s(n_s + n_p)$ variables together with the n_s entries of the state vector itself.

Their use goes beyond answering these questions and into the realm of the estimation problem, as will be seen in Ch. 4.

2.4. Describing Phobos' motion

This section will gather everything that was covered in the last two section, put it together, and particularize it for Phobos. The result will be a description of Phobos' state vector, its equations of motion and its variational equations.

2.4.1. The state vector

We will begin by defining Phobos' state vector. In this work, we are considering Phobos to be a rigid body that both translates and rotates. Therefore, the state vector will contain both its translational state - position $\vec{r}$ and velocity $\vec{v}$ - and its rotational state - by analogy, its orientation and angular velocity $\vec{\omega}$. Finding an efficient and singularity-free description of the orientation of a body is a problem that has troubled a lot of people for a long time. Luckily, Fukushima (2008) came close to an answer and suggests that the best way is to use quaternions (see App. C). Thus, the orientation of Phobos will be determined by quaternion $\boldsymbol{q}$. The state vector is written out in Eq.(2.29). Note the dimensions.

$$\vec{x} = \begin{bmatrix} \vec{r} \\ \vec{v} \\ \boldsymbol{q} \\ \vec{\omega} \end{bmatrix} \in \mathbb{R}^{13} \tag{2.29}$$

2.4.2. The equations of motion

The next step is to write the derivative of this state vector. It is straightforward that $\dot{\vec{r}} = \vec{v}$. The question now arises of how to write $\dot{\boldsymbol{q}}$. Luckily, the two forms that such a derivative accepts are given in Eq.(58-59) of Dirkx et al. (2019). They can be found here in Eq.(2.30). For convenience, we use the same notation as in the source. Note that $\boldsymbol{\Omega} \in \mathbb{R}^{4\times4}$ while $\boldsymbol{Q} \in \mathbb{R}^{4\times3}$.

$$\dot{\boldsymbol{q}} = \boldsymbol{\Omega}\boldsymbol{q} = \boldsymbol{Q}\vec{\omega} \qquad \text{with:}$$

$$\boldsymbol{\Omega} = \frac{1}{2}\begin{bmatrix} 0 & -\omega_1 & -\omega_2 & -\omega_3 \\ \omega_1 & 0 & \omega_3 & -\omega_2 \\ \omega_2 & -\omega_3 & 0 & \omega_1 \\ \omega_3 & \omega_2 & -\omega_1 & 0 \end{bmatrix} \qquad \boldsymbol{Q} = \frac{1}{2}\begin{bmatrix} -q_0 & -q_2 & -q_3 \\ q_0 & -q_3 & q_2 \\ q_3 & q_0 & -q_1 \\ -q_2 & q_1 & q_0 \end{bmatrix} \tag{2.30}$$

We now need to find $\dot{\vec{v}}$ and $\dot{\vec{\omega}}$. These can be extracted from Newton's laws of motion, namely Eq.(2.2) and Eq.(2.4). To gather them here, we will change the notation slightly. First, the term $\vec{F}/m$ in Eq.(2.2) will be called $\vec{a}$. Secondly, we will express $\vec{L}$ as $\boldsymbol{I}\vec{\omega}$ in Eq.(2.4). Note that, since Eq.(2.4) is written in a body fixed frame in which $\boldsymbol{I}$ is constant, we can take it out of the derivative, namely $\dot{\vec{L}} = \boldsymbol{I}\dot{\vec{\omega}}$. That allows to isolate $\dot{\vec{\omega}}$. Lastly, we will drop the summations over forces/torques in both equations. The derivatives of $\vec{v}$ and $\vec{\omega}$ are gathered in Eq.(2.31).

$$\frac{d\vec{v}}{dt} = \vec{a} \qquad\qquad \frac{d\vec{\omega}}{dt} = \boldsymbol{I}^{-1}\left(\vec{T} - \vec{\omega}\times\left(\boldsymbol{I}\vec{\omega}\right)\right) \tag{2.31}$$

The last thing we need is an expression for $\vec{a}$ and $\vec{T}$. These are pretty much given in Eq.(2.21) and Eq.(2.22). Before gathering them here, we will do some changes. First, we need to make the notation consistent, both between them and with the state vector in Eq.(2.29). First, we will define $\vec{r}$ to be Phobos' position in the Mars-Centered Inertial reference frame - i.e. the position vector in Eq.(2.29). Note that this is equivalent to $\vec{r}_{AB}$ in Eq.(2.21). Second, we will drop the summations over the different potential components and write the potential as a single unit. This is possible because all operations we will apply on it are distributive (matrix multiplication, derivatives, ...). Thirdly, we will have to consider the fact that the torque in Eq.(2.22) will be plugged into Eq.(2.4), which is written in Phobos' body frame. For this, we will define vector $\vec{\rho}_P^M$, which is Mars' position vector in Phobos' body frame. This is what we called $\vec{r}$ in Eq.(2.22) using old notation. Lastly, we will make explicit the fact that the gradients in Eq.(2.21) and Eq.(2.22) have to be evaluated not at $\vec{r}$ itself, but at the body-fixed position vectors of the other body. In other words, $\nabla_{\mathcal{P}} U_P$ has to be evaluated at $\vec{\rho}_P^M$. Similarly, we can define $\vec{\rho}_M^P$ to be the position vector of Phobos in Mars' body-frame. This way, $\nabla_{\mathcal{M}} U_M$ is to be evaluated at $\vec{\rho}_M^P$. The transformations between these $\vec{\rho}_M^P$ and $\vec{\rho}_P^M$, and $\vec{r}$ are given in Eq.(2.32). Note the negative sign in the second equation, meaning that $\vec{r}$ goes from Mars to Phobos while $\vec{\rho}_P^M$ goes the opposite way. Keep in mind that $\boldsymbol{R}^{\mathcal{P}/\mathcal{I}}$ is - in its way - part of the state vector because it depends on $\boldsymbol{q}$.

$$\vec{\rho}_M^P = \boldsymbol{R}^{\mathcal{M}/\mathcal{I}}\vec{r} \qquad\qquad \vec{\rho}_P^M = -\boldsymbol{R}^{\mathcal{P}/\mathcal{I}}\vec{r} \tag{2.32}$$

Putting everything together and performing the notation changes mentioned above, one finds a formulation of the dynamics governing Phobos *with origin in Mars*, i.e. all forces and torques that Mars exerts on Phobos. For a complete formulation of the equations of motion of Phobos, one needs to also include the forces and torques exerted by any number N of *third bodies*, that will be modelled as point masses. What bodies to include in this set is a study that will be carried out during the thesis following this text. Third body forces follow the shape in Eq. (2.10b), while third body torques are formulated in the same way af that of Mars. The complete equations of motion after including these terms are shown in Eq.(2.33).

$$\vec{x} = \begin{bmatrix} \vec{r} \\ \vec{v} \\ \boldsymbol{q} \\ \vec{\omega} \end{bmatrix} \implies \frac{d\vec{x}}{dt} = \begin{bmatrix} \vec{v} \\ \vec{a} \\ \boldsymbol{\Omega q} \\ \boldsymbol{I}^{-1}\left(\vec{T} - \vec{\omega} \times \left(\boldsymbol{I}\vec{\omega}\right)\right) \end{bmatrix} = \begin{bmatrix} \vec{v} \\ \vec{a} \\ \boldsymbol{Q}\vec{\omega} \\ \boldsymbol{I}^{-1}\left(\vec{T} - \vec{\omega} \times \left(\boldsymbol{I}\vec{\omega}\right)\right) \end{bmatrix} \tag{2.33a}$$

$$\vec{a} = (\mu_{\mathrm{M}} + \mu_{\mathrm{P}})\left(-\frac{\vec{r}}{r^3} + \frac{1}{\mu_{\mathrm{M}}}\boldsymbol{R}^{\mathcal{I}/\mathcal{M}}\nabla_{\mathcal{M}} U_{\mathrm{M}}(\vec{\rho}_M^P) - \frac{1}{\mu_{\mathrm{P}}}\boldsymbol{R}^{\mathcal{I}/\mathcal{P}}\nabla_{\mathcal{P}} U_{\mathrm{P}}(\vec{\rho}_P^M)\right) - \sum_{i=1}^{N}\mu_i\left(\frac{\vec{r}_{iP}}{r_{iP}^3} - \frac{\vec{r}_i}{r_i^3}\right) \tag{2.33b}$$

$$\vec{T} = -M\vec{\rho}_P^M \times \left(\boldsymbol{R}^{\mathcal{I}/\mathcal{P}}\nabla_{\mathcal{P}} U_{\mathrm{P}}(\vec{\rho}_P^M)\right) - \sum_{i=1}^{N} M_i\vec{\rho}_P^i \times \left(\boldsymbol{R}^{\mathcal{I}/\mathcal{P}}\nabla_{\mathcal{P}} U_{\mathrm{P}}(\vec{\rho}_P^i)\right) \tag{2.33c}$$

In principle, one would be able to integrate these equations of motion if an initial condition is provided and the necessary parameters - namely μ and the harmonic coefficients of both Mars and Phobos - are known.

2.4.3. The variational equations

It is now the time to give an expression for the variational equations. As seen in Eq.(2.27), the differential equations are completely determined by matrices $\boldsymbol{D}$ and $\boldsymbol{\Pi}$. The aim of this subsection will be to derive expression for these two matrices. Note that, in this context, $\vec{f}$ is no other than $d\vec{x}/dt$ given in Eq.(2.33a).

Let's begin by matrix $\boldsymbol{D}$. We will begin by the derivatives of $\vec{v}$ with respect to the components of $\vec{x}$. These are straight-forward and given in Eq.(2.34). The other easy partials are those of $\dot{\boldsymbol{q}}$, gathered in Eq.(2.35).

$$\frac{\partial\vec{v}}{\partial\vec{r}} = \boldsymbol{0}_{3\times3} \qquad \frac{\partial\vec{v}}{\partial\vec{v}} = \boldsymbol{I}_{3\times3} \qquad \frac{\partial\vec{v}}{\partial\boldsymbol{q}} = \boldsymbol{0}_{3\times4} \qquad \frac{\partial\vec{v}}{\partial\vec{\omega}} = \boldsymbol{0}_{3\times3} \tag{2.34}$$

$$\frac{\partial\dot{\boldsymbol{q}}}{\partial\vec{r}} = \boldsymbol{0}_{4\times3} \qquad \frac{\partial\dot{\boldsymbol{q}}}{\partial\vec{v}} = \boldsymbol{0}_{4\times3} \qquad \frac{\partial\dot{\boldsymbol{q}}}{\partial\vec{\omega}} = \boldsymbol{Q} \qquad \frac{\partial\dot{\boldsymbol{q}}}{\partial\boldsymbol{q}} = \boldsymbol{\Omega} \tag{2.35}$$

Next in line would be the partials of $\vec{a}$. However, some of these are very involved. The partials of $\dot{\vec{\omega}}$ will involve the partials of $\vec{T}$, some of which are also non-trivial. However, in the process, it will be useful to know that some others of them are nil. We will then indicate which partials of both $\vec{a}$ and $\vec{T}$ are nil, then move on to the partials of $\dot{\vec{\omega}}$, and then finish with the harder partials of $\vec{a}$ and $\vec{T}$.

The nil partials of $\vec{a}$ and $\vec{T}$ are given in Eq.(2.36). Although it might not seem so, the partials of these terms with respect to $\boldsymbol{q}$ are not nil because $\boldsymbol{R}^{\boldsymbol{I}/\boldsymbol{\mathcal{P}}}$ - and similarly $\boldsymbol{R}^{\boldsymbol{\mathcal{P}}/\boldsymbol{I}}$ - both depend on $\boldsymbol{q}$.

$$\frac{\partial \vec{a}}{\partial \vec{v}} = \frac{\partial \vec{a}}{\partial \vec{\omega}} = \mathbf{0}_{3\times 3} \qquad \frac{\partial \vec{T}}{\partial \vec{v}} = \frac{\partial \vec{T}}{\partial \vec{\omega}} = \mathbf{0}_{3\times 3} \tag{2.36}$$

The partials of $\dot{\vec{\omega}}$ are straight-forward if the partials of $\vec{T}$ are left indicated. The expressions are given in Eq.(2.37).

$$\frac{\partial \dot{\vec{\omega}}}{\partial \vec{r}} = \boldsymbol{I}^{-1}\frac{\partial \vec{T}}{\partial \vec{r}} \qquad \frac{\partial \dot{\vec{\omega}}}{\partial \vec{v}} = \mathbf{0}_{3\times 3} \qquad \frac{\partial \dot{\vec{\omega}}}{\partial \boldsymbol{q}} = \boldsymbol{I}^{-1}\frac{\partial \vec{T}}{\partial \boldsymbol{q}} \qquad \frac{\partial \dot{\vec{\omega}}}{\partial \vec{\omega}} = -\boldsymbol{I}^{-1}\left(\left[{}_{\wedge}\boldsymbol{I}\vec{\omega}\right] + \left[\vec{\omega}_{\wedge}\right]\boldsymbol{I}\right) \tag{2.37}$$

All we are left with are the difficult partials of $\vec{a}$ and $\vec{T}$. In the expressions in Eq.(2.33), we see very few $\vec{r}$ or $\boldsymbol{q}$, but a lot of $\vec{\rho}$ and rotation matrices. It would then be a good strategy to consider applying chain rules. For this, Eq.(2.38) will come in handy.

$$\frac{\partial \cdot}{\partial \vec{r}} = \frac{\partial \cdot}{\partial \vec{\rho}_M^P}\frac{\partial \vec{\rho}_M^P}{\partial \vec{r}} = \frac{\partial \cdot}{\partial \vec{\rho}_M^P}\boldsymbol{R}^{\boldsymbol{\mathcal{M}}/\boldsymbol{I}} \qquad \frac{\partial \cdot}{\partial \vec{r}} = \frac{\partial \cdot}{\partial \vec{\rho}_P^M}\frac{\partial \vec{\rho}_P^M}{\partial \vec{r}} = -\frac{\partial \cdot}{\partial \vec{\rho}_P^M}\boldsymbol{R}^{\boldsymbol{\mathcal{P}}/\boldsymbol{I}} \tag{2.38a}$$

$$\frac{\partial \cdot}{\partial \boldsymbol{q}} = \frac{\partial \cdot}{\partial \vec{\rho}_P^M}\frac{\partial \vec{\rho}_P^M}{\partial \boldsymbol{q}} = -\frac{\partial \cdot}{\partial \vec{\rho}_P^M}\frac{\partial \boldsymbol{R}^{\boldsymbol{\mathcal{P}}/\boldsymbol{I}}}{\partial \boldsymbol{q}}\vec{r} \tag{2.38b}$$

$$\frac{\partial \vec{\rho}_M^P}{\partial \boldsymbol{q}} = \mathbf{0}_{3\times 4} \qquad \frac{\partial \boldsymbol{R}^{\boldsymbol{I}/\boldsymbol{\mathcal{M}}}}{\partial \vec{r}} = \frac{\partial \boldsymbol{R}^{\boldsymbol{I}/\boldsymbol{\mathcal{P}}}}{\partial \vec{r}} = \mathbf{0}_{3\times 3\times 3} \tag{2.38c}$$

Taking the term-by-term derivative of Eq.(2.33b) and applying these chain rules on the necessary terms, we find the partials of $\vec{a}$ in Eq.(2.39).

$$\frac{\partial \vec{a}}{\partial \vec{r}} = (\mu_{\mathrm{M}} + \mu_{\mathrm{P}})\left(-\frac{\partial}{\partial \vec{r}}\left(\frac{\vec{r}}{r^3}\right) + \frac{1}{\mu_{\mathrm{M}}}\boldsymbol{R}^{\boldsymbol{I}/\boldsymbol{\mathcal{M}}}\nabla^2_{\mathcal{M}}U_{\mathrm{M}}\boldsymbol{R}^{\boldsymbol{\mathcal{M}}/\boldsymbol{I}} + \frac{1}{\mu_{\mathrm{P}}}\boldsymbol{R}^{\boldsymbol{I}/\boldsymbol{\mathcal{P}}}\nabla^2_{\mathcal{P}}U_{\mathrm{P}}\boldsymbol{R}^{\boldsymbol{\mathcal{P}}/\boldsymbol{I}}\right) \tag{2.39a}$$

$$\frac{\partial \vec{a}}{\partial \boldsymbol{q}} = -\frac{\mu_{\mathrm{M}} + \mu_{\mathrm{P}}}{\mu_{\mathrm{P}}}\left(\frac{\partial \boldsymbol{R}^{\boldsymbol{I}/\boldsymbol{\mathcal{P}}}}{\partial \boldsymbol{q}}\nabla_{\mathcal{P}}U_{\mathrm{P}} - \boldsymbol{R}^{\boldsymbol{I}/\boldsymbol{\mathcal{P}}}\nabla^2_{\mathcal{P}}U_{\mathrm{P}}\frac{\partial \boldsymbol{R}^{\boldsymbol{\mathcal{P}}/\boldsymbol{I}}}{\partial \boldsymbol{q}}\vec{r}\right) \tag{2.39b}$$

Proceeding in the same way with Eq.(2.33c), the partials of $\vec{T}$ are gathered in Eq.(2.40).

$$\frac{\partial \vec{T}}{\partial \vec{r}} = M\left(\left[{}_{\wedge}\boldsymbol{R}^{\boldsymbol{I}/\boldsymbol{\mathcal{P}}}\nabla_{\mathcal{P}}U_P\right] + \left[\vec{\rho}_P^M{}_{\wedge}\right]\boldsymbol{R}^{\boldsymbol{I}/\boldsymbol{\mathcal{P}}}\nabla^2_{\mathcal{P}}U_P\right)\boldsymbol{R}^{\boldsymbol{\mathcal{P}}/\boldsymbol{I}} \tag{2.40a}$$

$$\frac{\partial \vec{T}}{\partial \boldsymbol{q}} = M\left(\left[{}_{\wedge}\boldsymbol{R}^{\boldsymbol{I}/\boldsymbol{\mathcal{P}}}\nabla_{\mathcal{P}}U_P\right] + \left[\vec{\rho}_P^M{}_{\wedge}\right]\boldsymbol{R}^{\boldsymbol{I}/\boldsymbol{\mathcal{P}}}\nabla^2_{\mathcal{P}}U_P\right)\frac{\partial \boldsymbol{R}^{\boldsymbol{\mathcal{P}}/\boldsymbol{I}}}{\partial \boldsymbol{q}}\vec{r} - M\left[\vec{\rho}_P^M{}_{\wedge}\right]\frac{\partial \boldsymbol{R}^{\boldsymbol{I}/\boldsymbol{\mathcal{P}}}}{\partial \boldsymbol{q}}\nabla_{\mathcal{P}}U_P \tag{2.40b}$$

Having defined all terms in the $\boldsymbol{D}$ matrix, it is now time to turn our attention to the $\boldsymbol{\Pi}$ matrix. First, we should ask ourselves what parameters we are interested in, be it because a big uncertainty is associated to them or because they will be part of the parameters to estimate. With the position and orientation of Phobos being part of our state, the only other thing our dynamics depend on are the geophysical properties of Phobos, namely everything contained in Eq.(2.23) and Eq.(2.24). One can argue that the geophysical properties of Mars can also be taken as parameters. However, since this work focuses on Phobos itself, we will treat all information about Mars to be perfect, so that changes in, say, Mars' $C_{2,0}$ do not happen at all. Furthermore, Phobos' harmonic coefficients are involved in both acceleration/torque and the inertia tensor. This makes these parameters more interesting when it comes to couplings between translation and rotation. Thus, we will limit ourselves to Phobos' harmonic coefficients and mean moment of inertia. We will treat the partials with respect to a generic parameter α.

We will begin by the trivial derivatives. By looking at Eq.(2.33a), it is obvious that both $\vec{v}$ and $\dot{\boldsymbol{q}}$ are independent of any parameter. Thus, we can write Eq.(2.41).

$$\frac{\partial \vec{v}}{\partial \alpha} = \vec{0} \qquad \frac{\partial \dot{\boldsymbol{q}}}{\partial \alpha} = \boldsymbol{0} \tag{2.41}$$

Once again, we will begin by the partial of $\dot{\vec{\omega}}$, which will involve the partial of $\vec{T}$ and then we will move on to the partials of both $\vec{a}$ and $\vec{T}$. The partial of $\dot{\vec{\omega}}$ is straight-forward if one uses the expression in Eq.(2.42b). It's gathered in Eq.(2.42).

$$\frac{\partial \dot{\vec{\omega}}}{\partial \alpha} = -\boldsymbol{I}^{-1}\frac{\partial \boldsymbol{I}}{\partial \alpha}\dot{\vec{\omega}} + \boldsymbol{I}^{-1}\left(\frac{\partial \vec{T}}{\partial \alpha} - \vec{\omega} \times \left(\frac{\partial \boldsymbol{I}}{\partial \alpha}\vec{\omega}\right)\right) \tag{2.42a}$$

$$\frac{\partial \boldsymbol{I}^{-1}}{\partial \alpha} = -\boldsymbol{I}^{-1}\frac{\partial \boldsymbol{I}}{\partial \alpha}\boldsymbol{I}^{-1} \tag{2.42b}$$

Moving on to the partials of $\vec{a}$ and $\vec{T}$ and looking at Eq.(2.33b) and Eq.(2.33c), the only place where any of the parameters we are considering are involved is $\nabla_{\mathcal{P}} U_P$. The derivatives are therefore quite straight-forward as well. They are gathered in Eq.(2.43) and Eq.(2.44).

$$\frac{\partial \vec{a}}{\partial \alpha} = -\frac{\mu_{\mathrm{M}} + \mu_{\mathrm{P}}}{\mu_{\mathrm{P}}}\boldsymbol{R}^{\mathcal{I}/\mathcal{P}}\frac{\partial}{\partial \alpha}\nabla_{\mathcal{P}} U_P \tag{2.43}$$

$$\frac{\partial \vec{T}}{\partial \alpha} = -M\vec{\rho}_P^{\,M} \times \left(\boldsymbol{R}^{\mathcal{I}/\mathcal{P}}\frac{\partial}{\partial \alpha}\nabla_{\mathcal{P}} U_P\right) \tag{2.44}$$

The variational equations of this coupled model give insight on the kind of information that would be lost had an uncoupled model been used. It is intuitive to think that if a system of forces is different at one instant in time, the state vector at the next instant will be different. The variational equations go one step further and quantify these differences in time. Let's give an illustrative example. For that, we will consider a translational state $\vec{x}_t$ and a rotational state $\vec{x}_r$ that exist in our coupled model, and we will divide the $\boldsymbol{\Phi}$ and $\boldsymbol{D}$ matrices in blocks as in Eq.(2.45).

$$\boldsymbol{\Phi} = \begin{bmatrix} \boldsymbol{\Phi}_{tt} & \boldsymbol{\Phi}_{tr} \\ \boldsymbol{\Phi}_{rt} & \boldsymbol{\Phi}_{rr} \end{bmatrix} \qquad \boldsymbol{D} = \begin{bmatrix} \boldsymbol{D}_{tt} & \boldsymbol{D}_{tr} \\ \boldsymbol{D}_{rt} & \boldsymbol{D}_{rr} \end{bmatrix} \tag{2.45}$$

From Eq.(2.28) and Eq.(2.27), we can write Eq.(2.46).

$$\Delta\vec{x}_t = \boldsymbol{\Phi}_{tt}\Delta\vec{x}_{t,o} + \boldsymbol{\Phi}_{tr}\Delta\vec{x}_{r,o} \qquad \dot{\boldsymbol{\Phi}}_{tt} = \boldsymbol{D}_{tt}\boldsymbol{\Phi}_{tt} + \boldsymbol{D}_{tr}\boldsymbol{\Phi}_{rt} \tag{2.46}$$

We now consider an uncoupled model. This results in the cross-terms being nil, i.e. $\boldsymbol{\Phi}_{tr} = \boldsymbol{\Phi}_{rt} = \boldsymbol{0}$. Then, Eq.(2.46) turns into Eq.(2.47).

$$\Delta\vec{x}_t = \boldsymbol{\Phi}_{tt}\Delta\vec{x}_{t,o} \qquad \dot{\boldsymbol{\Phi}}_{tt} = \boldsymbol{D}_{tt}\boldsymbol{\Phi}_{tt} \tag{2.47}$$

Comparing both Eq.(2.46) and Eq.(2.47), we can see a difference in the first part. Since we now allow $\Delta\vec{x}_{r,o}$ to be non-zero, we can see a direct effect of the rotational state in the translational state: even if $\Delta\vec{x}_{t,o} = \vec{0}$, $\Delta\vec{x}_t \neq 0$. This might be somewhat intuitive and not add much to the game. It is the the second part, however, that is more interesting. Adding these couplings changes $\dot{\boldsymbol{\Phi}}_{tt}$ and therefore $\boldsymbol{\Phi}_{tt}$ itself. Even if $\Delta\vec{x}_{r,o} = \vec{0}$ and $\Delta\vec{x}_t = \boldsymbol{\Phi}_{tt}\Delta\vec{x}_{t,o}$, a case in which the coupled and uncoupled models "would be equivalent", $\Delta\vec{x}_t$ will still turn out to be different. In other words, the same analysis and conditions for the coupled and uncoupled models yields different results. It is these differences that an uncoupled model is blind to and what coupled models are needed for.

2.5. Overview of the Martian system

In the previous section, the dynamics of Phobos were studied in a theoretical way, meaning that a system of forces and torques was defined and the equations of motions and variational equations were written. The study of Phobos' motion, however, has historically been kinematical, i.e. its motion was *observed* rather than *described* with equations. This resulted in a very different approach, theories and lingo to be developed. Some of these aspects are general for many (natural) satellites in the solar system. Others, not so much. Furthermore, a context of the physical characteristics of Phobos and its motion will be beneficial in the following chapters. We will devote this section to knowing the Martian system a bit better.

Phobos is quite an amorphous rock - an object known by some as a *potatoid* - with characteristic lengths standing at $26.1 \times 22.8 \times 18.3$ km (Willner et al., 2014) - end to end - and full of craters - something like what can be seen on the cover of this document. It orbits Mars at an average distance of almost 6000km above the surface and has an orbital period of about 7h 40min, which means it completes a bit over 3 full revolutions around Mars each (Earth) day (Michel et al., 2015). Its orbit has an eccentricity of 0.0151 (see Sec. 2.1.2) and its inclination stands at about 1.1° with respect to the Martian equatorial plane. As many other planetary satellites, Phobos rotation rate about its polar axis equals its orbital mean motion (Burns, 1972) and its equatorial and orbital planes are coincident - or, what is the same, its rotation axis or *pole* is normal to the orbital plane. This phenomenon is known as *spin-orbit resonance* and the rotation is said to be *synchronous*. The result of this is that Phobos always shows the same face to Mars and also has a "dark side".

Superimposed on top of this resonance, the moon oscillates and wobbles back and forth around its three axes. These oscillations are called *(physical) librations*, and were first mentioned by Duxbury and Callahan (1981). There exist librations in latitude, and librations in longitude. The latter are more important, and are rotational oscillations about the axis of rotation of the moon, making it spin a bit faster or slower at times. This makes Mars oscillate in the East-West direction in Phobos' sky. Librations in latitude are those in which the moon tumbles up and down, nodding to the planet. This causes Mars to oscillate in the North-South direction in Phobos' sky. There exist librations in the third axis, but those are generally less important. The most relevant libration, and the one that has received the most attention, is the once-per-orbit longitudinal libration - i.e. an oscillation with a period equal to the orbital period - and we shall denote its amplitude as $\mathcal{A}$. The physics of librations will be expanded on in Sec. 3.1.1.

Another effect that is sometimes considered - but we are not going to in this work - is the tides that Phobos raises on Mars, the same way the Moon creates tides on Earth. However, without water on Mars, these tides are manifested through a slight stretch of the planet, usually known as *tidal bulge*. If Mars could instantly adapt to the changing location of Phobos in its sky, this tidal bulge would always point towards the moon. This would happen if Mars was perfectly liquid, or if the orbit of Phobos was "geostationary". That is however not the case, and the Martian structure needs some time to follow Phobos. This causes the stretch to *lag* behind the moon.

As a consequence of the tidal bulge following Phobos, the mass distribution of Mars changes with time, which renders the Martian spherical harmonic coefficients time-dependent. These changes will tend to modify the acceleration that Mars exerts on Phobos with a component that pulls Phobos back - effectively, there is a bunch of matter following Phobos from behind and attracting it back. The effect of this is similar to that of aerodynamic drag in Earth-bound satellites, but to a much lesser extent. This is to say that Phobos is decaying towards the Martian surface, and its orbit is in consequence getting faster and faster - its mean motion is increasing. This phenomenon is commonly referred to as *secular acceleration*. It may be caused by reasons other than tidal interactions, and an (old) account of historically proposed reasons is given by Burns (1972), with a more extensive explanation of tidal interactions in the *Orbital evolution under tidal forces* section. Thus, the *tidal effects* of Phobos can be implemented in many ways: by time-dependent spherical harmonics in numerical integrations, by the presence of an additional force term in the equations of motion, by the addition of the secular acceleration term in the kinematics of analytical models, ... Different authors have used different implementations, as we will see later.

Works that consider tides are often concerned about the elastic properties of the bodies, be it Mars or Phobos. Two important factors in these problems are the *quality factor, Q* and the *Love number,* k_2. We will not go into further details about what these numbers represent, because we will generally not be concerned with them, but the interested reader is referred to Mathews et al. (1995) and Nimmo and

Faul (2013). They might appear, however, when discussing works about other authors.

3

State of the art

Last chapter was dedicated to the physics governing the dynamics of Phobos, both in translation and rotation. The approach so far has been general and conceptual, and it has mostly focused on forces and accelerations. We will now look at how the motion of a body is described, namely its kinematics: position, velocity, orientation and angular velocity. There are two ways of doing this. On the one hand, we can describe the motion by *how it looks like*. This is a purely kinematical approach, also termed *analytical*. On the other hand, we can describe the motion by its root cause, i.e. linking back to forces and accelerations. This is a dynamical approach, usually also called *numerical* approach - because it requires (numerical) integration of the equations of motion.

Kinematical descriptions assume a shape for the different dynamical variables (position, velocity, orientation, ...) and attach some coefficients to these functions. These coefficients are then estimated through fits to real-life data and observations. Tradition has favoured these descriptions because they are very straightforward and do not require knowledge of the physical properties of the bodies involved. The drawbacks they present as compared with dynamical descriptions are also a consequence of this. Kinematical descriptions bundle the effects of all accelerations in these coefficients, and different forcing terms become indistinguishable from one another. They cannot therefore not offer information on the physical properties of the bodies involved - because these play no role in kinematical descriptions. Furthermore, their validity is very dependent on the type of data used to fit the coefficients and the time spanned by such data. Some functions might work well for small periods of time but longer tendencies might require other types of functions. On the other hand, they offer insight on the nature of the motion and they are able to transmit this information in an intuitive and straightforward manner. Things like periodicity/secularity or frequency analyses are trivial in this type of descriptions.

Dynamical descriptions, on the other hand, follow the inverse logic. They use forces and accelerations to build the equations of motion of a body and then (numerically) integrate them to find the trajectory or rotation of a body. The main disadvantage of these descriptions is that they require good knowledge of many things. On the one hand, the physical properties of the system (masses of the bodies, their moments of inertia, ...); on the other hand, building the equations of motion requires knowing what accelerations and forces are involved in the system; and lastly, one needs tools to be able to write these accelerations in a mathematical way. This can become complicated, and the spherical harmonics description of the gravity field is a good example. However, the real problem of this approach is, many times, evaluating these forces and accelerations. It is often the case that accelerations depend on the current state (gravity is a good example) and the differential equations of motion can become scarily complicated. Other times, the evaluation of these accelerations requires information that is to be obtained externally and whose quality might be better or worse - for example, the masses of Mars and Phobos or, more importantly, their harmonic coefficients. Such difficulties are more than compensated by the strengths of these descriptions. Dynamical descriptions allow to dissect the dynamics of the motion and perform a term-by-term assessment, where the impact of each individual third body or each individual harmonic can be quantified. Furthermore, the involvement of these descriptions with the physical properties of the bodies allows to infer them in an estimation procedure. Thus, things like a body's mass and mass distribution can be obtained.

This chapter will perform a systematic review of the existing models, both analytical and numerical, for both translation and rotation.

3.1. Attitude: rotational models

It is generally accepted that Phobos rotation is synchronous to its orbit (see Sec. 2.5), with its pole normal to its orbital plane. The subject of interest lies then in the librations, which make Phobos deviate from its otherwise permanent configuration. Describing the orientation of Phobos then reduces to characterizing the amplitude and frequency of these librations. This section presents an account of different ways in which different authors have tried to do this. Many have focused solely on the longitudinal libration (with amplitude $\mathcal{A}$).

This longitudinal libration is governed by the equations of rotational motion. If libration angles are small, these equations can be linearized and the longitudinal component reduced to Eq.(3.1), which is used by Rambaux et al. (2010) - with some change in notation - to study librations in Enceladus. In this equation, θ is the libration angle, n is Phobos' mean motion, $\gamma = (B - A)/C$ is a function of Phobos' three moments of inertia $A \leq B \leq C$ and f is a forcing torque. Note that, even in the absence of this torque, the homogeneous part of the solution to Eq.(3.1), θ_h, still oscillates. The frequency of this oscillation is called the *normal mode* or *proper mode* of the system[1]. In this case, the normal mode is given by $\omega_o = n\sqrt{3\gamma}$, i.e. a function of Phobos' mean motion and triaxiality, physical properties that are fixed to the system and do *not* depend on the motion. In other words, normal modes can be defined - and computed - independently of whether there are external torques or motion.

$$\ddot{\theta} + 3n^2\gamma\theta = f \tag{3.1}$$

Oscillatory systems present an interesting characteristic in the presence of certain forcing terms. The known function f can always be expanded in a Fourier series as in Eq.(3.2). In this case, the oscillatory homogeneous solution is superimposed with a series of particular oscillations as in Eq.(3.3). Note that, if f has some frequency component that is very close to the system's normal mode, i.e. $|\omega_o^2 - \omega_i^2| << 1$, the solution will blow up. This phenomenon is called *resonance* and it is critical in some cases. In particular, if resonance occurs, the oscillation becomes so big that the linearization assumption usually breaks down and the equation is no longer a valid reflection of reality.

$$f = \sum F_i \sin(\omega_i t + \varphi_i) \tag{3.2}$$

$$\theta(t) = \theta_h(t) + \sum \frac{F_i}{\omega_o^2 - \omega_i^2} \sin(\omega_i t + \varphi_i) \tag{3.3}$$

As it so happens, Phobos' normal mode for its longitudinal libration is close to its orbital period, the period at which torques will naturally oscillate as Phobos revolves around Mars. This makes the libration amplitude particularly sensitive to change in either γ - which are unlikely - and n - which it is known to be increasing with time. The fact that the motion is sensitive to these quantities means that these quantities can be inferred by studying the motion.

Normal modes are also particular in another way. Note that, in the presence of dissipation - no matter how small it is - the normal modes will die out over time, and only the forced solution will prevail, with stronger signals in the frequencies close to the normal modes. However, in the event that the forcing has some component exactly at the normal mode, the response will have a secular oscillatory term, whose amplitude will become arbitrarily large with time. The phenomenon of resonance is usually kept in check in rotational systems by the linearization assumption.

A mathematical discussion of the oscillatory motion of librations can be found in App. B.

3.1.1. Analytical models

Analytical models attempt to describe librations with closed-form expressions. This is often times synonymous to providing a more accurate value of $\mathcal{A}$ for an a-priori rotation model using a new set of observations. This a-priori model may be an already existing analytical model or the simple spin-orbit resonance with the pole normal to the orbit. There are several ways of reaching this result.

[1]These terms are used to refer to both the *frequency* and the *period* of the oscillations, as well as the oscillation itself and, sometimes, to its amplitude. Context is used to tell the difference.

Photogrammetry and inertia

The method that first gave an estimation of this libration was photogrammetry, in the form of the so-called *bundle block adjustments* - i.e. image analysis (the interested reader is referred to Burmeister et al. (2018) for an thorough explanation). The main objective of this method is actually generating a shape model of the body, estimating the axes of its reference ellipsoid. However, as a byproduct of this process, the orientation of the body is also obtained. For this, an a-priori reference frame is required, as well information of the body's ephemerides. Other information, main on spacecraft and camera, is also required. Duxbury (1974) was the first to do this. Assuming that Phobos was aligned with its RTN frame (see Sec. 2.1.4) - which is to say that he assumed spin-orbit resonance with pole normality - and that libration angles were small, he estimated the librations in all three directions, as did Burmeister et al. (2018). This time, the a-priori reference frame was not the synchronous rotation but rather the IAU distributed rotational elements (Archinal et al., 2011) as well as the ones derived by Stark et al. (2017).

When the size and shape of Phobos is obtained through photogrammetry, one can obtain the inertia properties of the Moon if a model of the interior composition is assumed. Usually this model takes Phobos as a rock with constant density. Duxbury and Callahan (1981) gave an expression for the once-per-orbit longitudinal libration of a synchronously rotating moon as a function of its moments of inertia $A \leq B \leq C$, written here in Eq.(3.4).

$$\mathcal{A} = \frac{2e}{1 - \frac{1}{3\gamma}} \tag{3.4}$$

In Eq.(3.4), $\gamma = (B - A)/C$ and $e = 0.0151$ is the orbital eccentricity of Phobos. This is a second way in which photogrammetry can predict Phobos' libration. This is the way that was used by (Duxbury and Callahan, 1989) and Duxbury (1991). Although both of these works take vastly different approaches on the computation of Phobos' shape, they are very similar in the way they compute the longitudinal libration amplitude. In these works, Duxbury assumed a synchronously rotating Phobos on top of which a force longitudinal libration is superimposed.

On the other hand, many bundle block adjustment works compute an *observed* libration through the fitting of the images and a *predicted* libration through Eq.(3.4). By comparing the two, the validity of the assumed interior model can be assessed. This is done by Willner et al. (2010), Nadezhdina and Zubarev (2014) and Oberst et al. (2014). The shape determination process is different in each source, but the longitudinal libration determination process is pretty much the same, with the exception of the a-priori rotation model - with respect to which estimation residuals are computed. In this respect, Willner et al. (2010) assumed a purely synchronous rotation on top of which a longitudinal libration was superimposed - like Duxbury and Callahan (1989) - while Nadezhdina and Zubarev (2014) and Oberst et al. (2014) used the IAU recommendations at the time (Archinal et al., 2011) - actually the rotations derived by Duxbury and Callahan (1989).

ESAPHO

In 1988, Chapront-Touze (1988) developed a formulation of the dynamics of Phobos in a dedicated reference frame that allowed for the integration of the equations of motion in a semi-analytical manner. This frame was used to discuss the librations of Phobos by both Chapront-Touze (1990) and Borderies and Yoder (1990). Due to the dynamical nature of these works, more librations other than the once-per-orbit longitudinal libration are studied, and lists are provided with amplitudes and frequencies of different ESAPHO angles. This means that all librations in all three axes can be extracted from these works.

In particular, Borderies and Yoder (1990) provide an expansion of the longitudinal libration into three terms scaled with different powers of the orbital eccentricity of Phobos, and provides an analytically integrable second order ODE for the evolution of each term. This allows him to provide a closed-form expression for the amplitudes of the main terms in each of the three librations.

As opposed to bundle block adjustments, the ESAPHO framework works with equations of motion that are (analytically) integrated. This means that geophysical parameters - more specifically the moments of inertia and the mass of Phobos - are to be provided as input, rather than obtained as output as in bundle block adjustments. The same thing happens with librations: purely analytical models have to "be made aware" that librations exist in order for their amplitudes to be estimated. An EOM approach will naturally give rise to these dynamics.

Direct orbit inference

Other authors have decided to use the spin-orbit resonance and forced libration to propose models for a rotation that follows the orbit perfectly. These models capture well long-period trends of the rotation that follow the orbit's secular acceleration and node precession. This is, for example, the approach taken by Duxbury and Callahan (1981), Stark et al. (2017) and Jacobson et al. (2018). The first of the three develops simplified expressions by using small-angle approximations. The inclusion of the longitudinal libration varies from source to source. Eq.(3.4) is used by Duxbury and Callahan (1981), with inertia moments taken from an unmentioned source, while Jacobson et al. (2018) decided to include the first two longitude librations from Borderies and Yoder (1990). On the other hand, Stark et al. (2017) provides an expression for the forced libration in longitude, although the source is not clear as to what the origin of the reported amplitudes and frequencies is.

Within this group, Jacobson (2010) and Lainey et al. (2021) take another approach. Although these works focus on ephemerides computation, the effect of the libration amplitude can be translated in a change of argument of periapsis, as given by Lagrange's planetary equations and recalled in Eqs.(7-10) by Jacobson (2010), collected here in Eq.(3.5). If one has an expression for the left hand sides of Eq.(3.5) and the orbital elements on the right hand sides, then the librational amplitude can be extracted from it. These elements, however, are outputs of an estimation problem that simultaneously provides the value of $\mathcal{A}$ (see Sec. 4), given that J_2 and $C_{2,2}$ are provided. These two inputs will have some uncertainty associated to them, that will translate into uncertainty in $\mathcal{A}$. As mentioned by Lainey et al. (2021), Phobos' harmonic coefficients have large uncertainties, which will map into big uncertainties in $\mathcal{A}$ as well. Nowadays, other methods are used to estimate all these parameters (see Sec. 2.3).

$$\Delta a = 3a\left(\frac{R}{a}\right)^2 (J_2 + 6C_{2,2})e\cos M \tag{3.5a}$$

$$\Delta\lambda = 3a\left(\frac{R}{a}\right)^2 (J_2 + 6C_{2,2})nt + \frac{21}{4}\left(\frac{R}{a}\right)^2 (J_2 + 6C_{2,2})e\sin M \tag{3.5b}$$

$$\Delta e = \frac{3}{2}\left(\frac{R}{a}\right)^2 (J_2 + 6C_{2,2})e\cos M \tag{3.5c}$$

$$\Delta\omega = \frac{3}{2}\left(\frac{R}{a}\right)^2 \left[J_2 - 2C_{2,2}\left(5 + \frac{4\mathcal{A}}{e}\right)\right] nt + \frac{3}{2}\left(\frac{R}{a}\right)^2 \frac{(J_2 + 6C_{2,2})}{e}\sin M \tag{3.5d}$$

3.1.2. Numerical models

By looking at Eq.(2.4) and Eq.(2.22), it is clear that the equations of motion can be integrated if we have:

- The moments of inertia of Phobos.
- The mass of Mars
- A model of the gravity field of Phobos and values for the harmonic coefficients.
- A model for the orbit of Phobos - so that $\vec{r}$ in Eq.(2.22) can be evaluated.

Notice that the evaluation of ∇U_P requires a rotation model for Phobos. However, that rotation is precisely what we are integrating for. The question still remains, however, of how far we should expand U_P. We will look at literature to aid us in making that decision.

Numerical approaches to the rotational motion of celestial bodies are scarce. In fact, for the case of Phobos, only two have been found in literature. The first one was developed by Rambaux et al. (2012). Here, the gravity field of Phobos is expanded to degree and order 3. The source computes the degree 3 coefficients from the model of the interior of Phobos given by Willner et al. (2010). Although not explicitly said in the source, it is safe to assume that all other coefficients are computed in the same way. The moments of inertia are also computed from the model by Willner et al. (2010). The trajectory of Phobos was taken from the numerical ephemerides of Lainey et al. (2007). As for Mars' rotation model and J_2 coefficient, nothing is explicitly said in the source, although it is suspected that they were taken from Konopliv et al. (2006). The source performed a characterization of the frequency spectrum of all three librations of Phobos, and proposed ways of extracting information about Phobos' interior from the these librational spectra.

A second integration was performed by Yang et al. (2020) in 2020. The same librational spectra characterization as Rambaux et al. (2012) was performed, and in fact the same tables are presented in the source. However, this time, Phobos was considered as a deformable body, a model for the inertia tensor was proposed dependent on the kinematical and dynamical state of Phobos, and the rotational equations of motion were integrated together with this variable inertia tensor. Additionally, two studies were performed. On the one hand, about the effect of the k_2 Love number of Phobos on the librational spectra; on the other, a sensitivity analysis of the spectra with respect to small errors in the ephemerides model was performed. In their dynamical model, this source considered the same external torques as Rambaux et al. (2012), with the Martian J_2 and rotation model taken from Konopliv et al. (2011). For Phobos, the gravity field was expanded up to degree and order 8, with coefficients computed using the shape model by Willner et al. (2014). Yang et al. (2020) say that Phobos' ephemerides model is a revised version of those by Lainey et al. (2007), supposedly done by Lainey himself in 2016. Such a source has not been found by the author, as the reference given by Yang does not contain a DOI. The reference does say, however, *submitted*. This makes the author believe that this revision is actually the one published the year after (Lainey et al., 2021), which are the same ephemerides model as Rambaux et al. (2012) used for his numerical rotation propagation.

Although not explicitly, numerical models do incorporate all the effects that were usually considered in analytical models, but in a dynamic way. The explicit effect of a perturbation is reflected in the kinematics, and the perturbations that are not in the dynamic model are not reflected in the kinematics. This is contrary to analytical models, where a parameter is present as a placeholder for all perturbations that have similar effects and different perturbations can be *absorbed* into a single parameter. In particular, these numerical integrations by Rambaux et al. (2012) and Yang et al. (2020) report values for the amplitudes of the different arguments defined in the ESAPHO theory, found through a Fourier decomposition of the resulting signal from the integration. These arguments can be traced back to the governing equations of these librations: each of the arguments represents a distinct frequency of libration, much like the different frequencies ω_i in Eq.3.3. The argument or that represents the popular once-per-orbit longitudinal libration is l, and its amplitude is what we have called $\mathcal{A}$ in this work. A table with the value of $\mathcal{A}$ obtained by all rotational models can be seen in Table 3.1. Note how the last two source, who computed their respective amplitudes through the Fourier analysis of their numerically integrated rotations, agree well with the analytical fits. These numerical models include the torque that Mars' center of mass exerts on the figure of Phobos, which is represented by its quadrupole coefficients - or up to degree and order 8 in the work by Yang et al. (2020). The good agreement indicates that the dynamics considered in these numerical models is representative enough of the real dynamics, which include in theory all degrees and orders of both Mars and Phobos, as well as all degrees and orders of all other planets and bodies in the universe. This supports further the decision of including only Phobos' quadrupole field.

3.2. Ephemerides: Translational models

3.2.1. Analytical models

The currently distributed ephemerides by JPL are the numerically integrated ephemerides generated by Jacobson and Lainey (2014). This source makes a review of analytically produced ephemerides. However, their use was abandoned early on in favor of numerical ephemerides. As a reference, the older planetary ephemerides in the JPL website were the numerically integrated DE102, already back in 1981 (Various, a). For Phobos and Deimos, their currently published ephemerides by JPL are the ones generated by Jacobson and Lainey (2014) (see Sec. 3.2.2).

Analytical efforts on the trajectories of the Martian satellites died out in the 90s. The strongest effort on a Martian-system dedicated dynamic model was probably the ESAPHO reference frame (Chapront-Touze, 1988). By writing the equations of motion in this particular frame, Chapront-Touze (1988) could integrate them analytically. This was done by Borderies and Yoder (1990) in 1990 and developed further by Chapront-Touze (1990) later that year.

Outside of the ESAPHO theory, the orbit of Phobos has been studied assuming an ellipse with constant shape, with precessing node and pericenter mostly due to Mars' oblateness (Burns, 1972), and periodic changes in inclination due to solar perturbations (Jacobson et al., 1989), as well as a secular acceleration due to tidal dissipation. This is described in Struve's theory and served as the basis for the

[2]Three values are reported in the source for three different harmonic coefficient sets.

Table 3.1: Values of $\mathcal{A}$ from different sources. If two are reported, it is a work that observes a value through fits and predicts a value through Eq.(3.4) as explained in Sec. 3.1.1.

Source	$\mathcal{A}$ [°]
Duxbury (1974)	5
Duxbury and Callahan (1981)	2.31
Duxbury and Callahan (1989)	0.78 / 1.99
Borderies and Yoder (1990)	1.187
Chapront-Touze (1990)	0.807/1.186/0.9746[2]
Duxbury (1991)	0.90
Willner et al. (2010)	1.2 / 1.1
Jacobson (2010)	1.03
Nadezhdina and Zubarev (2014)	1.09 / 0.83
Oberst et al. (2014)	1.09 / 1.09
Stark et al. (2017)	1.732
Burmeister et al. (2018)	1.143
Jacobson et al. (2018)	1.2
Lainey et al. (2021)	1.09
Rambaux et al. (2012)	1.1
Yang et al. (2020)	1.15

works by Born and Duxbury (1975) and Jacobson et al. (1989). An alternative theory was developed by Waż (1999), where the Hamiltonian of the Keplerian motion was developed in powers of Phobos' eccentricity and the zonal harmonic coefficients of Mars, while expressions were given for the perturbing Hamiltonians of Mars' asphericity, the tide created on Mars by the Sun, the third body forces from the Sun, Deimos and Jupiter and an additional perturbation due to the Mars-attached reference frame not being entirely inertial. Other analytical theories based on those used for Earth-bound artificial satellites were also used on Phobos and Deimos, as mentioned by Jacobson and Lainey (2014).

Additionally, Lagrange's planetary equations (see section 10.2 of Battin (1999)) offer another analytical solution to the orbit of Phobos, by implementing increments on the orbital elements of the otherwise static elliptical orbit of Phobos. The relevant equations can be seen collected by Jacobson (2010) as part of an effort to ascertain the impact of the libration of Phobos on its orbit.

In any case, as we will see later, all these analytical ephemerides started lacking the necessary precision for some applications as early as 1977 (Tolson et al., 1977), and the 2000s saw a lot of advancement on the development of numerical models that could be integrated by the machine. This will be the topic of the next subsection.

3.2.2. Numerical models

Translational numerical models will generally aim to integrate the F2BP equation of motion Eq.(2.21), with the addition of third bodies in the form of Eq.(2.8). Notice that, in order to include all these accelerations, they require:

- A gravity model for Mars - i.e. the values of the spherical harmonic coefficients.
- A gravity model for Phobos.
- A rotation model for Mars - for the evaluation of $\boldsymbol{R}^{\mathcal{I}/\mathcal{M}}$.
- A rotation model for Phobos - for the evaluation of $\boldsymbol{R}^{\mathcal{I}/\mathcal{P}}$.
- The ephemerides of the third bodies.
- What propagator they use.

This will be secondary yet necessary information for a complete description of each of the models. However, there are more important differences that we should look out for. These represent the questions we should ask ourselves when building the equations of motions. These are:

- What third bodies should we include?
- How far should we expand the gravity field of Mars?

- How far should we expand the gravity field of Phobos?
- What other perturbations should we include?

We will attempt to answer these questions by studying the choices other authors made in the past.

The first numerical integration of the trajectory of Phobos was that of Tolson et al. (1977), in 1977. The aim was to analyze data from the Viking I orbiter, which got as close to Phobos as 88km. Existing Phobos ephemerides at the moment were based on analytical orbital element theory (see Sec. 3.2.1), which did not offer the accuracy required by Tolson et al. (1977). However, the source does not provide any information as to what accelerations were included in the model, much less what ancillary information was used. Tolson et al. (1977) fit their results to the Born-Duxbury mean element theory (Born and Duxbury, 1975) to obtain a good estimate of the initial conditions of Phobos. A second fit was performed to real data observations in order to estimate the gravitational parameter of Phobos μ_P.

In 1981, Peters (1981) formalized the numerical integration of multi-moon systems, providing both equations of motion and variational equations of a general planetary system. The source integrated all moons simultaneously, including the J_2 and J_4 terms of all the moons and the primary planet. It also included a number m of perturbing external planets. The integration was performed in the barycentric reference frame. The source reports results of application of the presented formulation to the Jovian and Saturnian systems, providing computation times for different integration settings. However, nothing is said on the accuracy of the ephemerides.

In 2004, Lainey et al. (2004) developed a formulation of the equations of motion of the Jovian system, and they used the same approach in 2007 for both Phobos and Deimos (Lainey et al., 2007). The two moons were integrated simultaneously. The model included the third body forces of the Sun, Jupiter, Saturn, the Earth and the Moon. The gravity field of Mars was expanded to degree and order 10, while both Phobos and Deimos were treated as point masses. The MGM1041C Martian gravity field and the IAU2000 Martian rotation model (Seidelmann et al., 2002) were used for acceleration evaluation. Third body forces were evaluated using the JPL DE406 ephemerides (Standish and Newhall, 1996). The model also includes the tides created on Mars by both moons. The equations of motion were posed in a Cartesian propagator, expressed in planetocentric coordinates. During estimation of their parameters of interest, Lainey et al. (2007) obtained very high residuals. They tried to solve the problem by refining the dynamical model, and they decided to expand the gravity field to the quadrupole. An attempt at using "known" values from Borderies and Yoder (1990) resulted in a further increase in residuals, so they decided to treat these parameters as unknowns and estimate them, with satisfactory results. A footnote suggests that they used the IAU2000 rotation model (Seidelmann et al., 2002) for Phobos as well.

At the same time, Akim et al. (2007) and Shishov (2008) integrated the orbit of Phobos alone. The model expanded the gravity field of Mars to degree and order 8, with coefficients taken from Lemoine et al. (2001). Only two terms - beyond the central force - were used for the gravity field of Phobos: $(l, m) = (2, 0)$ and $(l, m) = (2, 1)$. The coefficients were taken from Martinec et al. (1989). The IAU2000 rotation models (Seidelmann et al., 2002) were used for both Mars and Phobos. The Sun and Deimos were included as third body forces, along with "the planets", although the sources do not give a list. As opposed to Lainey et al. (2007), Akim et al. (2007) and Shishov (2008) do not use Cartesian states to write the equations of motion, but rather pose Lagrange equations of orbital elements (see section 10.2 of Battin (1999)). These sources estimated μ_P and Phobos' secular acceleration.

In 2010, Jacobson (2010) updated his past ephemerides model from 1989 (Jacobson et al., 1989) and, this time, he numerically integrated the equations of motion for both Phobos and Deimos together. He expanded the gravity field of Mars to degree 8 for the zonal harmonics ($m = 0$) and to degree and order 5 to the tesseral harmonics. The coefficients were taken from Konopliv et al. (2006), while the rotation model was *adapted* from the same source (Konopliv et al., 2006) through fits to sine or cosine series. On the other hand, the quadrupole gravity field was used for Phobos, with coefficients taken from Willner et al. (2014). The rotation model for Phobos assumed spin-orbit resonance of the moon, on top of which longitudinal Duxbury-like librations (Duxbury, 1977) were superimposed. The amplitude of these librations were estimated in the source. Third body forces included the Sun, Jupiter, Saturn and the Earth-Moon system, with the JPL DE421 ephemerides (Folkner et al., 2009) for these bodies. The tides produced on Mars by Phobos were also considered, but not those of Deimos as Lainey et al. (2007) did. The equations of motion were posed in Cartesian states expressed in the ICRF reference frame. Jacobson estimated the amplitude of the longitudinal libration - among many other things - and attempted to estimate Phobos' quadrupole coefficients without success, concluding he didn't have enough data to isolate their effects.

A review of the state of the art in ephemerides generation of the Martian moons was performed in 2014 by Jacobson and Lainey (2014), accompanied by yet another integration of the orbits of both Phobos and Deimos. This was intended as an improvement on Jacobson's past integration (Jacobson, 2010). The gravity field of Mars was expanded from degree 8 to degree 10 in the zonal harmonics, and from degree and order 5 to degree and order 6 in the tesseral harmonics. The coefficients and rotation model for the planet were taken from a recent state of the art estimation by Konopliv et al. (2011). Phobos retained its quadrupole gravity field and the same rotation model from 2010 (Jacobson, 2010). This time, however, the libration amplitude was taken from an external source, namely Willner et al. (2010), while the $C_{2,0}$, $C_{2,2}$ and $S_{2,2}$ coefficients were estimated. The same third bodies were used as in the 2010 integration (Jacobson, 2010), but the newer JPL DE424 ephemerides where used this time. A particular aspect of this model, arising from the Martian field taken from Konopliv et al. (2011), is the fact that the $C_{3,0}$ coefficient is time-dependent to account for seasonal ice mass migrations from the Martian poles. Furthermore, this field includes the tides generated on Mars by the Sun. Although it is not explicitly said in the source, it is assumed that they integrate the equations of motion in the same way as in 2010 (Jacobson, 2010), i.e. with ICRF Cartesian states. The source estimates Phobos' quadrupole coefficients, together with its secular acceleration and Mars' tidal parameters. The ephemerides generated in this work are the ones published by JPL as part of their *Planetary Satellite Ephemerides* catalogue (Various, b).

The second half of the 2010's saw a lot of work in the estimation of the Martian gravity and rotation models, as well as on Phobos' own gravity field. This was used by Dirkx et al. (2019). This work was not a standard trajectory integration and parameter fitting process. Rather, the effect of considering different figure-figure effects between Mars and Phobos were studied. The gravity field coefficients were taken from a recent estimation (Genova et al., 2016) and the rotation model was taken from Konopliv et al. (2006). For the gravity field of Phobos, they took the quadrupole estimation of Jacobson and Lainey (2014). A particularity of this work is that the rotation model of Phobos does not follow a spin-orbit assumption anymore, but rather it is the result of the numerical integration of the rotational equations of motion performed by Rambaux et al. (2012). The source does not mention any third body perturbations and, by the extensive study of the F2BP performed in it, it is safe to assume that a purely F2BP was assumed in posing the equations of motion. Although nothing is said in the source, a planetocentric Cartesian propagator is assumed. Their parameter estimation process is also a particular one. They focus on Phobos' quadrupole coefficients and the error incurred in during estimation by neglecting figure-figure effects between Phobos and Mars. They conclude that neglecting figure-figure effects is reasonable for current models because formal errors are way above these model errors. However, they will need to be included in the future, as upcoming technologies will offer much lower formal errors (Dirkx et al., 2014).

The latest integration was performed in 2021 by Lainey et al. (2021). This was intended as an improvement on Lainey's 2007 integration (Lainey et al., 2007), and therefore the orbits of both Phobos and Deimos are integrated simultaneously. The gravity field of Mars was expanded all the way to degree and order 12, with coefficients and rotations taken from Konopliv et al. (2016) (this gravity model is called MRO120D). The rotation model was also taken from Konopliv et al. (2016). Again, a quadrupole gravity field was used for Phobos. Coefficients are computed in the source, but use results from Willner et al. (2014). The rotation model of Phobos, although not explicitly stated in the source, can be inferred to be the same as Jacobson (2010) used. Third bodies include, once again, the Sun, Jupiter, Saturn and the Earth-Moon system but, this time, the recent INPOP19a ephemerides (Fienga et al., 2019) are used, as opposed to the traditional JPL DE series. The effects of third body tides and relativity are included in the model for completeness, although the source states that they are "rather negligible at the current level of accuracy for Mars". The equations of motion were again posed in terms of planetocentric Cartesian states. The source estimates, among others, the amplitude of the longitudinal libration of Phobos.

The characteristics of all the models discussed in this subsection can be found summarized in Table 3.2. Every work after 2010 included the quadrupole gravity field of Phobos, and expansions around degree and order 10 for the Martian gravity seems to be a good approximation as well. Although not said explicitly in many of the sources or in the review we have just done here, it is assumed that all past integrations estimate the initial states of the moon(s); Tolson et al. (1977) and Lainey et al. (2007) make this clear in their works. Beyond that, none of them estimate *everything*, and different authors make different choices on what to estimate. There is good reasons for this. As it so happens, some parameters have the same effect and cannot be determined separately, but rather their combined effect has to be estimated. Otherwise, the estimation problem can't be solved. This is, for example, what Dirkx

encountered (Dirkx et al., 2019) with the degree 2 and degree 4 coefficients of Phobos.

Table 3.2: Numerical models of the ephemerides of Phobos.

Model	Mars			Phobos			Third bodies		Propagator	Estimation
	Deg/Ord	Grav. Mod.	Rot. Mod.	Deg/Ord	Grav. Mod.	Rot. Mod.	Bodies	Eph. Mod.		
Tolson et al. (1977)	???	???	???	???	???	???	???	???	???	μ_P
Peters (1981)	(2,0) & (4,0)	—	—	(2,0) & (4,0)	—	—	m	—	—	—
Lainey et al. (2007)	10/10	MGM1041C	IAU2000	QUAD	Estimated in source	From Seidelmann et al. (2002)	Sun, Jupiter, Saturn, Earth, Moon, Deimos*	JPL DE406	Cartesian (planetocentric)	Phobos' gravity field
Akim et al. (2007) / Shishov (2008)	8/8	From Lemoine et al. (2001)	From Seidelmann et al. (2002)	(2,0) & (2,1)	From Martinec et al. (1989)	From Seidelmann et al. (2002)	Sun, planets, Deimos	JPL DE405	Lagrange equations (orbital elements)	μ_P, Phobos' secular acceleration
Jacobson (2010)	8 (zonal) 5/5 (tesseral)	From Konopliv et al. (2006)	In source, computed from Konopliv et al. (2006)	QUAD	From Borderies and Yoder (1990)	Spin-orbit resonance + longitudinal librations (libration amplitude estimated in source)	Sun, Jupiter, Saturn, Earth, Moon, Deimos*	JPL DE421	Cartesian (ICRF)	$\mathcal{A}$
Jacobson and Lainey (2014)	10 (zonal) 6/6 (tesseral)	From Konopliv et al. (2011)	From Konopliv et al. (2011)	QUAD	Estimated in source	Spin-orbit resonance + longitudinal librations (libration amplitude from Willner et al. (2010))	Sun, Jupiter, Saturn, Earth, Moon, Deimos*	JPL DE424	Cartesian (ICRF)	Phobos' gravity field and secular acceleration.
Dirkx et al. (2019)	Various	From Genova et al. (2016)	From Konopliv et al. (2006)	QUAD	From Jacobson and Lainey (2014)	From Rambaux et al. (2012)	None	—	Cartesian (planetocentric)	—
Lainey et al. (2021)	12/12	MRO120D Konopliv et al. (2016)	From Konopliv et al. (2016)	QUAD	In source, computed from Willner et al. (2014)	Same as Jacobson (2010)	Sun, Jupiter, Saturn, Earth, Moon, Deimos*	INPOP19a	Cartesian (planetocentric)	$\mathcal{A}$

* The model integrates the trajectories of both Phobos and Deimos simultaneously.

3.3. Couplings: the interaction between rotation and translation

It was explicitly stated in Sec. 2.2 that the translational dynamics of Phobos depend on its rotational state through the $\boldsymbol{R}^{(P)}$ term in Eq.(2.21). Similarly, Eq.(2.22) shows that Phobos' rotational dynamics depend on its translational state.

In Sec. 3.1.1, the dependence of translation on rotation was made explicit through the libration amplitude effect on the argument of pericenter (Jacobson, 2010; Lainey et al., 2021). Works used this dependence to infer rotational properties from translational kinematics. Estimation of rotational parameters were sometimes made on a purely rotational basis (Stark et al., 2017; Jacobson et al., 2018). Furthermore, photogrammetric studies required a translational model to contextualize the figure of Phobos and estimate its size and rotation.

In Sec. 3.2.2, a rotational model was required as an input for every single integration (see Table 3.2). It is to be noted that many - if not all - of these models are tightly connected to a translation model. Those who assume spin-orbit resonance force the rotation to follow the translation at all levels - not only for the long trends. Akim et al. (2007) and Shishov (2008) are in a particularly delicate position because their rotation model, which is *fixed* to that of the IAU recommendations, is only compatible with the ephemerides model that it was derived from and might give way to discrepancies if used for the integration of an (in principle) unknown trajectory from a given initial state - which has to be, in any case, compatible with the rotational state. The approaches taken by Lainey et al. (2007, 2021) and Jacobson (2010); Jacobson and Lainey (2014) *at least* allow the rotation to adapt to the orbit. The rotation used by Dirkx et al. (2019) is the numerically integrated one by Rambaux et al. (2012), which is a good approach provided that initial states are compatible.

In Sec. 3.1.2, ephemerides models were required as basis for the integration of the rotational equations of motion (Eq.(2.4)). Rambaux et al. (2012) took the ephemerides from Lainey et al. (2007), which in turn assumed a pure spin-orbit resonance in his numerical model. Rambaux's numerical integration allowed to recover the librational spectrum from Lainey's ephemerides. One could propose a further step and recompute Lainey's ephemerides but using Rambaux's rotational model, then use those ephemerides to recompute the attitude, and so on. The discrepancies that may arise from this assumed rotation/ephemerides are resolved if the trajectory and orientation of Phobos are integrated simultaneously. In fact, Yang et al. (2020) performs a sensitivity analysis of the librational amplitudes to errors in the ephemerides, although in quite a rudimentary way. An offset of 170m in the latter cause the longitudinal libration amplitude to change up to 1.7" (rms) - which translates to a 11cm error at the submartian point - arising only from said longitudinal libration error. The latest ephemerides by Lainey et al. (2021) have uncertainties of up to 1km in 3D space, which would put the errors in the submartian point in the order of meters. Yang et al. (2020) also call for the simultaneous integration of translation and rotation at the same time: "*A simultaneous integration of orbit and rotation [...] will also give a clear answer to this problem.*" - referring to the sensitivity of the librations to changes in the ephemerides.

Besides Yang et al. (2020), no other source appears to assess the sensitivity of Phobos' rotation to its position - or, inversely, of Phobos' translation to its orientation.

4

The estimation problem

In Sec. 1.4, it was mentioned that the dynamical model of Phobos was at the intersection between state propagation - knowing Phobos' location/orientation - and data processing - using data to its fullest. If Ch. 2 described this dynamical model and Ch. 3 covered how propagation is currently performed, the present chapter will cover how data and measurements are used to infer characteristics and properties of, in this case, Phobos.

This is done in what is called the *(parameter) estimation problem*. This problem works on the basis of a mathematical model that, in principle, represents reality. Then, the estimation problem is concerned with computing the parameters of this mathematical model using observations. Although not necessarily so, such a mathematical model is often times a dynamical model, i.e. a model of the dynamics of a body. In the context of the present work, this will always be the case.

The required knowledge to understand an estimation problem, the so-called *normal equations* and concepts on covariance will be provided in the following sections. The author has (loosely) used Montenbruck and Gill (2005) as a basis for this chapter.

4.1. Unweighted least squares

Loosely said, the *least squares problem* is concerned with making a model fit with observations by providing the list or vector of parameters that minimizes the sum of squared distances between the points predicted by the model and the observations. Let's now put some rigor in that explanation.

Consider a model parameterized by n parameters collected in vector $\vec{y}$ and a set of m observations, collected in a vector $\vec{z}$. In trying to emulate the observations, the model is used to compute a set of values - referred to as *model values* by Montenbruck and Gill (2005) - and collected in the vector $\vec{h}$, dependent upon the used $\vec{y}$ vector. If the model was perfect and the observations flawless, it would happen that $\vec{z} = \vec{h}(\vec{y})$. This is sadly not the case, and there will exist discrepancies between the observations and the model's best attempt at emulating them. These discrepancies are usually called *residuals* and collected in a vector $\vec{\varepsilon}$. Note the dimensions: $\vec{y} \in \mathbb{R}^{n\times 1}$ and $\vec{z}, \vec{h}, \vec{\varepsilon} \in \mathbb{R}^{m\times 1}$. The relationship between model values and observations is therefore given in Eq(4.1). Note that the residual vector can be regarded as a function of $\vec{y}$ in itself.

$$\vec{z} = \vec{h}(\vec{y}) + \vec{\varepsilon} \quad \Longrightarrow \quad \vec{\varepsilon}(\vec{y}) = \vec{z} - \vec{h}(\vec{y}) \tag{4.1}$$

The aforementioned *sum of squared distances between the points predicted by the model and the observations* is commonly known as the *cost function* or *loss function*, J. It can be expressed in terms of the vector of residuals as $J = \vec{\varepsilon}^T\vec{\varepsilon}$. In mathematical terms, the aim of the least squares is finding $\vec{y}$ such that J is minimized. The standard procedure is taking the gradient of J with respect to $\vec{y}$ and equating it to $\vec{0}$. The $\vec{y}$ that can be solved for will minimize J. This is done in Eq.(4.2), where the fact that $d(\vec{x}^T\vec{x}) = 2\vec{x}^T d\vec{x}$ has been used. Keeping track of the dimensions, $\vec{z}^T - \vec{h}^T \in \mathbb{R}^{1\times m}$ and $\partial\vec{h}/\partial\vec{y} \in \mathbb{R}^{m\times n}$.

$$\frac{\partial J}{\partial \vec{y}} = 2\vec{\varepsilon}^T\frac{\partial \vec{\varepsilon}}{\partial \vec{y}} = -2\vec{\varepsilon}^T\frac{\partial \vec{h}}{\partial \vec{y}} \quad \Longrightarrow \quad (\vec{z}^T - \vec{h}^T)\frac{\partial \vec{h}}{\partial \vec{y}} = \vec{0} \tag{4.2}$$

The resulting equation is, at least, annoying to solve for $\vec{y}$, given that both $\vec{h}$ and its derivative (may) depend on it. Things simplify a great deal if the model is linear, so that we can write $\vec{h}(\vec{y}) = \boldsymbol{H}\vec{y}$, where $\boldsymbol{H}$ is an m-by-n matrix whose entries are not functions of $\vec{y}$. It is sometimes called the *design matrix* (Fayolle et al., 2022). The problem is then sometimes referred to as a *linear least squares problem* and the derivative of $\vec{h}$ then reduces to $\boldsymbol{H}$ itself. Then, Eq.(4.2) reduces to and is solved as in Eq.(4.3). Note the transposition of the whole equation in the second step.

$$(\vec{z}^T - \vec{y}^T\boldsymbol{H}^T)\boldsymbol{H} = \vec{z}^T\boldsymbol{H} - \vec{y}^T\boldsymbol{H}^T\boldsymbol{H} \quad \Longrightarrow \quad \boldsymbol{H}^T\boldsymbol{H}\vec{y} = \boldsymbol{H}^T\vec{z} \tag{4.3}$$

With $\boldsymbol{H}$ itself not being square, it cannot be inverted. The right-most part of Eq.(4.3) is often called the *normal equations*, and matrix $\boldsymbol{H}^T\boldsymbol{H}$ is known as the *normal matrix*, $\boldsymbol{N}$ (notice that it is a square matrix). This normal equations can be solved by any linear-system solution algorithms (LU factorization, Cholesky decomposition, ...), which is convenient if a machine is used, or by inverting the normal matrix. The solution to the least squares problem posed in Eq.(4.2) reads as in Eq.(4.4).

$$\vec{y} = (\boldsymbol{H}^T\boldsymbol{H})^{-1}\boldsymbol{H}^T\vec{z} \tag{4.4}$$

Sadly, linear least squares problems are hard to come by, and plainly non-existent in astrodynamics. Luckily, every non-linear problem can be linearized around a reference. That is how non-linear least squares problems are solved. Consider a reference parameter vector $\vec{y}_{\text{ref}}$, used by the model to compute a set of reference model values, $\vec{h}_{\text{ref}} = \vec{h}(\vec{y}_{\text{ref}})$. We can then expand the model values about their reference in a first order Taylor series as in Eq.(4.5). This way, the derivative becomes $\boldsymbol{H}$ once again through a convenient notation.

$$\vec{h}(\vec{y}) \approx \vec{h}_{\text{ref}} + \left.\frac{\partial\vec{h}}{\partial\vec{y}}\right|_{\vec{y}=\vec{y}_{\text{ref}}}(\vec{y} - \vec{y}_{\text{ref}}) \quad \Longrightarrow \quad \vec{h}(\vec{y}) = \vec{h}_{\text{ref}} + \boldsymbol{H}\Delta\vec{y} \qquad \text{with} \quad \boldsymbol{H} = \left.\frac{\partial\vec{h}}{\partial\vec{y}}\right|_{\vec{y}=\vec{y}_{\text{ref}}} \tag{4.5}$$

Note that, with this new expression, the residual vector reads $\vec{\varepsilon} = \vec{z} - \vec{h}_{\text{ref}} - \boldsymbol{H}\Delta\vec{y}$. The difference $\vec{z} - \vec{h}_{\text{ref}}$ is sometimes denoted as $\Delta\vec{z}$, given that $\vec{h}_{\text{ref}}$ can be regarded as a "reference value of the observations". Plugging Eq.(4.5) into Eq.(4.2) yields Eq.(4.6).

$$(\vec{z}^T - \vec{h}_{\text{ref}}^T - \Delta\vec{y}^T\boldsymbol{H}^T)\boldsymbol{H} = \Delta\vec{z}^T\boldsymbol{H} - \Delta\vec{y}^T\boldsymbol{H}^T\boldsymbol{H} \quad \Longrightarrow \quad \boldsymbol{H}^T\boldsymbol{H}\Delta\vec{y} = \boldsymbol{H}^T\Delta\vec{z} \tag{4.6}$$

Note the resemblance between the non-linear normal equations - Eq.(4.6) - and the linear normal equations - Eq.(4.3). They are essentially the same, but Eq.(4.6) works with increments from the reference, rather than absolute terms. Eq.(4.6) can be solved in the same way as Eq.(4.3), with linear system solving algorithms if a machine is used, or by inverting $\boldsymbol{H}^T\boldsymbol{H}$. The solution to these non-linear normal equations, call it $\Delta\vec{y}_{\text{lsq}}$, then reads as in Eq.(4.7).

$$\Delta\vec{y}_{\text{lsq}} = (\boldsymbol{H}^T\boldsymbol{H})^{-1}\boldsymbol{H}^T\Delta\vec{z} \tag{4.7}$$

Although it is the solution to the normal equations, Eq.(4.7) is not yet the solution to the non-linear least squares problem. The solution will only be an approximation because the normal equations are an approximation themselves: a linear approximation to the non-linear equations. If we call $\vec{y}_{\text{nl}}$ the actual solution to the non-linear problem, how close $\vec{y}_{\text{lsq}} = \vec{y}_{\text{ref}} + \Delta\vec{y}_{\text{lsq}}$ is to $\vec{y}_{\text{nl}}$ depends on how good the linear approximation is. And the linear approximation is better the closer we are to the reference. This is to say that the closer $\vec{y}_{\text{ref}}$ is to $\vec{y}_{\text{nl}}$ the closer $\vec{y}_{lsq}$ will be to $\vec{y}_{\text{nl}}$ as well. Therefore, an iterative process is usually performed by updating the reference $\vec{y}_{\text{ref}}$ with $\Delta\vec{y}_{\text{lsq}}$ and linearizing around this new reference to find another approximation $\vec{y}_{\text{lsq}}$, which is even closer to $\vec{y}_{\text{nl}}$. The question now lies in when to stop this iteration

The key is to realize that, as $\vec{y}_{\text{lsq}}$ approaches $\vec{y}_{\text{nl}}$, the corresponding cost function will approach its actual minimum, and its gradient will approach $\vec{0}$. For each iteration k, the difference $|J_k - J_{k-1}|$ will be smaller than $|J_{k-1} - J_{k-2}|$. Thus, a tolerance δ is usually established on the cost function and the iterative process is stopped when $|J_k - J_{k-1}| < \delta$.

Caveats are to be kept in mind. It has so far been assumed that the normal matrix is full rank/regular/invertible. However, it may happen that $\boldsymbol{H}^T\boldsymbol{H}$ is (near) singular, with some of its rows/columns being linearly dependent. The problem cannot be solved, and is said to be *ill posed*. The underlying

physics/assumptions should be thoroughly studied to find why this happens. As an example, Dirkx et al. (2019) reported to have encounterednd an ill-posed problem like this when trying to estimate the quadrupole harmonic coefficients together with the libration amplitude of Phobos. Additionally, smoothness has been assumed on the cost function J, such that the stopping criterion makes sense. If J does not "behave well" near its extrema, or its gradient is not even defined, the problem complicates. Luckily, this is hardly ever the case, and it will be safe for us to assume that J is smooth in the domains of interest.

4.2. Weighting

A characteristic of the least squares problem from last section was that all observations had the same informational value, they were all considered equal and, most importantly, they were all considered perfect. This is rarely - rather, never - the case. That is why *weights* are introduced to make some observations and residuals be more important than others and to represent their "imperfections". In particular, the uncertainty associated to each observation is used to scale the corresponding residual. This uncertainty - sometimes referred to as *noise* - is contained in the so-called *standard deviation*, σ. The bigger σ, the more uncertainty the observation has. Observation or *measurement* noise is always to be taken into account, and attention is always paid to them. Clear examples are seen in the works of Lainey et al. (2021) or Jacobson and Lainey (2014), where extensive discussion is presented on the different observation uncertainties. Such a discussion is always assumed to happen, either implicitly or explicitly, in every work.

Residuals are scaled with the inverse of this σ, so that more uncertain observations are less relevant to the problem. The scaling is then done as in Eq.(4.8), using the same nomenclature as in last section. Note that $\boldsymbol{S}^T = \boldsymbol{S}$ and $(\boldsymbol{S}^{-1})^T = \boldsymbol{S}^{-1}$.

$$\vec{\varepsilon}_{\mathrm{w}} = \boldsymbol{S}^{-1}\vec{\varepsilon} \qquad \text{with} \quad \boldsymbol{S} = \mathrm{diag}\{\sigma_i\} \quad \text{and therefore} \quad \boldsymbol{S}^{-1} = \mathrm{diag}\left\{\frac{1}{\sigma_i}\right\} \tag{4.8}$$

With this new definition, the cost function reads as in Eq.(4.9). This new $\boldsymbol{W}^{-1}$ that appears is the so-called *covariance matrix* of the observations. Note that $\boldsymbol{W}^T = \boldsymbol{W}$.

$$J = \vec{\varepsilon}_{\mathrm{w}}^T\vec{\varepsilon}_{\mathrm{w}} = \vec{\varepsilon}^T\boldsymbol{S}^{-1}\boldsymbol{S}^{-1}\vec{\varepsilon} = \vec{\varepsilon}^T\boldsymbol{W}\vec{\varepsilon} \qquad \text{with} \quad \boldsymbol{W} = \boldsymbol{S}^{-2} = \mathrm{diag}\left\{\frac{1}{\sigma_i^2}\right\} \tag{4.9}$$

The weighted least squares problem is that of minimizing this new *weighted cost function*. The procedure is exactly the same as for the unweighted case, but now there is a constant factor in between. The cost minimization equations are posed and solved as in Eq.(4.10). Note that a non-linear problem has been assumed, so that $\vec{\varepsilon} = \Delta\vec{z} - \boldsymbol{H}\Delta\vec{y}$ and $\partial\vec{h}/\partial\vec{y} = \boldsymbol{H}$.

$$\frac{\partial J}{\partial \vec{y}} = -2\vec{\varepsilon}^T\boldsymbol{W}\frac{\partial\vec{h}}{\partial\vec{y}} \quad \Longrightarrow \quad (\Delta\vec{z}^T - \Delta\vec{y}^T\boldsymbol{H}^T)\boldsymbol{W}\boldsymbol{H} = \vec{0} \quad \Longrightarrow \quad \boldsymbol{H}^T\boldsymbol{W}\boldsymbol{H}\Delta\vec{y} = \boldsymbol{H}^T\boldsymbol{W}\Delta\vec{z} \tag{4.10a}$$

$$\Delta\vec{y} = (\boldsymbol{H}^T\boldsymbol{W}\boldsymbol{H})^{-1}\boldsymbol{H}^T\boldsymbol{W}\Delta\vec{z} \tag{4.10b}$$

Note that now the normal matrix is $\boldsymbol{N} = \boldsymbol{H}^T\boldsymbol{W}\boldsymbol{H}$. As can be seen, the observation covariance matrix is used in estimating the parameter vector $\vec{y} = \vec{y}_{\mathrm{ref}} + \Delta\vec{y}$. Furthermore, it is intuitive that an uncertainty in the observations will lead to an uncertainty in the estimated parameters, and the "bigger" the former the "bigger" the latter. The information on this parameter uncertainty is gathered in the *parameter covariance matrix*, $\boldsymbol{P}$, given in Eq.(4.11).

$$\boldsymbol{P} = \boldsymbol{N}^{-1} = (\boldsymbol{H}^T\boldsymbol{W}\boldsymbol{H})^{-1} \tag{4.11}$$

This matrix $\boldsymbol{P}$ will no longer be diagonal, although will still be symmetric. By drawing a parallel with $\boldsymbol{W}$, there is an intuition of what the diagonal terms are: their square roots are the standard deviations of the parameters, often times called *formal errors*. The off-diagonal terms, however, are not as intuitive. They are called *covariances* σ_{ij}, i.e. the term in the i-th row and j-th column is the covariance between

the i-th and j-th entries of the estimated vector. The values of these covariances are not very informative, so a better indicator of this quantity is the so-called *correlation* ρ_{ij} defined in Eq.(4.12).

$$\rho_{ij} = \frac{\sigma_{ij}}{\sigma_i \sigma_j} \tag{4.12}$$

Correlations range always between -1 and 1. If $|\rho_{ij}|$ is close to 1, the i-th and j-th parameters are said to be *correlated*, while if it close to 0 they are said to be *uncorrelated*. High correlations indicate that changes in one parameter can be mimicked by appropriate changes in the other parameter. Thus, high correlations are usually a sign of a poor quality estimation process, where the results are very dependent on each other. On the other hand, low correlations associated to a parameter indicate that the effect such a parameter has on the observation model is quite unique, and can therefore be singled out and its estimation result is valuable.

4.3. Dynamical least squares

So far, the least squares has been considered to be static, i.e. time independent, and the observation equations $\vec{h}$ were also the same form of the parameters $\vec{y}$. Let's now consider, however, another scenario, which can be illustrated by the conveniently relevant example of a Martian rover taking pictures of Phobos. If the geometry of the picture is known - the rover's position, where it is looking at, ... - these pictures can be used to compute, for example, the right ascension and declination of Phobos in *a Martian reference frame*, α and δ. The values of all these α and δ are the *observations*, and are what is collected in the $\vec{z}$ vector. If we have m pictures, then $\vec{z} \in \mathbb{R}^{2m\times 1}$. On the other hand, we have a model for these observations. At the epoch of each picture, the position vector $\vec{r}$ of Phobos in the Martian reference frame can be manipulated to *emulate* the values of the observed α and δ. These values are the *model values*, and they go into the $\vec{h}$ vector. One can argue that the parameter vector will then be an inconveniently long vector composed by the three coordinates of Phobos' position at each epoch: $\vec{y} = [\vec{r}_1^T\ \vec{r}_2^T\ \vec{r}_3^T\ ...\ \vec{r}_m^T]^T \in \mathbb{R}^{3m\times 1}$. Well, yes. But also, no. This model $\vec{h}$ is a dynamical model in the sense that all $\vec{r}$ can be obtained through the integration of some equations $\vec{f}$ - namely Phobos' equations of motion - provided an initial state $\vec{x}_o$. This is nothing other than the dynamical model in Sec. 2.3, where $\vec{x} = [\vec{r}^T\ \vec{v}^T]^T$. All properties of that model can be applied here. In particular, the fact that $\vec{x}_o$ and $\vec{p}$ uniquely determine the evolution of $\vec{x}$. Therefore, our estimation parameter vector $\vec{y}$ - which gathers everything necessary to make the evolution of $\vec{x}$ unique - will contain $\vec{x}_o$ and $\vec{p}$ as in Eq.(4.13).

$$\vec{y} = \begin{bmatrix} \vec{x}_o \\ \vec{p} \end{bmatrix} \qquad \vec{x}_o \in \mathbb{R}^{n_s\times 1} \quad \vec{p} \in \mathbb{R}^{n_p\times 1} \quad \vec{y} \in \mathbb{R}^{n\times 1} \tag{4.13}$$

With all relevant quantities identified, it is time to solve the least squares problem. The question now arises of how to compute $\partial\vec{h}/\partial\vec{y}$. Although there doesn't exist a closed expression for that derivative, there exists a closed expression for $\partial\vec{h}/\partial\vec{x}$, because those are the "manipulations on the state vector" that we mentioned earlier. We can then apply the chain rule as in Eq.(4.14). Note how the notation has been reused to write $\boldsymbol{H} = \partial\vec{h}/\partial\vec{x}$ and how the state transition and sensitivity matrices from Sec. 2.3 arise naturally in the context of the estimation problem.

$$\frac{\partial\vec{h}}{\partial\vec{y}} = \frac{\partial\vec{h}}{\partial\vec{x}}\frac{\partial\vec{x}}{\partial\vec{y}} = \frac{\partial\vec{h}}{\partial\vec{x}}\begin{bmatrix} \frac{\partial\vec{x}}{\partial\vec{x}_o} & \frac{\partial\vec{x}}{\partial\vec{p}} \end{bmatrix} \quad \Longrightarrow \quad \frac{\partial\vec{h}}{\partial\vec{y}} = \boldsymbol{H}\begin{bmatrix} \boldsymbol{\Phi} & \boldsymbol{S} \end{bmatrix} \tag{4.14}$$

This expression poses a problem when introducing it into Eq.(4.10a). The state transition and sensitivity matrices are functions of time, and therefore cannot be plugged directly into any other part of the estimation problem. We can particularize them at some epoch, but then the normal equations become epoch-dependent. Luckily, this can be fixed by a mere *re-writing* of the cost function.

The process we have followed so far is perfectly valid in itself, only the problem is it can only apply for observations at a single epoch. We can use that fact to try to write the whole least squares problem for all epochs in terms of smaller least squares problems that apply to each observation epoch. In particular, the cost function of the whole problem can be written as the *sum* of "per-epoch" cost functions, such as in Eq.(4.15), where subindex e stands for "epoch". Each of these per-epoch problems will have a number

m_e of observations. Note that this per-epoch definition of the total cost function is exactly identical to the one we have been using so far.

$$J_e = \vec{\varepsilon}_e^T \boldsymbol{W}_e \vec{\varepsilon}_e \quad \Longrightarrow \quad J = \sum_e J_e = \sum_e \vec{\varepsilon}_e^T \boldsymbol{W}_e \vec{\varepsilon}_e \tag{4.15}$$

We can now follow the exact same procedures as in Sec. 4.1 and 4.2, assuming a non-linear model and with the same notation as in this section. The derivative in Eq.(4.2) can still be taken on Eq.(4.15), only that it will apply term by term. And inside each individual term, we can use the result in Eq.(4.14). This procedure is presented in Eq.(4.16). Note that the terms $\vec{y}$ and $\Delta\vec{y}$ is the same *for all epochs*, as it contains the initial conditions and dynamical parameters.

$$\begin{gathered}
\frac{\partial J}{\partial \vec{y}} = \sum_e 2\vec{\varepsilon}_e^T \boldsymbol{W}_e \frac{\partial \vec{\varepsilon}_e}{\partial \vec{y}} = -2 \sum_e \vec{\varepsilon}_e^T \boldsymbol{W}_e \frac{\partial \vec{h}}{\partial \vec{y}} \\
\sum_e \vec{\varepsilon}_e^T \boldsymbol{W}_e \frac{\partial \vec{h}}{\partial \vec{y}} = \vec{0} \quad \Longrightarrow \quad \sum_e (\Delta\vec{z}_e - \boldsymbol{H}_e \begin{bmatrix} \boldsymbol{\Phi}_e & \boldsymbol{S}_e \end{bmatrix} \Delta\vec{y})^T \boldsymbol{W}_e \boldsymbol{H}_e \begin{bmatrix} \boldsymbol{\Phi}_e & \boldsymbol{S}_e \end{bmatrix} = \vec{0} \\
\sum_e \begin{bmatrix} \boldsymbol{\Phi}_e & \boldsymbol{S}_e \end{bmatrix}^T \boldsymbol{H}_e^T \boldsymbol{W}_e \boldsymbol{H}_e \begin{bmatrix} \boldsymbol{\Phi}_e & \boldsymbol{S}_e \end{bmatrix} \Delta\vec{y} = \sum_e \begin{bmatrix} \boldsymbol{\Phi}_e & \boldsymbol{S}_e \end{bmatrix}^T \boldsymbol{H}_e^T \boldsymbol{W}_e \Delta\vec{z}_e \quad \Longrightarrow \quad \boldsymbol{N}\Delta\vec{y} = \vec{b} \\
\text{with} \quad \boldsymbol{N} = \sum_e \begin{bmatrix} \boldsymbol{\Phi}_e & \boldsymbol{S}_e \end{bmatrix}^T \boldsymbol{H}_e^T \boldsymbol{W}_e \boldsymbol{H}_e \begin{bmatrix} \boldsymbol{\Phi}_e & \boldsymbol{S}_e \end{bmatrix} \quad \text{and} \quad \vec{b} = \sum_e \begin{bmatrix} \boldsymbol{\Phi}_e & \boldsymbol{S}_e \end{bmatrix}^T \boldsymbol{H}_e^T \boldsymbol{W}_e \Delta\vec{z}_e
\end{gathered} \tag{4.16}$$

As can be seen, the resulting normal equations are the *accumulated* normal equations over all epochs. It is again intuitive that uncertainty in the observations will somehow translate into uncertainty in the estimated parameters. The parameter covariance matrix associated to these accumulated normal equations turns out to be the same as that for the regular case, i.e. the inverse of the normal matrix, Eq.(4.17).

$$\boldsymbol{P} = \boldsymbol{N}^{-1} \tag{4.17}$$

The presented method for solving a dynamical least squares problem is known as a *batch* least squares estimation. This is only one of the many methods that exist to solve such a problem - the most popular of which might be a Kalman filter - but their discussion is outside of the scope of this work.

4.4. Consider parameters and a priori information

The discussion so far has neglected very likely scenarios that often occur in real life. On the one hand, it is usually - if not always - that some (constant) parameters in out model that we consider known have some uncertainty associated to them. These are the so-called *consider parameters*. Their uncertainty will combine with the observation noise and result in an increased uncertainty of the estimated parameters. Although this might seem like a bad thing - because it is - it is also a real thing, and if a study is to be valuable it should consider this fact. Sometimes this uncertainty is very small and can be neglected; other times it is a source of estimation uncertainty even bigger than observation noise. On the other hand, we usually know things about the parameters we want to estimate, usually an a-priori value and some uncertainty about it. In some cases, we have an a-priori value for the whole vector and a full covariance matrix, obtained for example from a past estimation. It is then good practice to include this information into the present estimation. This section will focus on these two topics.

4.4.1. Consider parameters

Consider parameters are those whose values are *known* but with some uncertainty. If we gather these parameters in a vector $\vec{c}$ and define the associated covariance matrix $\boldsymbol{C}$, we will answer the following question: how does this $\boldsymbol{C}$ affect the estimation covariance matrix $\boldsymbol{P} = \boldsymbol{N}^{-1}$?

We start by linearizing the observation equation $\vec{h}(\vec{y}, \vec{c})$ around reference estimation and consider parameter vectors and writing the residuals with this linearization, as in Eq.(4.18a). Then, we recover the first bit of Eq.(4.10a) and we minimize the cost function, noting that $\partial\vec{\varepsilon}/\partial\vec{y} = -\boldsymbol{H}_y$, as in Eq.(4.18b).

$$\vec{h} \approx \vec{h}_{\text{ref}} + \boldsymbol{H}_y \Delta\vec{y} + \boldsymbol{H}_c \Delta\vec{c} \quad \Longrightarrow \quad \vec{\varepsilon} = \vec{z} - \vec{h} = \Delta\vec{z} - \boldsymbol{H}_y \Delta\vec{y} - \boldsymbol{H}_c \Delta\vec{c} \tag{4.18a}$$

$$\frac{\partial J}{\partial \vec{y}} = -2(\Delta\vec{z} - \boldsymbol{H_y}\Delta\vec{y} - \boldsymbol{H_c}\Delta\vec{c})^T \boldsymbol{W}\boldsymbol{H_y} \tag{4.18b}$$

Equating Eq.(4.18b) to $\vec{0}$ yields the normal equations of Eq.(4.19). Note that this solution only deviates from the result in Eq.(4.10a) if the consider parameters deviate from the established reference.

$$\boldsymbol{N}\Delta\vec{y} = \boldsymbol{H_y}^T\boldsymbol{W}(\Delta\vec{z} - \boldsymbol{H_c}\Delta\vec{c}) \qquad \text{with} \quad \boldsymbol{N} = \boldsymbol{H_y}^T\boldsymbol{W}\boldsymbol{H_y} \tag{4.19}$$

If we solve for $\Delta\vec{y}$, we can write $\Delta\vec{y} = \boldsymbol{A}\Delta\vec{z} + \boldsymbol{B}\Delta\vec{c}$, where $\boldsymbol{A} = \boldsymbol{N}^{-1}\boldsymbol{H_y}^T\boldsymbol{W}$ and $\boldsymbol{B} = -\boldsymbol{N}^{-1}\boldsymbol{H_y}\boldsymbol{W}\boldsymbol{H_c}$. The covariance associated to $\vec{y}$ will then be given as in Eq.(4.20).

$$\boldsymbol{P} = \boldsymbol{A}\boldsymbol{W}^{-1}\boldsymbol{A}^T + \boldsymbol{B}\boldsymbol{C}\boldsymbol{B}^T \quad \Longrightarrow \quad \boldsymbol{P} = \boldsymbol{N}^{-1} + (\boldsymbol{H_y}^{-1}\boldsymbol{H_c})\boldsymbol{C}(\boldsymbol{H_y}^{-1}\boldsymbol{H_c})^T \tag{4.20}$$

A more popular form of the covariance matrix in Eq.(4.20) - the one presented in Eq.(8.42) of Montenbruck and Gill (2005) or Eq.(19) of Dirkx et al. (2014) - can be seen in Eq.(4.21), where $\boldsymbol{P_o} = \boldsymbol{N}^{-1}$, and, by inversion of $\boldsymbol{N}$ in Eq.(4.20), $\boldsymbol{P_o} = \boldsymbol{H_y}^{-1}\boldsymbol{W}^{-1}\boldsymbol{H_y}^{-T}$.

$$\boldsymbol{P} = \boldsymbol{P_o} + \boldsymbol{H_y}^{-1}(\boldsymbol{H_c}\boldsymbol{C}\boldsymbol{H_c}^T)(\boldsymbol{H_y}^{-1})^T \quad \Longrightarrow \quad \boldsymbol{P} = \boldsymbol{P_o} + (\boldsymbol{P_o}\boldsymbol{H_y}^T\boldsymbol{W})(\boldsymbol{H_c}\boldsymbol{C}\boldsymbol{H_c}^T)(\boldsymbol{P_o}\boldsymbol{H_y}^T\boldsymbol{W})^T \tag{4.21}$$

Study of the uncertainty generated by consider parameters is usually called *consider covariance analysis*. As important as this might seem, it is interesting that very few sources mention consider covariance in their work. Sometimes uncertainty in model parameters is mentioned lightly and superficially, as Jacobson (2010) did, and one can venture to assume they take this aspect into account. Other times it is explicitly stated that a consider covariance analysis is carried out and the consider parameters are discussed, as done by Tolson et al. (1977). Other sources just don't mention consider covariance at all. Consider covariance can be used to determine how errors in model parameters translate into errors in estimated parameters, namely through Eq.(4.20) or Eq.(4.21). This serves to compare the impact of different sources of errors in the uncertainty of the estimated parameters. Such a study was carried out by Dirkx et al. (2014) and the results were used by Dirkx et al. (2019) to assess whether errors arising from unmodelled figure-figure effects would be bigger than measurement errors from Phobos laser ranging.

4.4.2. A priori information

In this subsection we will have an a priori estimation vector, $\vec{y}_{\text{apr}}$, and the associated (symmetric) covariance matrix $\boldsymbol{\Lambda}^{-1}$. The approach here is to construct an alternative cost function so that we try to minimize both the residuals and the difference between our a priori estimation and the solution of the current one. Such a cost function is given in Eq.(4.22), were the increments are measured from $\vec{y}_{\text{ref}}$. Note that each component of the a priori vector is scaled so that elements with less uncertainty are worth more.

$$J = (\vec{y} - \vec{y}_{\text{apr}})^T\boldsymbol{\Lambda}(\vec{y} - \vec{y}_{\text{apr}}) + \vec{\varepsilon}^T\boldsymbol{W}\vec{\varepsilon} = (\Delta\vec{y} - \Delta\vec{y}_{\text{apr}})^T\boldsymbol{\Lambda}(\Delta\vec{y} - \Delta\vec{y}_{\text{apr}}) + \vec{\varepsilon}^T\boldsymbol{W}\vec{\varepsilon} \tag{4.22}$$

In taking the gradient, note that Eq.(4.10a) computes the gradient of the second term, while the gradient of the first term is trivial. The minimization process and the resulting normal equations are gathered in Eq.(4.23).

$$\frac{\partial J}{\partial \vec{y}} = 2(\Delta\vec{y} - \Delta\vec{y}_{\text{apr}})^T\boldsymbol{\Lambda} - 2(\Delta\vec{z} - \boldsymbol{H}\Delta\vec{y})^T\boldsymbol{W}\boldsymbol{H} \quad \Longrightarrow \quad \boldsymbol{\Lambda}(\Delta\vec{y} - \Delta\vec{y}_{\text{apr}}) - \boldsymbol{H}^T\boldsymbol{W}(\Delta\vec{z} - \boldsymbol{H}\Delta\vec{y}) = \vec{0} \tag{4.23a}$$

$$(\boldsymbol{\Lambda} + \boldsymbol{H}^T\boldsymbol{W}\boldsymbol{H})\Delta\vec{y} = \boldsymbol{\Lambda}\Delta\vec{y}_{\text{apr}} + \boldsymbol{H}^T\boldsymbol{W}\Delta\vec{z} \tag{4.23b}$$

Note that, contrary to the case of consider parameters, the solution now changes even if $\Delta\vec{y}_{\text{apr}} = \vec{0}$. The covariance matrix is computed in a similar way as for consider parameters, writing $\Delta\vec{y} = \boldsymbol{A}\Delta\vec{y}_{\text{apr}} + \boldsymbol{B}\Delta\vec{z}$. After the algebra, the resulting covariance matrix is gathered in Eq.(4.24), which turns out to be the inverse of the normal matrix of these normal equations with a priori information.

$$\boldsymbol{P} = (\boldsymbol{\Lambda} + \boldsymbol{H}^T\boldsymbol{W}\boldsymbol{H})^{-1} \tag{4.24}$$

Interestingly enough, examples of the use of a-priori information are hard to find in the literature - at least in the relevant literature for this text - be it because it does not happen or because it is not explicitly stated in the sources. Past results are usually presented - like Jacobson (2010) does for example - but their role seems to be mostly comparative. One source has been found, however, that not only mentions but also discusses the use of a-priori information, giving a thorough list of the parameters they estimate and their a-priori covariance, namely Dirkx et al. (2014).

4.5. Dynamics absorption and residual analysis

The description of Phobos' dynamics that is used in estimation problems is not perfect. It never will. It is intuitive to think that this will make the estimation results not be perfect. That is to say that the unmodelled/mismodelled terms will change the estimated parameters, which will adapt to still minimize the cost function. In this sense, the estimated parameters will try as much as they can to emulate the effect of the unmodelled/mismodelled terms so that observations are replicated as best as possible and residuals are as close to 0 as possible - which is what is sought by minimizing their summed squares. When this happens, the estimated parameters are said to *absorb* the mismodelled terms. If this absorption was *perfect*, the estimated parameters alone could identically replicate the mismodelled terms, all residuals would be 0, and we would never know there are unmodelled terms. We wouldn't even need to know that.

Such a thing, however, never happens, and absorption always occurs partially, at best. Then, some of the mismodelled terms are absorbed by the estimated parameters, while the remaining part is still left mismodelled and contributes to the residuals. Residuals are therefore a window to those mismodelled terms - or the part thereof - that are not absorbed by estimated parameters. To better understand how absorption works and how residuals can be used to improve a model, we will use a simple yet illustrative example.

Consider the *reality* model in Eq.(4.25), which will provide the observations. Here, $a_o = 3$, $b_o = 1$, $A_o = 2$ and $\omega_o = 0.4$.

$$z(t) = a_o + b_o t + A_o \sin(\omega_o t) \tag{4.25}$$

This reality model is actually unknown, and we will propose our own model to replicate reality. In a first approach, we assume a linear function as in Eq.(4.26), where a and b are yet unknown and are the parameters we will try two estimate using least squares.

$$h(t) = a + bt = \boldsymbol{H}(t)\vec{y} \qquad \text{where } \boldsymbol{H}(t) = [1 \;\; t] \quad \text{and } \vec{y} = [a \;\; b]^T \tag{4.26}$$

We can collect the value of the observations and model values at each epoch in vectors, so that the vector of residuals is given as in Eq.(4.27). Here, each row of $\boldsymbol{H}$ is the per epoch $\boldsymbol{H}(t)$ from Eq.(4.26) particularized at each epoch.

$$\vec{\varepsilon} = \vec{z} - \boldsymbol{H}\vec{y} \tag{4.27}$$

Note that the residuals in this equations are given in the same way as in Eq.(4.1) with $\vec{h} = \boldsymbol{H}\vec{y}$. Thus, the normal equations read as in Eq.(4.3). Solving these, we find that $a = 3.1094467$ and $b = 0.9995870$, as opposed to $a = a_o = 3.0$ and $b = b_o = 1.0$. This means that a tiny part of the sine can be absorbed by a and b, while the rest will go into the residuals. Fig.[4.1a] shows a comparison between the model values computed with the estimated a and b and the observations. It is obvious that the oscillations are lost in the estimation. On the other hand, Fig.[4.1b] shows the time series of the residuals[1] computed with the estimated parameters in $\vec{h}$. Here we can see that even at $t = 0$, where the unmodelled sine is 0, we have a residual. This arises from the difference between a and a_o.

A periodic evolution is observed in the residuals in Fig.[4.1b], which indicates that we have left some sinusoidal term unmodelled. A Fourier transform of this signal will provide insight on its frequency components. It's decomposition is showed in Fig.[4.1c], where a strong amplitude for a frequency *below* 0.4 rad/s. It was numerically checked to correspond to $\omega \approx 0.37$ rad/s. However, all frequencies in the shown range - between 0 rad/s and 1.4 rad/s - are also present. The question might arise of why is the peak not at 0.4 rad/s and why are the other frequencies present.

[1] Residuals computed in this manner are known as *post fit* residuals, as they are computed after the model fit to observations and with the estimated parameters.

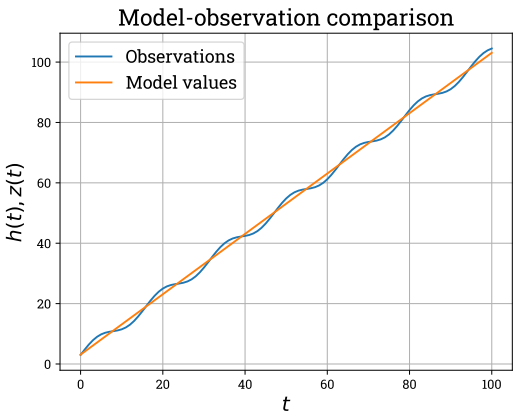

(a) Comparison between observations and model values

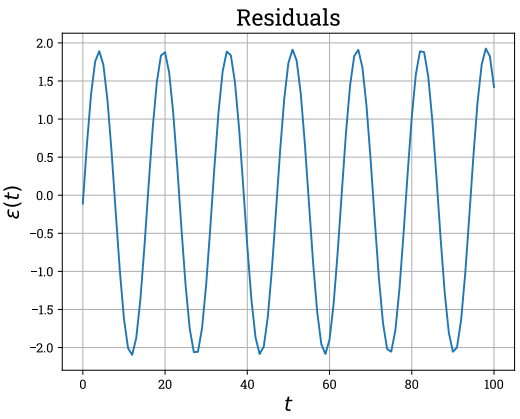

(b) Residuals

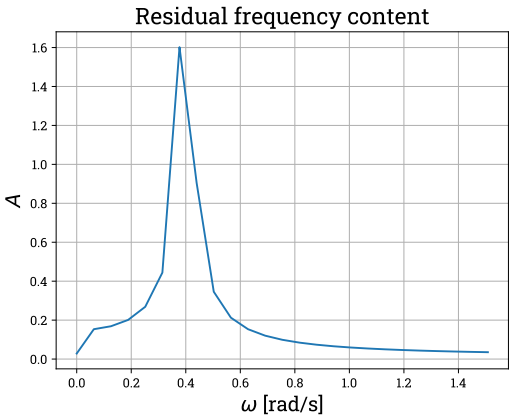

(c) Residual frequency content for a linear fit

Figure 4.1: Results of the estimation with a linear fit

We can answer in a quantitative manner by looking at the equation for the residual, namely Eq.(4.28), where we have written $\Delta a = a_o - a$ and $\Delta b = b_o - b$. The residuals follow this equations, rather than just a pure sinusoid. A constant and secular terms are also present in this expression and contaminate the Fourier transform of the pure sine.

$$\varepsilon(t) = z(t) - h(t) = a_o + b_o t + A_o \sin(\omega_o t) - a - bt = \Delta a + \Delta b t + A_o \sin(\omega_o t) \tag{4.28}$$

By *mis-estimating* a and b such that $\Delta a, \Delta b \neq 0$, the frequency content of the observations - of *reality* - is masked and contaminated. This effect is particularly relevant when the original signal has some frequency component that was not included in the estimation model, like it happened in this case where we left the sine out of the estimation model. For the case of Phobos, this is very much the case when modelling its rotation, which is often represented by the spin-orbit resonance plus the once-per-orbit longitudinal libration, while all other frequencies are disregarded.

Nevertheless, remember that we in principle don't know the real model $z(t)$, so these contaminated residuals are the only thing we have to follow with the investigation. Thus, we can build a new, improved model as in Eq.(4.29) to try to estimate this new sine component, where $\omega = 0.37$.

$$h(t) = a + bt + A \sin(\omega t) \tag{4.29}$$

The estimation can be carried out in two ways. In a first approach, we reuse the previous results of a and b to try and estimate A, meaning this is a *partial* estimation. On a second approach, we estimate all three parameters at the same time, so we perform a *complete* estimation. The estimation result for both choices is collected Table 4.1, and the residuals are shown in Fig.[4.2].

Table 4.1: Result of both estimation approaches

Parameter	Partial	Complete
a	3.1094467	3.1007425
b	0.9995870	0.9997576
A	0.0562082	0.0570707

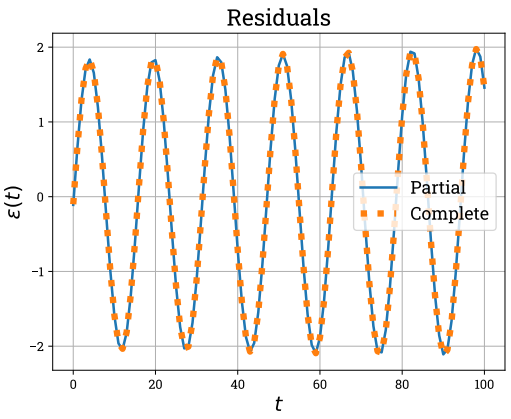

Figure 4.2: Residual signal for both estimation approaches

The estimated parameters are slightly closer to their *real* values in the complete estimation, but the residuals don't improve at all. This inability to reduce residuals lies in the fact that the assumed frequency for the sine was wrong.

This example is a simple one that illustrates the principles of absorption and residual analysis. However, notice that we did *not* use a dynamical model - something like what is seen in Eq.(2.25) - and we did not need the state transition or sensitivity matrices to build the normal equations. The impact of our estimated parameters on both $\vec{h}$ and $\vec{\varepsilon}$ was straightforward and the concept of initial conditions plays no role in this model. Phobos' dynamics add one layer of difficulty because the effect of parameters on $\vec{h}$ is not direct - the impact that Phobos' $C_{2,0}$ has on its position is anything but trivial - and the residual analysis requires some knowledge of the situation. Furthermore, working with a dynamical model makes your estimation involve both initial conditions and dynamical parameters, and an additional layer of interest appears when the former can absorb effects of the latter - and viceversa. All this only extends to a theoretical setup, but real life observations have errors and uncertainty associated to them, which are also partially absorbed by the estimated quantities.

However, the basis of mismodelling errors being absorbed by parameters that was depicted by the presented example, and the fact that it is residuals that can aid in improving the dynamical model, still stand in real life applications.

The phenomenon of absorption is present in any estimation problem and examples of their discussion are countless. In the context of the dynamics of the Galilean moons, Lainey et al. (2004) suggest that the oblateness of the satellites can be absorbed into the oblateness of the central body. In this same context, Dirkx et al. (2016) explore the possibility of using several different absorptions to come up with a minimal model that, with as few parameters as possible, can faithfully emulate the complex dynamics of the Jovian system. In a more relevant scenario, Dirkx et al. (2019) find that figure-figure effects in the Mars-Phobos system can be efficiently absorbed by Phobos' degree 4 coefficients. A prior work by Lainey et al. (2007) mentions that observational errors and uncertainties associated to the relative position between the two Martian satellites can be absorbed by the dynamics of one of them.

Along another line, absorption is often times used purposefully, in particular in the context of Earth orbiters, where the concept of *empirical accelerations* is used. These are artificial dynamical parameters that are introduced in a model and estimated with the only aim of absorbing mismodellings that occur in the highly uncertain environment of Earth's orbit.

5

Future work

So far, the key theoretical concepts have been thoroughly explained and all relevant literature has been deeply examined. An inconsistency was discovered between the actual dynamical behaviour of Phobos and the way it is presently studied. Sec. 2.4 clearly presented translational and rotational dynamics that affect each other: orientation affects accelerations, position affects torques. However, these facts are ignored in the study of Phobos' motion, as seen in Ch. 3 and explicitly stated in Sec. 3.3. The subsequent thesis will aim to cover this yet uncovered ground. This chapter will discuss the specifics of this thesis.

5.1. Research questions and answer approach

The aim of this thesis will be to explore the couplings between Phobos' translational and rotational motion. The findings of this "exploration" will be a quantitative description of the effect that (not) modelling these couplings has on different aspects and products of Phobos' dynamical model. For this, it is intuitive to think that the differences between a coupled and an uncoupled model will have to be examined. We will set-up this exploration as an effort to answer a question - which will serve as the research question for the upcoming thesis - and which will be the higher level question of two lower level subquestions. These question/subquestions are:

- To what extent can an uncoupled dynamical model of Phobos' translation and rotation emulate a coupled dynamical model?
  - How well can an uncoupled estimation model of Phobos' translation and rotation extract information from a coupled dynamical model?
  - How could a coupled model improve the current state of the art results?
  - To what extent are initial conditions transferable between models?

The first subquestion will be a direct assessment of the state-of-the-art estimation scheme. As seen in Ch. 3, uncoupled models are used to estimate parameters from real observations - which are provided by inherently coupled dynamics. The couplings in the *real* model will, to some extent, be absorbed into the parameters estimated by the uncoupled model (see Sec. 4.5). These parameters can however not absorb all of them, and the leftover effects will go into the residuals - that would otherwise be 0 if all the couplings could be absorbed into parameters. Answering the first subquestion will provide a quantitative measure of what couplings can be absorbed by what (combinations of) parameters.

The second subquestion can be regarded as a follow up of the first. It will be the first look into the potential of a coupled model to minimize absorption of couplings into estimated parameters and, consequently, bring residuals as close to 0 as possible. On the one hand, this will give a measure of the extent to which a coupled model can *fix* the deficiencies of the uncoupled model, when such a technique is required and in what cases the uncoupled model suffices. Furthermore, comparing the estimation results between the coupled and uncoupled models will help quantify the contribution of unmodelled couplings to residuals, which will in turn allow to single out the contribution of other mismodellings, such as higher spherical harmonics that were left unmodelled or accelerations/torques that were not considered at all.

The third subquestion represents a limiting case. Assuming everything else is perfect - i.e. dynamical parameters and initial conditions are known to infinite precision - the aim is to quantify the differences in Phobos' trajectory and orientation between integration with a coupled model and integration with an uncoupled model. Answering this question may put constraints on the usefulness of certain initial conditions, or provide different sets of initial conditions to use depending on the model they are to be used with.

5.2. Thesis outline

The previous section explained what answering the presented question/subquestions could bridge the gap identified in Ch. 3. This section will cover what has to be done to answer said question/subquestions.

5.2.1. The tasks

For this, consider the models listed below. The reasons for the choices in harmonic coefficients will be explained later in this section.

- **Model A:** Uncoupled model. Mars' gravity field is expanded to degree and order 12. Phobos' gravity field is represented by the $C_{2,0}$ and $C_{2,2}$ coefficients.
- **Model B:** Coupled model. Mars' gravity field is expanded to degree and order 12. Phobos' gravity field is represented by the $C_{2,0}$ and $C_{2,2}$ coefficients.
- **Model C:** Coupled model. Mars' gravity field is expanded to degree and order 12. Phobos' gravity field is expanded to degree and order 4.

The first subquestion can be answered by using model A to estimate parameters from observations[1] generated by model B. The difference between these two models lies only in the couplings. The results of these estimation - both in terms of estimated parameters and residuals - will represent a direct quantification of leaving the couplings unmodelled.

The second subquestion requires a scenario that resembles reality a bit more. Furthermore, a model used to estimate its own parameters will return - or *should* return - the same inputs it was given, so although useful for validation it is not an interesting exercise. A third model is therefore required. This question will be answered by using both models A and B to estimate parameters from observations generated by model C. This time, parameters estimated by model A will absorb both the unmodelled couplings and the unmodelled higher harmonics. The parameters estimated by model B will only absorb the latter. Thus, comparing the results of both models will provide a measure of how much improvement a coupled model can provide over an uncoupled model in a situation in which the dynamics are not perfectly modelled by either of them.

The choices for the spherical harmonics included in each model are not arbitrary. On the one hand, models A and B will be used as estimation models. As was seen in Ch. 3, the quadrupole field was the most popular way of representing Phobos' gravity field. Furthermore, Dirkx et al. (2019) explains that these two coefficients are "of prime interest for geophysical analyses", and a Phobos lander will allow their estimation down to the 9^{th} decimal place. Including more terms was deemed unnecessary if their estimation is not relevant. On the other hand, model C will not be used for estimation and also requires to have more complete dynamics than models A and B. Higher harmonics of Phobos have not yet been used in estimation or propagation efforts, but rather their theoretical values attending to an assumed internal composition have been computed from shape models. The only exception to this is when Dirkx et al. (2019) tried to estimate Phobos' harmonic coefficients up to degree and order 4 and found an ill-posed problem due to the identical way in which $C_{2,0}$ and $C_{4,0}$ manifest in the dynamics. Thus, restricting Phobos' gravity field at degree and order 4 is expected to provide sufficient value while keeping computational time as low as possible. Finally, for Mars' gravity field, a maximum degree and order 12 was selected because it is the one used in the most recent propagation - that of Lainey et al. (2019). Nevertheless, these choices are susceptible to change if they are found to be insufficient or unnecessary during the thesis.

Finally, it would be convenient to have a preliminary plan of what kind of simulations will be run and, more specifically, to define what the "observations" generated with models B and C will look like,

[1] When an *observation* is generated using a simulation rather than from real life experiments - telescopes, ranges, Doppler, ... - they are called *simulated* observations. These observations don't have any kind of observational uncertainty or error - no aberration to correct for, no light time, ... - and are therefore said to be *ideal*.

and what parameters models A and B will be made to estimate. For this, it will be key to have in mind that the uncoupled model described above, model A, will be inherently composed of 2 sub-models:

- **Sub-model A1:** It is a translational model that uses an assumed a-priori rotation of Phobos to integrate the translational EOMs (the upper half of Eq.(2.33a)).
- **Sub-model A2:** It is a rotational model that uses the assumed a-priori ephemerides of Phobos to integrate the rotational EOMs (the lower half of Eq.(2.33a)).

The parameters to be estimated are those that were found important in Ch. 3 and can appear in any of the presented models. These are $C_{2,0}$, $C_{2,2}$ and $\mathcal{A}$. Furthermore, all estimation runs will be used to estimate the corresponding initial condition. On the other hand, the observations that will be used - besides being ideal - can be separated in two groups:

- **Position:** These are ideal observations of the position of Phobos in the form of the position vector $\vec{r}$. They resemble currently available observations.
- **Orientation:** These are ideal observations of the orientation of Phobos in the form of Euler angles (see App. C), more specifically the 3-1-3 Euler angles. These observation do not currently exist because Phobos' orientation has only been observed through photography of a Mars orbiter (see Sec. 3.1) and had to be estimated together with its shape. However, a Phobos lander equipped with a start-tracker can provide direct observations of Phobos' orientation.

Combining these observations with suitable models and estimated parameters is not trivial. To begin with, note that $\mathcal{A}$ does not appear in the coupled model at all. Thus, its estimation cannot be performed with such a model. A table containing what parameters can be estimated attending to the combination of model and observations used is presented in Table 5.1. Notice how $\mathcal{A}$ can only be estimated with a very specific combination of model/observation. And even in this case, there is a caveat. For this to be possible, the *assumed a-priori rotation of Phobos* from model A1 needs to be described in such a way that $\mathcal{A}$ appears explicitly in it. Otherwise, the sensitivity matrix term $\partial\vec{f}/\partial\mathcal{A}$ cannot be defined.

Table 5.1: Parameters that each model (columns) can estimate using each type of observations (rows).

	A1	**A2**	**B**
Position	$C_{2,0}$, $C_{2,2}$, $\mathcal{A}$	—	$C_{2,0}$, $C_{2,2}$
Orientation	—	$C_{2,0}$, $C_{2,2}$	$C_{2,0}$, $C_{2,2}$

Estimation runs will be performed to estimate the harmonic coefficients when possible, the libration amplitude when possible, and all three at the same time when possible. The latter is only doable with model A1. There is an alternative way of "estimating" $\mathcal{A}$ using orientation observations. Note that such observations are basically a time series of the Euler angles, which can be very well be written as explicit functions of time $\theta(t)$. These functions will present a certain frequency content, and performing a Fourier analysis of these functions can provide the same insight that Rambaux et al. (2012) presents in his work, namely Phobos' librational spectrum.

A list of the specific dynamical least squares problems that will be inverted, with the observation type (position/orientation), estimation model (A1/A2/B) and estimated parameters ($C_{2,x}$/$\mathcal{A}$/both), is given below.

- **Alpha:** Position, A1, $C_{2,x}$
- **Bravo:** Position, A1, $\mathcal{A}$
- **Charlie:** Position, A1, both
- **Delta:** Position, B, $C_{2,x}$
- **Echo:** Orientation, A2, $C_{2,x}$
- **Foxtrot:** Orientation, B, $C_{2,x}$

Estimations *Alpha*, *Bravo*, *Charlie* and *Echo* will be run once using observations generated by model B. They will provide the answer to the first subquestion when their results are compared to the *real* parameters used to generate the observations. The value of $\mathcal{A}$ will be compared to what is obtained

from the frequency analysis of the orientation obtained with model B. Then, all estimations, from *Alpha* to *Foxtrot*, will be run using observations generated by model C, and analysis and comparison of their results will provide the answer to the second subquestion.

We have so far not concerned ourselves with the *assumed a-priori* rotation and translation of models A1 and A2 respectively. It is now a good point to do so. To this respect, it has been decided to follow the approach that it is currently used in literature. The assumed rotation for model A1 will be the one used by Lainey et al. (2021), namely a spin-orbit resonance together with a once-per-orbit libration. Then, following the approach by Rambaux et al. (2012), these ephemerides will be used as assumed translation for model A2.

Lastly, we still need an outline of how we will answer the third subquestion. For a clearer view of what it will entail, consider a translational state $\vec{x}_t$ and a rotational state $\vec{x}_r$. In a coupled model, they are integrated simultaneously, while in an uncoupled model integration of the former requires an a-priori model of the latter, and vice-versa. With their derivatives and dynamical parameters being the same between the coupled and uncoupled models, the solution of the uncoupled model is completely defined by the choice of initial conditions and the a-priori models for each state. This is illustrated in Eq.(5.1).

$$\dot{\vec{x}}_t = \vec{f}_t\left(\vec{x}_t, \vec{x}_r; \vec{p}\right) = \vec{f}_t\left(\vec{x}_{t,o}, \vec{x}_r\right) \tag{5.1a}$$

$$\dot{\vec{x}}_r = \vec{f}_r\left(\vec{x}_t, \vec{x}_r; \vec{p}\right) = \vec{f}_r\left(\vec{x}_t, \vec{x}_{r,o}\right) \tag{5.1b}$$

At this, point, we will have performed an integration with model B to provide to the observations. The translational and rotational evolution output by this model can very well be used as a-priori models for Eq.(5.1a) and Eq.(5.1b). If this is done, then using the same $\vec{x}_{t,o}$ and $\vec{x}_{r,o}$ as in B will yield the exact same solution because the derivatives will be the same at all times. Nevertheless, other choices of any of these two elements will yield different trajectories and rotational states. Thus, different propagations will be performed with model A using different combinations of a-priori $\vec{x}_r/\vec{x}_t$ and initial conditions $\vec{x}_{t,o}/\vec{x}_{r,o}$.

In particular, a common choice of a-priori $\vec{x}_r$ is that of the spin orbit resonance with a once-per-orbit libration - we will call this model *SORA*. That will be our first attempt, namely propagating model A1 using the same $\vec{x}_{t,o}$ that was used in model B but using the $\vec{x}_r$ from SORA. The ephemerides generated in this way are the ones that Rambaux et al. (2012) used to propagate the rotational equations of motion. We will try to replicate this process, so we will then propagate model A2 with $\vec{x}_t$ from model A1. For this, we will need to choose an initial condition $\vec{x}_{r,o}$. We will try two different things. First, we will use the initial condition from B. The effect of the new translational model on this initial condition will be assessed. However, it is expected that things don't work exactly as they should.

As explained by Rambaux et al. (2012), the initial conditions should be compatible with the current motion of Phobos. That is, the combination of its translation and rotation should produce an orientation evolution that does not contain the normal modes. In the source, Rambaux et al. (2012) select these conditions by introducing an artificial damping in the rotational EOMs and propagating a generic initial state until the normal modes fade away. By propagating this state back in time without the damping - i.e. using the original undamped equations - an initial state without normal modes is obtained. This is then used as initial condition.

In the thesis, we will use the same initial conditions as in B nevertheless, and see how the integration responds. In particular, we will look at the appearance of normal modes in the solution to assess the quality of such a solution. Later, we will follow the same approach as Rambaux et al. (2012) and find an initial condition that will not generate any normal modes. We will assess how different this initial condition is from the original one - the one used in B - and what differences appear in the integrated solution - which, although normal-mode free, will be different from the orientation evolution in B.

The fact that normal modes cannot be present in the integrated solution can be useful in more ways. Estimations like Delta, Echo or Foxtrot have not been performed as of yet in literature. How this *constraint* enters the estimation is a problem in itself that goes beyond the scope of the thesis. In our work, we will only assess the quality of the solutions - namely the estimated parameters/initial states - by using the presence/absence of normal modes in the integrated rotation as a figure of merit.

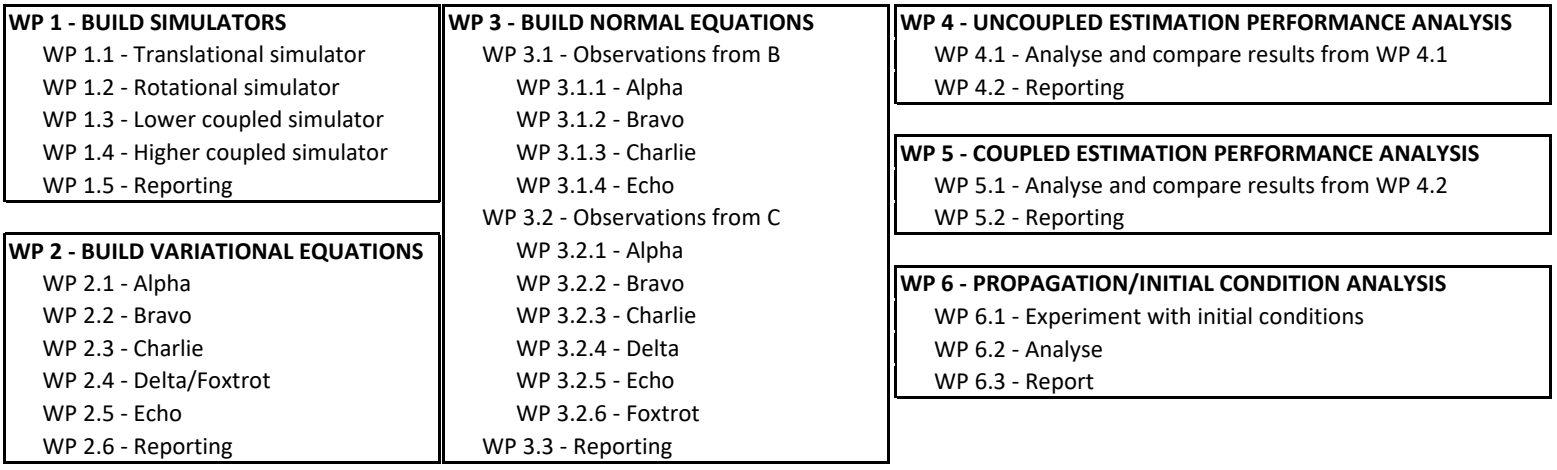

Figure 5.1: Work packages

5.2.2. The tools

All the software development pertaining these simulations will be done with the help of TU Delft Astrodynamics Toolbox[2] (Tudat). Tudat is a C++ software package developed and maintained by staff and students from TU Delft that contains implementations of various integrators, dynamical models for both translational and rotational dynamics, integration of the variational equations and the inversion of least squares problems. It also implements a plethora of ancillary operations, like element conversions - position/velocity to COE, Euler angles to quaternions, ... - as well as some I/O and post-processing utilities. Thus, none of those tools will need to be implemented as part of the thesis following this text. However, Tudat is thought as a modular tool - making it very versatile - which means that an important task will be that of putting together all necessary pieces to yield a working problem. Past experience - mainly from the *Numerical Astrodynamics* and the *Propagation and Optimization* courses - has proven this to be far from trivial. To avoid the "complexities" of C++ at user level, Tudat features a Python wrapper. The author, as a user, will therefore work mostly on Python. Some of the pieces that will be used, however, appear to not have been used extensively, and *minor* bugs will have to be fixed along the way. These fixes might have to be done by either the author or members of the staff. The former might be more likely given the urgency and familiarity of the author with the topic. If this is required, quite some time will have to be allocated for this, given the author's limited experience with C++.

As a final note, Tudat also provides a function to compute the undamped initial state that will have no normal modes in its propagation (see Sec. 5.2.1).

5.2.3. The plan

The work presented in Sec. 5.2.1 can be organized in work packages as in Fig [5.1]. They follow a natural division in two halves. The first half - WP1 through WP3 - consists on building the setup and generating *the numbers* for later analysis. The second half - WP4 through WP6 - consists on analyzing the data and answering the three research subquestions. The relationship in this second half is a 1-to-1 between research (sub)question and work package.

The first half is expected to take around 3 natural months, including writing the corresponding part of the thesis. Starting the code will probably take an unfairly big amount of time, seeing that the author has no experience with Tudat's variational equations or estimation interface. Once the first of those is written, however, the rest follow almost from copy-pasting the first tweaking a coupled of lines here and there.

The second half will probably take 5 months. This part involves a great deal of post processing and plot generation, often times more time-consuming than writing the code for a simulation. It will also entail writing the most part of the thesis, comprising results, interpretations and, in the end, the answers to the research questions.

[2]Documentation: https://tudat-space.readthedocs.io. Source code: https://github.com/tudat-team/tudat-bundle.

6

Conclusions

Since its discovery, Mars' inner moon Phobos has generated plenty of questions and controversy. Observing this moon from the Earth allowed to estimate its orbit and mass, while the second half of the 20th century provided humans with spacecraft that could take pictures of it and allowed to visually inspect the moon. By the turn of the 21st century, Phobos was known to be small and amorphous, in a near-circular, near-equatorial orbit around Mars, and presented the dark surface of a carbonaceous body, heavily cratered and traversed by grooves. It was also the moon that orbited the closest to its parent planet, so close that tidal dissipation was causing it to fall inward - so much so that it is expected to disintegrate inside the Martian gravity field in around 50 million years. The only thing it seemed to have in common with other natural satellites was that it is in spin-orbit resonance and features the famous physical librations, the biggest of them being the once-per orbit longitudinal libration. As it is natural, questions on its origin and formation quickly arose. Its regular orbit is very well explained if Phobos was created in the planetary disk around a proto-Mars. This, however, seems very unlikely by attending to its surface characteristics, which are very compatible with Phobos being a captured asteroid. In an attempt to shed some light on this mystery, 21st -century efforts focus on landing on Phobos and bringing a sample of Phobian soil to Earth, something that has never been done before.

This new type of mission presents new challenges. On one hand, landing on Phobos requires new levels of accuracy on both position and orientation of the moon. On the other hand, a lander-type mission will provide novel measurements of Phobos' orientation and new ranging technologies can provide cm and mm level accuracy measurements. These measurements will be required both for engineering purposes - lander/spacecraft tracking - and scientific purposes - knowing Phobos' orientation/position can help estimate its mass/interior properties. At the intersection of all these elements sits Phobos' dynamical model - i.e. Phobos' equations of motion.

Current models of Phobos' motion resemble the models used for other moons in the solar system - except our own. This means that its rotation and translation are studied separately. For each of these motions, the study can be done either analytically or numerically. Analytical models are kinematical descriptions of the motion that try to write the components of the state vector based on a-priori shapes. Analytical efforts were abandoned early on for describing Phobos' translation, but are still the main way of describing its orientation. There are also numerical descriptions. These originate from the equations of motion, i.e. they describe the systems of forces and torques that govern Phobos and then integrate the equations of motion to yield a trajectory/orientation. These are the go-to when describing translation, but are not as popular when describing rotation.

In any case, the accuracy of state-of-the art ephemerides degrades up to 1km with time (see Sec. 3.3), which yield errors in the location of surface points on Phobos in the order of meters. Therefore, better models are required to assist in and process the data of a lander type mission. Main improvements to current models lie in the inclusion of the couplings between Phobos' translational and rotational motion. Theoretical knowledge on the dynamics of the full two body problem (see Sec. 2.2) reveals that the location of Phobos influences the torques that act on it, while its orientation impacts acting accelerations. This interaction is not represented in uncoupled models. These couplings cannot be implemented in an analytical model, but rather a coupled numerical model is required. These couplings have not only been left unrepresented in current models, but have also not been explored at all. That is precisely what

the thesis following this text will attempt to do.

The aim will be to give a quantitative description of these couplings, and we will do so in a question-answer format. There are three questions that are of relevance. The main question is how these couplings affect the propagation of a given initial condition. Quantifying the difference between a coupled and an uncoupled propagation will aid in better understanding of ephemerides and rotation models of Phobos, which combined provide the location in 3D space of its surface points and will therefore provide necessary improvements in the guidance of a lander mission. On the other hand, a question to answer would be how these couplings affect the estimation of different dynamical parameters. Answering this question will help bridge the gap in data processing capacities for a lander type mission. These two aspects are synthesized in three sciences questions that the thesis will need to provide quantitative answers for (see Sec. 5.1).

To answer these three questions, a number of estimations will be performed with estimation models of Phobos' equations of motion and observations generated by some *truth* models (see Sec. 5.2.1 for a detailed description of these models and the estimations). One of these models will resemble the currently available uncoupled models. By using known models as *truth*, the performance of this uncoupled model can be assessed in estimation. A coupled model will also be used to perform a similar estimation and their results will be compared. Lastly, both models will be compared in propagation of some initial conditions. Such an effort, however, has implications that address the validity of the initial conditions themselves. Thus, an exploration of these initial conditions will be performed as well.

The efforts required by all these tasks can be divided in 6 work packages as described in Sec. 5.2.3, which will extend over the course of 9-10 natural months. The work will be based on numerical simulations performed with *Tudat* (see Sec. 5.2.2), an astrodynamics toolbox written in C++ with a Python interface that provides the required classes and methods to perform integration of equations of motion and variational equations, as well as the generation of observations and building and inversion of normal equations for estimation problems.

By the end of the coming thesis, the research questions should be answered and documented. The developed code will be available in a yet-to-be-discussed online repository and a thesis defence - in the form of a presentation - will be given to all interested public.

Bibliography

Akim, E., Stepanyants, V., Tuchin, A., Shishov, V., 2007. Motion parameters determination of the sc and phobos in the project phobos-grunt, in: Proceedings of the 20th International Symposium on Space Flight Dynamics, pp. 1–15.

Archinal, B.A., Acton, C.H., A'Hearn, M.F., Conrad, A., Consolmagno, G.J., Duxbury, T., Hestroffer, D., Hilton, J.L., Kirk, R.L., Klioner, S.A., McCarthy, D., Meech, K., Oberst, J., Ping, J., Seidelmann, P.K., Tholen, D.J., Thomas, P.C., Williams, I.P., 2018. Report of the IAU working group on cartographic coordinates and rotational elements: 2015. Celestial Mechanics and Dynamical Astronomy 130. doi:10.1007/s10569-017-9805-5.

Archinal, B.A., A'Hearn, M.F., Bowell, E., Conrad, A., Consolmagno, G.J., Courtin, R., Fukushima, T., Hestroffer, D., Hilton, J.L., Krasinsky, G.A., Neumann, G., Oberst, J., Seidelmann, P.K., Stooke, P., Tholen, D.J., Thomas, P.C., Williams, I.P., 2011. Report of the IAU working group on cartographic coordinates and rotational elements: 2009. Celestial Mechanics and Dynamical Astronomy 109, 101–135. doi:10.1007/s10569-010-9320-4.

Ball, A.J., Price, M.E., Walker, R.J., Dando, G.C., Wells, N.S., Zarnecki, J.C., 2009. Mars phobos and deimos survey (m-PADS) – a martian moons orbiter and phobos lander. Advances in Space Research 43, 120–127. doi:10.1016/j.asr.2008.04.007.

Barnard, E., 1897. Measures of the diameters of mars and the positions of his satellites in 1894. The Astronomical Journal 17, 145–147.

Barraclough, S., Ratcliffe, A., Buchwald, R., Scheer, H., Chapuy, M., Garland, M., Rebuffat, D., 2014. Phootprint: A european phobos sample return mission, in: LPI Editorial Board (Ed.), 11th International Planetary Probe Workshop, p. 8030. URL: https://ui.adsabs.harvard.edu/abs/2014LPICo1795.8030B.

Battin, R.H., 1999. An introduction to the mathematics and methods of astrodynamics. American Institute of Aeronautics and Astronautics.

Borderies, N., Yoder, C., 1990. Phobos' gravity field and its influence on its orbit and physical librations. Astronomy & Astrophysics 233, 235–251.

Born, G.H., Duxbury, T.C., 1975. The motions of phobos and deimos from mariner 9 TV data. Celestial Mechanics 12, 77–88. doi:10.1007/bf01228626.

Burmeister, S., Willner, K., Schmidt, V., Oberst, J., 2018. Determination of phobos' rotational parameters by an inertial frame bundle block adjustment. Journal of Geodesy 92, 963–973. doi:10.1007/s00190-018-1112-8.

Burns, J.A., 1972. Dynamical characteristics of phobos and deimos. Reviews of Geophysics 10, 463. doi:10.1029/rg010i002p00463.

Campbell, W., 1892. Observations of mars and his satellites. The Astronomical Journal 12, 137–139.

Chapront-Touze, M., 1988. Esapho - a semi-analytical theory for the orbital motion of phobos. AAP 200, 255–268. URL: https://ui.adsabs.harvard.edu/abs/1988A&A...200..255C.

Chapront-Touze, M., 1990. Phobos' physical libration and complements to the esapho theory for the orbital motion of phobos. AAP 235, 447–458. URL: https://ui.adsabs.harvard.edu/abs/1990A&A...235..447C.

Chung, M., Dalton, K., Davidson, R., 2008. Tensor-based cortical surface morphometry via weighted spherical harmonic representation. IEEE Transactions on Medical Imaging 27, 1143–1151. doi:10.1109/tmi.2008.918338.

Colaprete, A., Bellerose, J., Andrews, D., 2012. Pcross — phobos close rendevous observation sensing satellite, in: LPI Editorial Board (Ed.), Concepts and Approaches for Mars Exploration, p. 4180. URL: https://ui.adsabs.harvard.edu/abs/2012LPICo1679.4180C.

Correspondent, O.A., 1969. Mars: Mariner pictures discussed. Nature 224, 750–751.

Dirkx, D., 2022. Tudat mathematical model definition.

Dirkx, D., Lainey, V., Gurvits, L., Visser, P., 2016. Dynamical modelling of the galilean moons for the JUICE mission. Planetary and Space Science 134, 82–95. doi:10.1016/j.pss.2016.10.011.

Dirkx, D., Mooij, E., Root, B., 2019. Propagation and estimation of the dynamical behaviour of gravitationally interacting rigid bodies. Astrophysics and Space Science 364. doi:10.1007/s10509-019-3521-4.

Dirkx, D., Vermeersen, L., Noomen, R., Visser, P., 2014. Phobos laser ranging: Numerical geodesy experiments for martian system science. Planetary and Space Science 99, 84–102. doi:10.1016/j.pss.2014.03.022.

Dobrovolskis, A.R., 1982. Internal stresses in phobos and other triaxial bodies. Icarus 52, 136–148. doi:10.1016/0019-1035(82)90174-9.

Duxbury, T.C., 1974. Phobos: Control network analysis. Icarus 23, 290–299. doi:10.1016/0019-1035(74)90007-4.

Duxbury, T.C., 1977. Phobos and deimos: Geodesy, in: IAU Colloq. 28: Planetary Satellites, p. 346. URL: https://ui.adsabs.harvard.edu/abs/1977plsa.conf..346D.

Duxbury, T.C., 1991. An analytic model for the phobos surface. Planetary and Space Science 39, 355–376. doi:10.1016/0032-0633(91)90157-6.

Duxbury, T.C., Callahan, J.D., 1981. Pole and prime meridian expressions for PHOBOS and deimos. The Astronomical Journal 86, 1722. doi:10.1086/113056.

Duxbury, T.C., Callahan, J.D., 1989. Phobos and deimos control networks. Icarus 77, 275–286. doi:10.1016/0019-1035(89)90090-0.

Elifritz, T.L., 2012. Osiris-rex ii to mars — mars sample return from phobos and deimos, in: LPI Editorial Board (Ed.), Concepts and Approaches for Mars Exploration, p. 4017. URL: https://ui.adsabs.harvard.edu/abs/2012LPICo1679.4017E.

Fayolle, M., Dirkx, D., Lainey, V., Gurvits, L., Visser, P., 2022. Decoupled and coupled moons' ephemerides estimation strategies application to the JUICE mission. Planetary and Space Science 219, 105531. doi:10.1016/j.pss.2022.105531.

Fienga, A., Avdellidou, C., Hanuš, J., 2019. Asteroid masses obtained with INPOP planetary ephemerides. Monthly Notices of the Royal Astronomical Society 492, 589–602. doi:10.1093/mnras/stz3407.

Folkner, W.M., Williams, J.G., Boggs, D.H., 2009. The planetary and lunar ephemeris de 421. The Interplanetary Network Progress Report 42-178, 1–34. URL: https://ipnpr.jpl.nasa.gov/progress_report/42-178/178C.pdf.

Fukushima, T., 2008. SIMPLE, REGULAR, AND EFFICIENT NUMERICAL INTEGRATION OF ROTATIONAL MOTION. The Astronomical Journal 135, 2298–2322. doi:10.1088/0004-6256/135/6/2298.

Genova, A., Goossens, S., Lemoine, F.G., Mazarico, E., Neumann, G.A., Smith, D.E., Zuber, M.T., 2016. Seasonal and static gravity field of mars from MGS, mars odyssey and MRO radio science. Icarus 272, 228–245. doi:10.1016/j.icarus.2016.02.050.

Golub', A.P., Popel, S.I., 2021. Nonstationary processes in the formation of a dusty plasma near the surface of phobos. JETP Letters 113, 428–432. doi:10.1134/s0021364021070079.

Hall, A., 1878. Discovery of satellites of mars. Monthly Notices of the Royal Astronomical Society 38, 205–209. URL: https://ui.adsabs.harvard.edu/abs/1878MNRAS..38..205H/abstract.

Hall, A., 1880. Satellites of mars: Data for ephemierides of the satellites of mars in the opposition of 1881. Science , 543–543.

Illés, E., Horváth, A., Horváth, F., Gesztesi, A., 1985. In situ measurements to determine if phobos is layered. Acta Astronautica 12, 455–464. doi:10.1016/0094-5765(85)90052-9.

Jacobson, R., Konopliv, A., Park, R., Folkner, W., 2018. The rotational elements of mars and its satellites. Planetary and Space Science 152, 107–115. doi:10.1016/j.pss.2017.12.020.

Jacobson, R., Lainey, V., 2014. Martian satellite orbits and ephemerides. Planetary and Space Science 102, 35–44. doi:10.1016/j.pss.2013.06.003.

Jacobson, R.A., 2010. The orbits and masses of the martian satellites and the libration of phobos. The Astronomical Journal 139, 668–679. doi:10.1088/0004-6256/139/2/668.

Jacobson, R.A., Synnott, S.P., Campbell, J.K., 1989. The orbits of the satellites of mars from spacecraft and earthbased observations. AAP 225, 548–554. URL: https://ui.adsabs.harvard.edu/abs/1989A&A...225..548J.

Jeffreys, H., 1957. The secular accelerations of satellites. Monthly Notices of the Royal Astronomical Society 117, 585–589. doi:10.1093/mnras/117.6.585.

JPL, 2000. Mgs photojournal. URL: https://photojournal.jpl.nasa.gov/targetFamily/Mars?subselect=Target:Phobos:Instrument:Mars+Orbiter+Camera+(MOC):Mission:Mars+Global+Surveyor+(MGS):Spacecraft:Mars+Global+Surveyor+Orbiter.

Keeler, J.E., 1888. Micrometer observations of the satellites of mars. The Astronomical Journal 8, 73–78.

Keeler, J.E., 1890. Observations of the satellites of mars. The Astronomical Journal 10, 89–91.

Kerr, F.J., Whipple, F.L., 1951. Possible explanations of the secular acceleration of phobos and jupiter v. The Astronomical Journal 56, 131. URL: https://ui.adsabs.harvard.edu/abs/1951AJ.....56R.131K, doi:10.1086/106617.

Konopliv, A.S., Asmar, S.W., Folkner, W.M., Özgür Karatekin, Nunes, D.C., Smrekar, S.E., Yoder, C.F., Zuber, M.T., 2011. Mars high resolution gravity fields from MRO, mars seasonal gravity, and other dynamical parameters. Icarus 211, 401–428. doi:10.1016/j.icarus.2010.10.004.

Konopliv, A.S., Park, R.S., Folkner, W.M., 2016. An improved JPL mars gravity field and orientation from mars orbiter and lander tracking data. Icarus 274, 253–260. doi:10.1016/j.icarus.2016.02.052.

Konopliv, A.S., Yoder, C.F., Standish, E.M., Yuan, D.N., Sjogren, W.L., 2006. A global solution for the mars static and seasonal gravity, mars orientation, phobos and deimos masses, and mars ephemeris. Icarus 182, 23–50. doi:10.1016/j.icarus.2005.12.025.

Lainey, V., Dehant, V., Pätzold, M., 2007. First numerical ephemerides of the martian moons. Astronomy & Astrophysics 465, 1075–1084. doi:10.1051/0004-6361:20065466.

Lainey, V., Duriez, L., Vienne, A., 2004. New accurate ephemerides for the galilean satellites of jupiter. Astronomy & Astrophysics 420, 1171–1183. doi:10.1051/0004-6361:20034565.

Lainey, V., Noyelles, B., Cooper, N., Rambaux, N., Murray, C., Park, R., 2019. Interior properties of the inner saturnian moons from space astrometry data. Icarus 326, 48–62. doi:10.1016/j.icarus.2019.01.026.

Lainey, V., Pasewaldt, A., Robert, V., Rosenblatt, P., Jaumann, R., Oberst, J., Roatsch, T., Willner, K., Ziese, R., Thuillot, W., 2021. Mars moon ephemerides after 14 years of mars express data. Astronomy & Astrophysics 650, A64. doi:10.1051/0004-6361/202039406.

Le Maistre, S., Rivoldini, A., Rosenblatt, P., 2019. Signature of phobos' interior structure in its gravity field and libration. Icarus 321, 272–290. doi:10.1016/j.icarus.2018.11.022.

Lee, P., Bicay, M., Colaprete, A., Elphic, R., Genova, A., Hine, B., Horanyi, M., Jaroux, B., Korsmeyer, D., Lewis, B.S., Worden, S.P., 2014. Phobos and deimos and mars environment (padme): A ladee-derived mission to explore mars's moons and the martian orbital environment, in: 45th Annual Lunar and Planetary Science Conference, p. 2288. URL: https://ui.adsabs.harvard.edu/abs/2014LPI...45.2288L.

Lee, P., Hildebrand, A.R., Richards, R., Team, P.M., 2008. The prime (phobos reconnaissance and international mars exploration) mission and mars sample return, in: 39th Annual Lunar and Planetary Science Conference, p. 2268. URL: https://ui.adsabs.harvard.edu/abs/2008LPI....39.2268L.

Lee, P., Veverka, J., Bellerose, J., Boucher, M., Boynton, J., Braham, S., Gellert, R., Hildebrand, A., Manzella, D., Mungas, G., Oleson, S., Richards, R., Thomas, P.C., West, M.D., 2010. Hall: A phobos and deimos sample return mission, in: 41st Annual Lunar and Planetary Science Conference, p. 1633. URL: https://ui.adsabs.harvard.edu/abs/2010LPI....41.1633L.

Lemoine, F.G., Smith, D.E., Rowlands, D.D., Zuber, M., Neumann, G., Chinn, D., Pavlis, D., 2001. An improved solution of the gravity field of mars (gmm-2b) from mars global surveyor. Journal of Geophysical Research 106, 23359–23376. doi:https://doi.org/10.1029/2000JE001426.

Ma, C., Arias, E.F., Eubanks, T.M., Fey, A.L., Gontier, A.M., Jacobs, C.S., Sovers, O.J., Archinal, B.A., Charlot, P., 1998. The international celestial reference frame as realized by very long baseline interferometry. The Astronomical Journal 116, 516–546. doi:10.1086/300408.

Marov, M., Avduevsky, V., Akim, E., Eneev, T., Kremnev, R., Kulikov, S., Pichkhadze, K., Popov, G., Rogovsky, G., 2004. Phobos-grunt: Russian sample return mission. Advances in Space Research 33, 2276–2280. doi:10.1016/s0273-1177(03)00515-5.

Marth, A., 1879. On the satellites of mars. Astronomische Nachrichten 95, 369–379.

Martinec, Z., Pěč, K., Burša, M., 1989. The phobos gravitational field modeled on the basis of its topography. Earth, Moon and Planets 45, 219–235. doi:10.1007/bf00057745.

Mathews, P.M., Buffett, B.A., Shapiro, I.I., 1995. Love numbers for a rotating spheroidal earth. Geophysical Research Letters 22, 579–582. doi:10.1029/95gl00161.

Michel, P., Agnolon, D., Brucato, J., Gondet, B., Korablev, O., Koschny, D., Schmitz, N., Willner, K., Zacharov, A., 2011. Mmsr - a study for a martian moon sample return mission, in: EPSC-DPS Joint Meeting 2011, p. 849. URL: https://ui.adsabs.harvard.edu/abs/2011epsc.conf..849M.

Michel, P., DeMeo, F.E., Bottke, W.F., 2015. Asteroids IV. University of Arizona Press.

Montenbruck, O., Gill, E., 2005. Satellite Orbits. Springer.

Murchie, S., Eng, D., Chabot, N., Guo, Y., Arvidson, R., Yen, A., Trebi-Ollennu, A., Seelos, F., Adams, E., Fountain, G., 2014. MERLIN: Mars-moon exploration, reconnaissance and landed investigation. Acta Astronautica 93, 475–482. doi:10.1016/j.actaastro.2012.10.014.

Murray, J.B., Iliffe, J.C., Muller, J.P.A.L., Neukum, G., Werner, S., Balme, M.R., 2006. New evidence on the origin of phobos' parallel grooves from hrsc mars express, in: Mackwell, S., Stansbery, E. (Eds.), 37th Annual Lunar and Planetary Science Conference, p. 2195. URL: https://ui.adsabs.harvard.edu/abs/2006LPI....37.2195M.

Nadezhdina, I.E., Zubarev, A.E., 2014. Formation of a reference coordinate network as a basis for studying the physical parameters of phobos. Solar System Research 48, 269–278. doi:10.1134/s003809461404008x.

Nakamura, T., Ikeda, H., Kouyama, T., Nakagawa, H., Kusano, H., Senshu, H., Kameda, S., Matsumoto, K., Gonzalez-Franquesa, F., Ozaki, N., Takeo, Y., Baresi, N., Oki, Y., Lawrence, D.J., Chabot, N.L., Peplowski, P.N., Barucci, M.A., Sawyer, E., Yokota, S., Terada, N., Ulamec, S., Michel, P., Kobayashi, M., Sasaki, S., Hirata, N., Wada, K., Miyamoto, H., Imamura, T., Ogawa, N., Ogawa, K., Iwata, T., Imada, T., Otake, H., Canalias, E., Lorda, L., Tardivel, S., Mary, S., Kunugi, M., Mitsuhashi, S., Doressoundiram, A., Merlin, F., Fornasier, S., Reess, J.M., Bernardi, P., Imai, S., Ito, Y., Ishida, H., Kuramoto, K., Kawakatsu, Y., 2021. Science operation plan of phobos and deimos from the MMX spacecraft. Earth, Planets and Space 73. doi:10.1186/s40623-021-01546-6.

Newall, H.F., 1895. Micrometer measurements of phobos, the inner satellite of mars, during the opposition of 1894. Monthly Notices of the Royal Astronomical Society 55, 348–353. doi:10.1093/mnras/55.7.348.

Nimmo, F., Faul, U.H., 2013. Dissipation at tidal and seismic frequencies in a melt-free, anhydrous mars. Journal of Geophysical Research: Planets 118, 2558–2569. doi:10.1002/2013je004499.

Oberst, J., Wickhusen, K., Willner, K., Gwinner, K., Spiridonova, S., Kahle, R., Coates, A., Herique, A., Plettemeier, D., Díaz-Michelena, M., Zakharov, A., Futaana, Y., Pätzold, M., Rosenblatt, P., Lawrence, D.J., Lainey, V., Gibbings, A., Gerth, I., 2018. DePhine – the deimos and phobos interior explorer. Advances in Space Research 62, 2220–2238. doi:10.1016/j.asr.2017.12.028.

Oberst, J., Zubarev, A., Nadezhdina, I., Shishkina, L., Rambaux, N., 2014. The phobos geodetic control point network and rotation model. Planetary and Space Science 102, 45–50. doi:10.1016/j.pss.2014.03.006.

Peters, C., 1981. Numerical integration of the satellites of the outer planets. Astronomy & Astrophysics 104, 37–41.

Pickering, E.C., Searle, A., Upton, W., 1879. Photometric observations. part ii. appendix f. satellites of mars 1879. Annals of Harvard College Observatory 11, 311–317. URL: https://ui.adsabs.harvard.edu/abs/1879AnHar..11..311P.

Pollack, J., Veverka, J., Noland, M., Sagan, C., Hartmann, W., Duxbury, T., Born, G., Milton, D., Smith, B., 1972. Mariner 9 television observations of phobos and deimos. Icarus 17, 394–407. doi:10.1016/0019-1035(72)90007-3.

Prettyman, T.H., Diniega, S., Raymond, C.A., 2014. Pandora - unlocking the mysteries of the moons of mars, in: AAS/Division for Planetary Sciences Meeting Abstracts #46, p. 304.08. URL: https://ui.adsabs.harvard.edu/abs/2014DPS....4630408P.

Pritchett, C.W., 1880. Observations of phobos and deimos. Astronomische Nachrichten 97, 45. URL: https://ui.adsabs.harvard.edu/abs/1880AN.....97...45P, doi:10.1002/asna.18800970307.

Rambaux, N., Castillo-Rogez, J.C., Maistre, S.L., Rosenblatt, P., 2012. Rotational motion of phobos. Astronomy & Astrophysics 548, A14. doi:10.1051/0004-6361/201219710.

Rambaux, N., Castillo-Rogez, J.C., Williams, J.G., Özgür Karatekin, 2010. Librational response of enceladus. Geophysical Research Letters 37. doi:10.1029/2009gl041465.

Samuel, H., Lognonné, P., Panning, M., Lainey, V., 2019. The rheology and thermal history of mars revealed by the orbital evolution of phobos. Nature 569, 523–527. doi:10.1038/s41586-019-1202-7.

Schelling, H.V., 1964. Comments on the paper by g.f. schilling, 'on exospheric drag as the cause of the supposed secular accelerations of phobos'. Journal of Geophysical Research 69, 4174–4175. doi:10.1029/jz069i019p04174.

Schilling, G.F., 1964a. On exospheric drag as the cause of the supposed secular accelerations of phobos. Journal of Geophysical Research 69, 1825–1829. doi:10.1029/jz069i009p01825.

Schilling, G.F., 1964b. Reply [to "comments on the paper by g, f. schilling, 'on exospheric drag as the cause of the supposed secular accelerations of phobos'"]. Journal of Geophysical Research 69, 4176–4176. doi:10.1029/jz069i019p04176.

Seidelmann, P.K., Abalakin, V.K., Bursa, M., Davies, M.E., de Bergh, C., Lieske, J.H., Oberst, J., Simon, J.L., Standish, E.M., Stooke, P., Thomas, P.C., 2002. Report of the iau/iag working group on cartographic coordinates and rotational elements of the planets and satellites: 2000. Celestial Mechanics and Dynamical Astronomy 82, 83–111. doi:10.1023/a:1013939327465.

Sharpless, B.P., 1945. Secular accelerations in the longitudes of the satellites of mars. The Astronomical Journal 51, 185–186. URL: https://ui.adsabs.harvard.edu/abs/1945AJ.....51..185S, doi:10.1086/105871.

Shishov, V.A., 2008. Determination of spacecraft and phobos parameters of motion in the phobos-grunt project. Solar System Research 42, 319–328. doi:10.1134/s0038094608040047.

Siddiqi, A.A., 2018. Beyond Earth A Chronicle of Deep Space Exploration, 1958-2016. National Aeronautis & Space Administration.

Smith, B.A., 1970. Phobos: Preliminary results from mariner 7. Science 168, 828–830. doi:10.1126/science.168.3933.828.

Standish, E. M., J., Newhall, X.X., 1996. New accuracy levels for solar system ephemerides. (lecture), in: Ferraz-Mello, S., Morando, B., Arlot, J.E. (Eds.), Dynamics, Ephemerides, and Astrometry of the Solar System, p. 29. URL: https://ui.adsabs.harvard.edu/abs/1996IAUS..172...29S.

Stark, A., Willner, K., Burmeister, S., Oberst, J., 2017. Geodetic framework for martian satellite exploration i: Reference rotation models, in: European Planetary Science Congess 2017, pp. 1–2.

Thomas, P., Veverka, J., Bloom, A., Duxbury, T., 1979. Grooves on phobos: Their distribution, morphology and possible origin. Journal of Geophysical Research 84, 8457. doi:10.1029/jb084ib14p08457.

Tolson, R.H., Blackshear, W.T., Mason, M.L., Kelly, G.M., 1977. The mass of phobos. Geophysical Research Letters 4, 551–554. doi:10.1029/gl004i012p00551.

Usui, T., ichi Bajo, K., Fujiya, W., Furukawa, Y., Koike, M., Miura, Y.N., Sugahara, H., Tachibana, S., Takano, Y., Kuramoto, K., 2020. The importance of phobos sample return for understanding the mars-moon system. Space Science Reviews 216. doi:10.1007/s11214-020-00668-9.

Various, a. Jpl solar system dynamics - planetary and lunar ephemerides. URL: https://ssd.jpl.nasa.gov/planets/eph_export.html.

Various, b. Jpl solar system dynamics - planetary satellite ephemerides. URL: https://ssd.jpl.nasa.gov/sats/ephem/.

Veverka, J., 1978. The surfaces of phobos and deimos. Vistas in Astronomy 22, 163–192. doi:10.1016/0083-6656(78)90014-4.

Villalba, M., Cavallaro, R., Chen, X., Correyero, S., Fajardo, P., Gonzalo, A., Moriche, M., Sánchez, A., Álvaro Sánchez, Sanjurjo, M., Merino, M., 2018. Mechanics applied to aerospace engineering.

Wakker, K.F., 2015. Fundamentals of Astrodynamics.

Waż, P., 1999. Analytical theory of the motion of phobos: Analysis of the perturbational function. Reports on Mathematical Physics 44, 283–290. doi:10.1016/s0034-4877(99)80170-0.

Willner, K., Oberst, J., Hussmann, H., Giese, B., Hoffmann, H., Matz, K.D., Roatsch, T., Duxbury, T., 2010. Phobos control point network, rotation, and shape. Earth and Planetary Science Letters 294, 541–546. doi:10.1016/j.epsl.2009.07.033.

Willner, K., Shi, X., Oberst, J., 2014. Phobos' shape and topography models. Planetary and Space Science 102, 51–59. doi:10.1016/j.pss.2013.12.006.

Woolard, E.W., 1944. The secular perturbations of the satellites of mars. The Astronomical Journal 51, 33. URL: https://ui.adsabs.harvard.edu/abs/1944AJ.....51...33W, doi:10.1086/105793.

Yang, Y., Yan, J., Guo, X., He, Q., Barriot, J.P., 2020. An elastic model of phobos' libration. Astronomy & Astrophysics 636, A27. doi:10.1051/0004-6361/202037446.

A

Torque in the F2BP

Back in 2.2.3, it was stated that the torque that Mars' center of mass exerts on the figure of Phobos is given by Eq.(2.22). This equation is used by Rambaux et al. (2012) without proof. The author thought it best to explain where this equation comes from, for the enjoyment of the interested reader.

Consider a body A, with center of mass at point O, and an arbitrary point P outside of the body. Define vectors $\vec{r}$, $\vec{r}_a$ and $\vec{\rho}$ as depicted in Fig.A.1, such that $\vec{\rho} = \vec{r} - \vec{r}_a$.

The acceleration that a differential mass dm of body A creates at point P is given by Eq.(A.1). The acceleration that the whole body A creates on P is obtained by integration. Note that $\vec{r}$ is constant over the whole integration domain. However, the acceleration that A creates on P is also defined as $\vec{a} = \nabla U_A$. Thus, we find the relationship in Eq.(A.2).

$$d\vec{a} = \frac{Gdm}{\rho^3}(-\vec{\rho}) = \frac{Gdm}{\rho^3}(\vec{r}_a - \vec{r}) \quad \rightarrow \quad \vec{a} = \int_A d\vec{a} = \int_A \frac{Gdm}{\rho^3}(\vec{r}_a - \vec{r}) \tag{A.1}$$

$$\boxed{\nabla U_A = \int_A \frac{Gdm}{\rho^3}\vec{r}_a - \vec{r}\int_A \frac{Gdm}{\rho^3}} \tag{A.2}$$

We now want to obtain the torque that a particle of mass M located at point P would create on body A. We begin by considering the torque that the particle exerts on a differential mass dm of body A. The force that M exerts on dm is given by Newton's law of gravitation. This force and the corresponding torque are written out in Eq.(A.3). Note that $\vec{r}_a \times \vec{\rho} = \vec{r}_a \times (\vec{r} - \vec{r}_a) = \vec{r}_a \times \vec{r}$. The total torque can then be found by integrating, which is done in Eq.(A.4). Again, note that $\vec{r}$ is constant over the whole domain of integration.

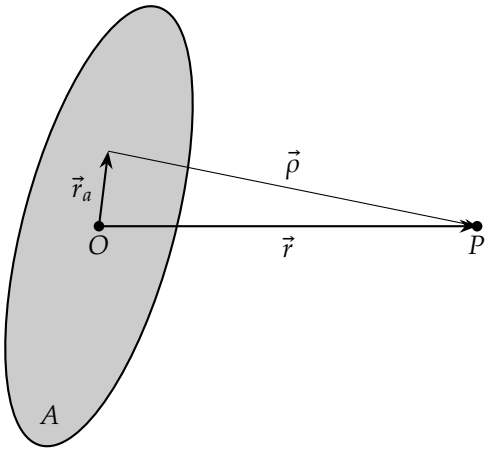

Figure A.1

$$d\vec{F} = \frac{GMdm}{\rho^3}\vec{\rho} \quad \rightarrow \quad d\vec{T} = \vec{r}_a \times d\vec{F} = \frac{GMdm}{\rho^3}\vec{r}_a \times \vec{\rho} = -\frac{GMdm}{\rho^3}\vec{r} \times \vec{r}_a \tag{A.3}$$

$$\vec{T} = \int_A d\vec{T} = -M\vec{r} \times \int_A \frac{Gdm}{\rho^3}\vec{r}_a \tag{A.4}$$

The integral in Eq.(A.4) is no other than the first term on the right hand side of Eq.(A.2). We can therefore substitute it and carry out the cross product, noting that $\vec{r} \times \vec{r} = \vec{0}$. The result is Eq.(2.22). This is done in Eq.(A.5), where body A is Phobos, M is the mass of Mars and $\vec{r}$ is the position vector of Mars with respect to Phobos. Rambaux et al. (2012) refers to this vector is as the "relative distance vector of Mars and Phobos", without specifying where it starts or ends.

$$\vec{T} = -M\vec{r} \times \left(\nabla U_A + \vec{r} \int_A \frac{Gdm}{\rho^3}\right) \quad \rightarrow \quad \boxed{\vec{T} = -M\vec{r} \times \nabla U_A} \tag{A.5}$$

B

Librations: Solving the linearized ODE

In the linear approximation, librations can be modelled by the harmonic oscillator. A summary of the equations and solutions relevant to the applications to librations will be given here for the interested reader. More particularly, the aim will be to give mathematical expressions for the solution of Eq.(3.1), to show how the forcing in Eq.(3.2) leads to the solution in Eq.(3.3), and to provide a mathematical expression for $\theta_h(t)$ in this equation. The concept of resonance will also be discussed.

We will begin by posing the homogeneous version of Eq.(3.1) (i.e. $f = 0$) and solving it, and then moving to the damped homogeneous equation. Finally, we will introduce a periodic forcing and show how Eq.(3.3) comes to be. Solving these equations can be done by means of the Laplace transform. However, we will use a more traditional approach.

B.1. Undamped oscillator

The general equation for an undamped harmonic oscillator reads as in Eq.(B.1), where $\omega_o > 0$ is the so-called *natural frequency*.The solution to this second order ODE is a combination of exponentials of the form shown in the equation. The λ factor characterizes the solution and is sometimes called the *eigenvalue* of the equation.

$$\ddot{\theta} + \omega_o^2 \theta = 0 \quad \Longrightarrow \quad \theta \sim e^{\lambda t} \tag{B.1}$$

The characteristic polynomial of this equation reads $P(\lambda) = \lambda^2 + \omega_o^2$, which equated to 0 yields $\lambda = \pm i\omega_o$. The general solution to Eq.(B.1) reads as in Eq.(B.2), where $A_c, B_c \in \mathbb{C}$ are arbitrary constants such that $\theta(t) \in \mathbb{R}$ at any instant of time.

$$\theta(t) = A_c e^{i\omega_o t} + B_c e^{-i\omega_o t} \tag{B.2}$$

We can impose further constraints on these constants by taking the imaginary part of θ and setting it to 0. This is done in Eq.(B.3), where the overhead bar denotes the complex conjugate. For that expression to *always* be 0, the two factors multiplying the time-dependent exponentials should be 0. The two yield the same constraint on A_c and B_c, namely that the two constants are complex conjugates.

$$\Im\{\theta\} = \frac{\theta - \bar{\theta}}{2} = \frac{A_c - \bar{B}_c}{2} e^{i\omega_o t} + \frac{B_c - \bar{A}_c}{2} e^{-i\omega_o t} = 0 \quad \Longrightarrow \quad B_c = \bar{A}_c \tag{B.3}$$

This allows to write θ as in Eq.(B.4), where we have written $2A_c = A + iB$.

$$\theta(t) = 2\Re\{A_c e^{i\omega_o t}\} \quad \Longrightarrow \quad \theta(t) = A\cos(\omega_o t) + B\sin(\omega_o t) \tag{B.4}$$

This is the solution to the homogeneous version of Eq.(3.1), where the constants A and B are to be fixed by initial conditions. In that equation, $\omega_o^2 = 3n^2\gamma$.

B.2. Damped oscillator

We now add a damping to the system. This damping will be characterized by a constant $\gamma > 0$ that, for reasons that will become apparent later, we will write as $\gamma = 2\zeta\omega_o$, where $\zeta > 0$ will be called *damping ratio*. The (homogeneous) ODE for this damped oscillator reads as in Eq.(B.5), with θ still being given as exponentials.

$$\ddot{\theta} + 2\zeta\omega_o\theta + \omega_o^2\theta = 0 \quad \Longrightarrow \quad \theta \sim e^{\lambda t} \tag{B.5}$$

The characteristic polynomial of this ODE now reads $P(\lambda) = \lambda^2 + 2\zeta\omega_o\lambda + \omega_o^2$. Equating it to 0 and solving for λ yields the eigenvalue and solution in Eq.(B.6), where we have written $\zeta\omega_o = \beta > 0$

$$\lambda = \omega_o\left(-\zeta \pm \sqrt{\zeta^2 - 1}\right) \quad \Longrightarrow \quad \theta(t) = e^{-\beta t}\left(Ae^{\omega_o t\sqrt{\zeta^2-1}} + Be^{-\omega_o t\sqrt{\zeta^2-1}}\right) \tag{B.6}$$

If $\zeta \geq 1$ (and $\gamma \geq 2\omega_o$), the solution reads as presented and does *not* oscillate. The oscillator is said to be *overdamped*. In the particular case where $\zeta = 1$, the oscillator is said to be *critically damped* (yet still does not oscillate). If $\zeta < 1$, then $\zeta^2 - 1 < 0$ and $\sqrt{\zeta^2 - 1} = i\sqrt{1 - \zeta^2}$. In this case, and by writing $\omega = \omega_o\sqrt{1 - \zeta^2}$, the solution reads as in Eq.(B.7). Note that we now have written A_c and B_c to make explicit that these are complex constants that, combined with the complex exponentials, shall yield a θ that is always real. This term in parenthesis reads exactly as the one from the undamped case in Eq.(B.2), but with ω instead of ω_o. We can then apply the exact same reasoning as earlier and write this solution with sines and cosines, as shown in this same Eq.(B.7).

$$\theta(t) = e^{-\beta t}\left(A_c e^{i\omega t} + B_c e^{-i\omega t}\right) \quad \Longrightarrow \quad \theta(t) = e^{-\beta t}\left(A\cos(\omega t) + B\sin(\omega t)\right) \tag{B.7}$$

These solutions for the homogeneous cases of both the damped and undamped oscillators are sometimes referred to as the *normal modes*. Note that, no matter how small β is - as long as it is larger that 0 - the normal mode will decay in amplitude and will eventually vanish. Notice also how the frequency of the damped oscillator is no longer the natural frequency ω_o but rather a *damped frequency* ω.

B.3. Forced oscillator

We will now consider the case of a (damped) forced oscillator. For this, we will consider the ODE as an operator, such that $L(\theta) = 0$ is equivalent to Eq.(B.5). Note that it is a linear operator, so that $L(ax + by) = aL(x) + bL(y)$. The homogeneous solution of L - sometimes called *eigenfunction* - that was found in the last section will be called θ_h and $L(\theta_h) = 0$. We are now interested in the solution to the equation $L(\theta) = f$, where f is a function that might depend on time but does not depend on θ. If we take θ_p to be a solution to this equation - i.e. $L(\theta_p) = f$ - it turns out that $L(\theta_h + \theta_p) = L(\theta_h) + L(\theta_p) = 0 + f$, which means that $\theta = \theta_h + \theta_p$ is also a solution to the equation $L(\theta) = f$. Thus, a general solution is composed of a *homogeneous part* θ_h - the normal mode found in the previous section - and a *particular solution*.

Using the operator also allows for the following analysis. If we write f as a composition of different forcings f_i and take θ_i to be the solution to the equation $L(\theta) = f_i$ - in other words, $L(\theta_i) = f_i$ - we can write Eq.(B.8) using the linearity of L.

$$L(\theta) = f = \sum f_i = \sum L(\theta_i) = L\left(\sum \theta_i\right) \quad \Longrightarrow \quad \theta = \sum \theta_i \quad \Longrightarrow \quad \theta = \theta_h + \sum \theta_i \tag{B.8}$$

The final expression in Eq.(B.8) already somewhat resembles Eq.(3.3). We only need to provide an expression for θ_i. For that, we will use the fact that $L(\theta_i) = f_i$, where f_i is a periodic forcing of the form $f_i = F_i\cos(\omega_i t)$. The equation reads as in Eq.(B.9a). Note that the only way a cosine can arise from a function and its derivatives is if said function itself contains a sine and a cosine, so that the first and second derivatives combine into a sine term and a cosine term. The coefficients of the sine and cosine are fixed by plugging this solution and its derivatives back into the original ODE and balancing the sine and cosine parts between both sides of the equality. The resulting system is solved for the constants A_i and B_i. This process is depicted in Eq.(B.9).

$$\ddot{\theta}_i + \gamma\dot{\theta}_i + \omega_o^2\theta_i = F_i\cos(\omega_i t) \tag{B.9a}$$

$$\begin{aligned}\theta_i(t) &= A_i\cos(\omega_i t) + B_i\sin(\omega_i t)\\ \dot{\theta}_i(t) &= \omega_i\left(-A_i\sin(\omega_i t) + B_i\cos(\omega_i t)\right)\\ \ddot{\theta}_i(t) &= -\omega_i^2\left(A_i\cos(\omega_i t) + B_i\sin(\omega_i t)\right) = -\omega_i^2\theta_i(t)\end{aligned} \tag{B.9b}$$

$$\left(\left(\omega_o^2-\omega_i^2\right)A_i + \gamma\omega_i B_i\right)\cos(\omega_i t) + \left(\left(\omega_o^2-\omega_i^2\right)B_i - \gamma\omega_i A_i\right)\sin(\omega_i t) = F_i\cos(\omega_i t) \tag{B.9c}$$

$$\begin{cases}\left(\omega_o^2-\omega_i^2\right)A_i + \gamma\omega_i B_i = F_i\\ \gamma\omega_i A_i - \left(\omega_o^2-\omega_i^2\right)B_i = 0\end{cases} \tag{B.9d}$$

The found A_i and B_i are used to write θ_i, which is given as in Eq.(B.10). The ratio of the response θ_i to the forcing magnitude F_i, that we have called Θ_i, is often times referred to as the *transfer function*.

$$\Theta_i(\omega_i) = \frac{\theta_i}{F_i} = \frac{\left(\omega_o^2-\omega_i^2\right)\cos(\omega_i t) + \gamma\omega_i\sin(\omega_i t)}{\left(\omega_o^2-\omega_i^2\right)^2 + (\gamma\omega_i)^2} \tag{B.10}$$

The particular case of Eq.(3.3) is that in which $\gamma = 0$. Note the importance of damping when a forcing exists, represented by the two cases in Eq.(B.11).

$$\lim_{\omega_i\to\omega_o}\Theta_i = \frac{\sin(\omega_o t)}{\gamma\omega_o} \qquad \text{if} \quad \gamma > 0 \tag{B.11a}$$

$$\lim_{\omega_i\to\omega_o}\Theta_i = \infty \qquad \text{if} \quad \gamma = 0 \tag{B.11b}$$

In the presence of damping, the normal modes will not die out if the forcing has terms oscillating in the normal frequency. Of course $\theta_h(t)$ - which oscillates at $\omega = \omega_o\sqrt{1-\zeta^2}$ - will vanish with time, but the component introduced by the forcing will stabilize at a magnitude inversely proportional to ω_o and γ, and will additionally be completely phased by 90°. On the other hand, if the oscillator is undamped, the components of f oscillating at ω_o will make θ blow up. This phenomenon is called *resonance*. As θ gets bigger, the linearization assumption will break and the original equation - i.e. Eq.(B.9a) - will no longer be a faithful representation of reality.

B.4. Application to Phobos

After this theoretical discussion, we will discuss how this applies to Phobos' librations. The most important libration, i.e. the longitudinal one, is modelled by Eq.(B.9a) with $\gamma = 0$ (Rambaux et al., 2010), which works well for small oscillations - i.e. if linearization holds - and represents an *undamped* oscillator. In the context of the longitudinal libration, $\omega_o = n\sqrt{3\gamma}$. Here, n is Phobos' mean motion and γ is the ratio of inertia moments $A \le B \le C$. For Phobos, $\omega_o = 12.275\text{rad/day}$ (Rambaux et al., 2012) using the moments of inertia computed by Willner et al. (2010).

In the context of the rotation of Phobos, the forcings in Eq.(3.1) are the torques exerted on Phobos, which are given in Eq.(2.33c). There are two important terms in this equation: $\vec{\rho}_P^{\,M}$ and $\boldsymbol{R}^{\mathcal{I}/\mathcal{P}}$. The former is related to the position of Phobos, while the latter is related to Phobos' orientation. If any of these two are periodic, then the forcings in Eq.(B.9a) will also be periodic. Phobos' position is periodic as it orbits Mars, so its frequency will be related to its orbital period such that $\omega_\rho = 19.694\text{rad/day}$. Phobos rotation oscillates, precisely, with the librations. However, it would be unwise to say that the oscillation period of the torques is also ω_o, because the librational motion of Phobos is known to be much more complicated than a simple longitudinal libration and a rich spectral content is known to exist. In fact, Rambaux et al. (2012) provides the frequencies of quite a few of these librations. One of these frequencies lies at $\omega_{\text{lib}} = 12.284\text{rad/day}$, which is extremely close to ω_o - so much so that $\omega_{\text{lib}}/\omega_o = 0.9978$. Knowing the magnitude of the torque component at this frequency and how Phobos responds to it is important because it can allow us to follow the inverse reasoning: knowing F_i, ω_i and Θ_i, we can better estimate the value of ω_o which will in turn provide a better measure of Phobos' moments of inertia and therefore of Phobos' interior.

Nevertheless, this simple scenario does not allow for more insight in the librational spectra of Phobos, but rather a numerical integration like that of Rambaux et al. (2012) or an analytical integration like that of Chapront-Touze (1990) is required for a complete characterisation of Phobos' librations.

C

Quaternions

A quaternion can be interpreted in many ways. For us, a quaternion will mathematically behave as a 4-by-1 matrix. We will denote it as $\boldsymbol{q}$ and its entries will be denoted by q_0, q_1, q_2 and q_3. Sometimes, the first entry is denoted s and the other three are gathered in a 3-by-1 matrix or *vector* $\vec{v}$. Physically, it represents a rotation by an angle θ about an axis given by the unitary vector $\hat{n}$. This information is gathered in the entries of the quaternion as in Eq.(C.1).

$$s = q_0 = \cos\frac{\theta}{2} \qquad \vec{v} = \begin{bmatrix} q_1 \\ q_2 \\ q_3 \end{bmatrix} = \hat{n}\sin\frac{\theta}{2} \tag{C.1}$$

If we define the *norm* of the quaternion, $|\boldsymbol{q}|$, as in Eq.(C.2), note that $|\boldsymbol{q}| = 1$. By the definition of a rotation quaternion, this is always the case and, if integrated numerically, this should always be imposed at every integration step.

$$|\boldsymbol{q}| = \sqrt{\boldsymbol{q}^T\boldsymbol{q}} = \sqrt{q_0^2 + q_1^2 + q_2^2 + q_3^2} \tag{C.2}$$

Consider a time-dependent quaternion $\boldsymbol{q}(t)$. Its derivative $\dot{\boldsymbol{q}}$ is defined as a quaternion whose entries are the time derivatives of $\boldsymbol{q}$. Constraints are imposed on both $\dot{\boldsymbol{q}}$ and $\ddot{\boldsymbol{q}}$ because $|\boldsymbol{q}| = 1$, namely Eq.(C.3).

$$\frac{d\,|\boldsymbol{q}|^2}{dt} = 2\boldsymbol{q}^T\dot{\boldsymbol{q}} = 0 \quad \Longrightarrow \quad \boldsymbol{q}^T\dot{\boldsymbol{q}} = 0 \tag{C.3a}$$

$$\frac{d^2\,|\boldsymbol{q}|^2}{dt^2} = 2\frac{d\,\boldsymbol{q}^T\dot{\boldsymbol{q}}}{dt} = 2\left(\dot{\boldsymbol{q}}^T\dot{\boldsymbol{q}} + \boldsymbol{q}^T\ddot{\boldsymbol{q}}\right) = 0 \quad \Longrightarrow \quad \dot{\boldsymbol{q}}^T\dot{\boldsymbol{q}} + \boldsymbol{q}^T\ddot{\boldsymbol{q}} = 0 \tag{C.3b}$$

Quaternions where shown by Fukushima (2008) to be the most computationally efficient way of expressing orientation in an integration framework. However, how the derivative of a quaternion relates with a change in orientation is not intuitive. The rate of change of orientation of a body is given in the angular velocity *vector*, while the orientation itself is given by a quaternion. The bridge between $\dot{\boldsymbol{q}} \in \mathbb{R}^4$ and $\vec{\omega} \in \mathbb{R}^3$ is also given by Fukushima (2008) in Eq.(13), and is gathered below in Eq.(C.4). Notice that, if written in matrix form, this is just Eq.(2.30).

$$\begin{aligned}
\dot{q}_0 &= \frac{1}{2}\left(-q_1\omega_1 - q_2\omega_2 - q_3\omega_3\right) \\
\dot{q}_1 &= \frac{1}{2}\left(+q_0\omega_1 - q_3\omega_2 + q_2\omega_3\right) \\
\dot{q}_2 &= \frac{1}{2}\left(+q_3\omega_1 + q_0\omega_2 - q_1\omega_3\right) \\
\dot{q}_3 &= \frac{1}{2}\left(-q_2\omega_1 + q_1\omega_2 + q_0\omega_3\right)
\end{aligned} \tag{C.4}$$

Although the orientation of Phobos is integrated using quaternions, *the orientation of Phobos* that is present in the equations of motion and the variational equations - namely Eq.(2.33) and Eq.(2.27) -

enters in the form of rotation matrices. Luckily, Eq.(15) of Fukushima (2008) relates one and the other - quaternions and rotation matrices. Call $\hat{e}_x$, $\hat{e}_y$ and $\hat{e}_z$ the unit vectors that conform Phobos' body-fixed frame. Therefore, they are aligned with Phobos' three axes of principal inertia. By the definition of the rotation matrix, $\boldsymbol{R}^{\mathcal{I}/\mathcal{P}}$ is defined as in Eq.(C.5). These vectors can be expressed in terms of the components of the rotation quaternion as shown in the same equation.

$$\begin{gathered}\boldsymbol{R}^{\mathcal{I}/\mathcal{P}} = \begin{bmatrix}\hat{e}_x & \hat{e}_y & \hat{e}_z\end{bmatrix} \iff \boldsymbol{R}^{\mathcal{P}/\mathcal{I}} = \begin{bmatrix}\hat{e}_x & \hat{e}_y & \hat{e}_z\end{bmatrix}^T \\ \hat{e}_x = \begin{bmatrix}q_0^2+q_1^2-q_2^2-q_3^2 \\ 2(q_0q_3+q_1q_2) \\ 2(q_1q_3-q_0q_2)\end{bmatrix} \quad \hat{e}_y = \begin{bmatrix}2(q_1q_2-q_0q_3) \\ q_0^2-q_1^2+q_2^2-q_3^2 \\ 2(q_0q_1+q_2q_3)\end{bmatrix} \quad \hat{e}_z = \begin{bmatrix}2(q_0q_2+q_1q_3) \\ 2(q_2q_3-q_0q_1) \\ q_0^2-q_1^2-q_2^2+q_3^3\end{bmatrix}\end{gathered} \tag{C.5}$$

This is essentially an expression for $\boldsymbol{R}^{\mathcal{P}/\mathcal{I}}(\boldsymbol{q})$, which allows for the evaluation of $\partial \boldsymbol{R}^{\mathcal{P}/\mathcal{I}}/\partial \boldsymbol{q}$ in Eq.(2.38). Note that this partial will be a 3-by-3-by-4 tensor of order 3, which will follow the rules for higher order tensors defined at the beginning of the document. Finally, the *rotation observations* mentioned in Sec. 5.2.1 come in the form of 3-1-3 Euler angles. Understanding the relationship between quaternions and these Euler angles is then the last step in the basic knowledge of quaternions required for this text. The link between the two is the rotation matrix. Consider again Phobos' body-fixed frame vectors $\hat{e}_x$, $\hat{e}_y$ and $\hat{e}_z$, and the 3-1-3 Euler angles ψ, θ and ϕ. The former are given as functions of the latter as shown below in Eq.(C.6), which corresponds to Eq(A5) of Fukushima (2008).

$$\hat{e}_x = \begin{bmatrix}\cos\phi\cos\psi - \sin\phi\cos\theta\sin\psi \\ \cos\phi\sin\psi + \sin\phi\cos\theta\cos\psi \\ \sin\phi\sin\theta\end{bmatrix} \quad \hat{e}_y = \begin{bmatrix}-\sin\phi\cos\psi - \cos\phi\cos\theta\sin\psi \\ -sin\phi\sin\psi + \cos\phi\cos\theta\cos\psi \\ \cos\phi\sin\theta\end{bmatrix} \quad \hat{e}_z = \begin{bmatrix}\sin\theta\sin\psi \\ -\sin\theta\cos\psi \\ \cos\theta\end{bmatrix} \tag{C.6}$$

Conversion between the quaternion components and the three Euler angles requires the inverse of one of these two equations - Eq.(C.5) and Eq.(C.6). For conversion of a quaternion into Euler angles, θ is assumed to be in the range $0 \leq \theta < \pi$. For the reverse conversion, specific transformations between the vectors and the quaternion components are defined by Fukushima (2008) in the events that any of q_0, q_1 or q_2 are (close to) 0.